UNIVERSIDADE FEDERAL DE MINAS GERAIS

PROGRAMA DE PÓS-GRADUAÇÃO EM

ENGENHARIA MECÂNICA

NUMERIC MODEL OF A DIRECT EXPANSION SOLAR ASSISTED HEAT PUMP WATER HEATER OPERATING WITH LOW GWP REFRIGERANTS (R1234YF, R290, R600A AND R744) FOR REPLACEMENT OF R134A

WILLIAN MOREIRA DUARTE

Belo Horizonte, September 20, 2018

Willian Moreira Duarte

NUMERIC MODEL OF A DIRECT EXPANSION SOLAR ASSISTED HEAT PUMP WATER HEATER OPERATING WITH LOW GWP REFRIGERANTS (R1234YF, R290, R600A AND R744) FOR REPLACEMENT OF R134A

Submitted in partial fulfillment of the requirements for the degree of Doctorate in Mechanical Engineering in the Programa de Pós Graduação em Engenharia Mecânica da Universidade Federal de Minas Gerais.
Concentration area: Energy and Sustainability
Advisor: Prof Dr. Luiz Machado (UFMG)
Co-advisor: Prof Dr. Antônio A. T. Maia (UFMG)

Belo Horizonte
Engineering School of UFMG
2018

Duarte, Willian Moreira.
D812n Numeric model of a direct expansion solar assisted heat pump water heater operating with low GWP refrigerants (R1234yf, R290, R600a and R744) for replacement of R134a [manuscrito] / Willian Moreira Duarte. – 2018.
107 f., enc.: il.

Orientador: Luiz Machado.
Coorientador: Antônio A. T. Maia.

Tese (doutorado) - Universidade Federal de Minas Gerais, Escola de Engenharia.

Bibliografia: f. 97-107.

1. Engenharia mecânica - Teses. 2. Bombas de calor - Teses. 3. Impacto ambiental - Teses. I. Machado, Luiz. II. Maia, Antônio Augusto Torres. III. Universidade Federal de Minas Gerais. Escola de Engenharia. VI. Título.

CDU: 621(043)

UNIVERSIDADE FEDERAL DE MINAS GERAIS
PROGRAMA DE PÓS-GRADUAÇÃO EM ENGENHARIA MECÂNICA
Av. Antônio Carlos, 6627 - Campus Universitário
31270-901 – Belo Horizonte – MG
Tel.:+55 31 3409.5145
E-mail: cpgmec@demec.ufmg.br

"NUMERIC MODEL OF A DIRECT EXPANSION SOLAR ASSISTED HEAT PUMP WATER HEATER OPERATING WITH LOW GWP REFRIGERANTS (R1234YF, R290, R600A AND R744) FOR REPLACEMENT OF R134A"

WILLIAN MOREIRA DUARTE

Tese submetida à Banca Examinadora designada pelo Colegiado do Programa de Pós-Graduação em Engenharia Mecânica da Universidade Federal de Minas Gerais, como parte dos requisitos necessários à obtenção do título de **"Doutor em Engenharia Mecânica"**, na área de concentração de **"Energia e Sustentabilidade".**

Tese aprovada no dia 20 de setembro de 2018.

Por:

Prof. Luiz Machado
Orientador - Departamento de Engenharia Mecânica/ UFMG

Prof. Antônio Augusto Torres Maia
Co-orientador - Departamento de Engenharia Mecânica/ UFMG

Profª. Sinthya Gonçalves Tavares
Centro Universitário de Belo Horizonte

Prof. Ralney Nogueira de Faria
Centro Federal de Educação Tecnológica de Minas Gerais

Prof. Rudolf Huebner
Departamento de Engenharia Mecânica/ UFMG

Prof. Matheus Pereira Porto
Departamento de Engenharia Mecânica/ UFMG

PREFACE

This PhD thesis is the result of research conducted in the last three years and three months at the group of refrigeration and heating (GREA) at Universidade Federal de Minas Gerais (UFMG) under the supervision of Prof. Luiz Machado and Prof. Antônio Maia and at the division of Applied Thermodynamics at Royal Institute of Technology (KTH), under the supervision of Prof. Björn Palm. During this time, three journal papers and seven conference/congress papers related to this research were produced and they are listed below:

1. **Duarte, W. M.**; Paulino, T. F.; Garcia, J.; Sawalha, S.; Machado, L.; Refrigerants selection for a direct expansion solar assisted heat pump for domestic hot water. Submitted to International Journal of Refrigeration.

2. **Duarte, W. M.**; Garcia, J.; Maia, A. A. T.; Machado, L.; Non-isentropic phenomenological model of a R134a reciprocating compressor. Submitted to Applied Thermal Engineering.

3. **Duarte, W. M.**; Diniz, H. A. G.; Paulino, T. F.; Rabelo, S. N.; Machado, L. Performance comparison of direct expansion solar assisted heat pump working with R1234yf as a drop-in replacement for R134a. In: 17TH Brazilian Congress of Thermal Sciences and Engineering - ENCIT (to appear). Águas de Lindóia-SP: ABCM, 2018.

4. **Duarte, W. M.**; Paulino, T. F.; Rabelo, S. N.; Maia, A. A. T.; Machado, L. Optimal high pressure correlation for R744 direct expansion solar assisted heat pump for domestic hot water. In: 17TH Brazilian Congress of Thermal Sciences and Engineering - ENCIT (to appear). Águas de Lindóia-SP: ABCM, 2018.

5. **Duarte, W. M.**; Rabelo, S. N.; Paulino, T. F.; Palm, B.; Machado, L. Economic and energetic analysis of solar collector size of a direct expansion solar assisted heat pump. In: 17TH Brazilian Congress of Thermal Sciences and Engineering - ENCIT (to appear). Águas de Lindóia-SP: ABCM, 2018.

6. Garcia, J.; Ali, T.; **Duarte, W. M.**; Khosravi, A.; Machado, L.; Comparison of transient response of an evaporator model for water refrigeration system working with R1234yf as a drop-in replacement for R134a. International Journal of Refrigeration, Elsevier, vol 91, pp. 211-222, 2018.

7. Rabelo, S. N.; Paulino, T. F.; **Duarte, W. M.**; Sawalha, S.; Machado, L. Experimental Analysis of the Influence of Water Mass Flow Rate on the Performance of a CO2 Direct-Expansion Solar

Assisted Heat Pump. 20th International Conference on Energy, Environmental and Chemical Engineering. Estocolmo. v.7, p.556 - 560, 2018.

8. Rabelo, S. N.; **Duarte, W. M.**; Paulino, T. F.; Garcia, J.; Machado, L. Analysis of the refrigerant mass charge for a direct expansion solar assisted heat pump system. In: 17TH Brazilian Congress of Thermal Sciences and Engineering - ENCIT (to appear). Águas de Lindóia-SP: ABCM, 2018.

9. Santos, F. N. Q.; Diniz, H. A. G.; **Duarte, W. M.**; Koury, R. N. N. Avalição experimental do desempenho térmico do ciclo de compressão a vapor ao se alterar as temperaturas das fontes quentes e fria. In: CONEM - Congresso Nacional de Engenharia Mecânica, Fortaleza, 2016.

10. Ali, T.; **Duarte, W. M.**; Haberschil, P.; Maia, A. A. T.; Machado, L. Dynamic model for an evaporator operating with R-1234yf and R-134a. In: XXXVI Ibero-Latin American Congress on Computational Methods in Engineering - CILAMCE. Rio de Janeiro, 2015.

From articles 1 to 5, and 8 the author of this thesis was responsible for the modelling and calculations, in articles 2, 6, 7, 9 and 10 the authors was responsible for experimental tests or part of them and assisted in the writing and result analysis of all the articles. The article number 7 was chosen as the best paper of the 20th International Conference on Energy, Environmental and Chemical Engineering.

This document was written considering the guidelines of Associação Brasileira de Normas Técnicas (ABNT), however, for the decimal separator it was used point (.) instead of comma (,).

ACKNOWLEDGMENT

First of all, I have to thank God for giving me the ability to get here. I would like to thank my family for the understanding and support of everyone who, in some way, participated in this stage of my career: My mother Célia, my father Tarcísio, my brother Wendel, my son Alyson, and, specially, my wife Riva.

I would like to thank my advisor, Prof. Luiz Machado, and co-advisor, Prof. Antonio Maia, for the traditional patience and attention. The Prof. Börn Palm and Prof. Samer Sawalha for hosted me at KTH on the last year. They helped me with important orientations which shaped this research.

I would like to thank my colleagues Tiago, Sabrina, Juan and Hamayun Maqbool that have worked with me during the PhD course. I would like to thank Prof. Sinthya for helping me at UniBH.

This work was supported by Foundation for Research Support of the State of Minas Gerais, through the project FAPEMIG AUC-00032-16.

ABSTRACT

Heating water through of heat pump has a reduced consumption of electric energy due to the use of the energy available in the environment. This work explores the lack of studies of direct expansion solar assisted heat pump (DX-SAHP) using refrigerants with low Global Warming Potential (GWP). The numeric model proposed uses a lumped parameter model for the heat exchangers and a semi-empirical model for the compressor. This model was validated from an experimental setup running with R134a, equipped with two types of condenser, comparing the experimental and theoretical results of Coefficient of Performance (COP). These results are available in the literature and were obtained under a solar radiation from 0 to 1100W/m^2, an ambient temperature between 24.8 and 34.5^{o}C, a final water temperature around 45^{o}C, and a wind velocity between 0 and 2.4 m/s. The mean difference between measured and calculated COP is 2%. The refrigerants with low GWP analyzed are R290, R600a, R744, and R1234yf. R290 has better COP for solar radiation between 50 W/m^2 and 700 W/m^2, as well as for environment temperature between 10^{o}C and 35^{o}C. On the other hand, for solar radiation less than 50 W/m^2, the R134a has better COP than R290. Environmental analysis indicates that the indirect emissions are the most important effect, and then, the Total Equivalent Warming Impact (TEWI) results almost followed the COP outcome. The lowest TEWI was obtained using R290 and an economic analysis was performed using this refrigerant. An optimum collector area and condenser length were found in the simulations to reduce the payback time. The optimum size of the condenser increases with the augment of solar radiation, but the optimum collector size remains approximately constant with the increase of solar radiation. The payback time of a R290 DX-SAHP in Belo Horizonte is 3.9 years and is 13% higher than the payback time available in the literature for R134a DX-SAHP.

Keywords: Numeric model; Low Environmental Impact; Economic; DX-SAHP; R1234yf; R290; R600a; R744; Solar Assisted Heat Pump;

RESUMO

O uso de bomba de calor para o aquecimento de água reduz o consumo de energia elétrica devido ao uso de energia térmica disponível no meio ambiente. Este trabalho explora a falta de estudos de bomba de calor solar de expansão direta utilizando refrigerantes com baixo *Global Warming Potential* (GWP). O modelo numérico proposto utiliza modelos de parâmetros concentrados para os trocadores de calor e um modelo semi empírico para o compressor. Esse modelo foi validado experimentalmente a partir de uma bomba de calor solar que usa o R134a, equipada com dois tipos de condensadores, comparando resultados experimentais e teóricos de *Coefficient of Performance* (COP). Esses resultados experimentais estão disponíveis na literatura e foram obtidos sob radiação solar de 0 e 1100 W/m^2, temperatura ambiente entre 24.8 e 34.5^{o}C, temperatura final da água em torno de 45^{o}C e velocidade do vento entre 0 e 2.4 m/s. A diferença média entre o COP medido e calculado é de 2%. Os refrigerantes com baixo GWP analisados foram o R290, o R600a, o R744 e o R1234yf. O R290 tem melhor COP para radiação solar entre 50 W/m^2 e 700 W/m^2, bem como para temperatura ambiente entre 10^{o}C e 35^{o}C. Por outro lado, para radiação solar menor que 50 W/m^2, o R134a tem melhor COP que o R290. A análise ambiental indica que as emissões indiretas é o efeito mais importante e os resultados de *Total Equivalent Warming Impact* (TEWI) quase seguiram o resultado do COP. O menor TEWI foi obtido usando o R290 e uma análise econômica foi realizada usando este refrigerante. Uma área ótima para o coletor e um comprimento para o condensador foram encontrados nas simulações afim de reduzir o tempo de retorno. O tamanho ótimo do condensador aumenta com o aumento da radiação solar, mas o tamanho ótimo do coletor fica aproximadamente constante com o aumento da radiação solar. O tempo de retorno de uma bomba de calor solar a R290 em Belo Horizonte é de 3.9 anos e é 13% maior que o tempo de retorno disponível na literatura para o uma bomba de calor solar a R134a.

Palavras chaves: Modelo numérico; Baixo impacto ambiental; Análise econômica; Bomba de calor solar; R1234yf; R290; R600a; R744

ABBREVIATIONS

ABNT	Associação Brasileira de Normas Técnicas
ASHRAE	American Society of Heating, Refrigerating and Air-Conditioning Engineers
ANEEL	Brazilian Electricity Regulatory Agency
ASHP	Air source heat pump
COP	Coefficient of performance.
CBFP	Covered bare flat plat
DHC	Domestic hot water
DWC	Dropwise condensation
DX	Direct expansion
EES	The Engineering Equation Solver
EP	European Parlament
ETUP	Evacuated Tube U-Pipe collector
FORTRAN	FORmula TRANslation.
FWC	Filmwise condensation
GREA	Group of cooling and heating.
GSHP	Ground Source Heat Pump
GWP	Global Warming Potential
HCF	Hydrochlorofluorocarbons.
HTC	Heat Transfer Coefficient
LCCP	Life-cycle climate performance
MAD	Mean absolute deviation or mean absolute relative deviation.
MMA	Brazilian Ministry of the Environment
MATLAB	MATrix LABoratory.
MAX	Function that returns the largest value of the list of value.
MD	Mean deviation or mean relative deviation.
NTU	Number of transfer units
ODP	Potential depletion of the ozone layer.
IX	Indirect expansion
IR	Annual inflation rate

PVC	Polyvinyl is a general purpose plastic.
PV-T	Photovoltaic thermal hybrid solar collector
R12	Refrigerant dichlorodifluoromethane known as Freon-12.
R22	Refrigerant chlorodifluoromethane or 22 Freon
R134a	Refrigerant also known as HFC-134a
R1234yf	Refrigerant 2,3,3,3-Tetrafluoropropene
R1270	Code used to identify propene when used as refrigerant.
R152a	Refrigerant 1,1-Difluoroethane
R290	Code used to identify propane when used as refrigerant.
R404A	Refrigerant blend (44% of R125, 52% of R143a and 4% of R134a)
R407C	Refrigerant blend (23% of R32, 25% of R125 and 52% of R134a.)
R410A	Refrigerant blend (50% of R125, 50% of R32)
R600	Code used to identify butane when used as refrigerant.
R600a	Code used to identify isobutane when used as refrigerant.
R717	Code used to identify ammonia when used as refrigerant.
R744	Code used to identify carbon dioxide or CO_2 when used as refrigerant.
SAHP	Solar Assisted Heat Pump
SH	Space heating
SI	International System of Units
TEWI	Total Equivalent Warming Impact
UBFP	Uncovered bare flat plat
UFMG	Universidade Federal de Minas Gerais
UNEP	United Nations Environment Programme
UNFCCC	United Nations Framework Convention on Climate Change.

NOMENCLATURE

Exceptions

$\overline{Y}$	Average of variable Y, page 60
B_n	Generics constants or auxiliary variables (n= 1, 2, 3...) [$dimensionless$], page 35
i_{lv}	Specific enthalpy of vaporization [J/kg] , page 38
r^*	Ratio between the inner tube outside diameter and the outer tube inner diameter at concentric annular ducts [$dimensionless$], page 34
r^2	Coefficient of determination [$dimensionless$], page 70

Greek and special symbols

α	Void fraction [$dimensionless$], page 36
β	Coefficient of thermal expansion [$1/K$], page 42
δ	Collector thickness [m], page 61
$\dot{\forall}$	Volumetric flow rate [m^3/s], page 57
η	efficiency [$dimensionless$], page 62
$\forall$	Volume [m^3], page 62
Γ	Bond thermal conductance [$W/(m^2K)$], page 27
λ	Leakage rate in the system [$kg/year$], page 58
μ	Dynamic viscosity [$Pa \cdot s$], page 33
Φ	Carbon dioxide emission factor [kg/kWh], page 58
ϕ	Relative humidity [$dimensionless$], page 54
ρ	Density [kg/m^3], page 36
σ	Stefan-Boltzmann constant [$5,670367(13) \cdot 10^{-8} W/(m^2K^4)$], page 61
σ'	Surface tension [N/m], page 36
τ	Transmissivity [$dimensionless$], page 27
θ	Inclination [^{o}], page 41
ε	Emissivity [$dimensionless$], page 61
ξ	Heat exchanger effectiveness [$dimensionless$], page 65
ζ	Heat leakage coefficient [$dimensionless$], page 64

Latin symbols

$\dot{C}$	Heat capacity rate [W/K], page 65

$\dot{m}$ Mass flow rate [kg/s], page 27

$\dot{W}$ Work rate [W], page 57

COP Coefficient of performance [$dimensionless$], page 57

GWP Global Warming Potential [$dimensionless$], page 58

IR Annual inflation rate [$dimensionless$], page 58

MAD Mean absolute deviation [$dimensionless$], page 32

MD Mean deviation [$dimensionless$], page 32

NTU Number of transfer units [$dimensionless$], page 65

TEWI Total equivalent warming impact [$kgofCO_2$-eq], page 58

A Area [m^2], page 27

a Solar absorptivity [$dimensionless$], page 27

C Specific heat at constant pressure [$J/(kgK)$], page 45

c Flow coefficient [$dimensionless$], page 67

D Diameter [m], page 27

E Energy consumption [$kWh/year$], page 58

F Fin efficiency [$dimensionless$], page 27

f Friction factor [$dimensionless$], page 33

F' Collector efficiency factor [$dimensionless$], page 27

G Mass flux [$kg/(m^2s)$], page 36

g Gravitational acceleration [m/s^2], page 36

h Convective heat transfer coefficient[$W/(m^2K)$], page 27

I Solar irradiance [W/m^2], page 27

i Specific entalphy [J/kg], page 27

I' Initial investment [R\$], page 58

k Thermal conductivity [$W/(m^2K)$], page 38

L Lenght [m], page 33

M Molecular weight [$kg/kmol$], page 38

m Mass [kg], page 67

N Rotational speed [Hz], page 62

n Number of data points or divisions [$dimensionless$], page 32

N' Lifetime of the system [$years$], page 58

P Pressure [Pa], page 45

p Reduced pressure [$dimensionless$], page 38

P' Payback period [$year$], page 58

Q Heat transfer rate [W], page 45

q Heat flux [W/m^2], page 38

R Gas constant [$J/(kgK)$], page 45

r Rugosity [m], page 35

S Net radiation absorbed by the collector [W/m^2], page 60

s Annual savings [$R\$$], page 58

T Temperature [K], page 27

t Time [s], page 63

T' Electricity tariff [$R\$/kWh$], page 59

U Overall heat transfer coefficient [$W/(m^2K)$], page 27

V Velocity [m/s], page 44

v Vapor velocity [$dimensionless$], page 41

W Work [J], page 58

w Distance between the tubes [m], page 27

x Vapor quality [$dimensionless$], page 36

z Position [m], page 33

Dimensionless numbers

Bd Bond , page 38

Bo Boiling , page 38

Co Convection , page 39

Fr Froude, page 39

Gr Grashof number, page 42

Nu Nusselt, page 33

Pr Prandtl, page 33

Ra Rayleigh, page 42

Re Reynolds, page 33

We Weber, page 39

Common subscripts

0 For a inclination of 0^o, page 41

1 Compressor inlet or evaporator outlet, page 52

2 Compressor outlet or condenser inlet, page 52

3 valve inlet or condenser outlet, page 52

4 Evaporator inlet or valve outlet, page 52

90 For a inclination of 90^o, page 41

∞ Quiescent fluid or free stream, page 42

a Ambient, page 27

air Air or dry air, page 45

ann Annular flow or annular regions, page 35

atm Atmospheric, page 45

bo Boiling region, page 61

$C1$ Vapor only region in the condenser, page 63

$C2$ Condensation region in the condenser, page 63

$C3$ Liquid only region in the condenser, page 63

ch Characteristic, page 42

$circ$ Circular duct, page 33

col Collector, page 58

col Solar collector, page 45

$cond$ Condensation or condenser, page 45

$cond$ Condenser, page 64

$crit$ Critical, page 33

d Compressor displacement volume, page 62

ed Expansion device, page 67

ele Electrical, page 59

ev Evaporator or evaporating, page 27

exp Experimental, page 32

flm Liquid film, page 46

gco Gas cooler outlet, page 48

h Hydraulic, page 33

hel Helical coil, page 33

hom Homogeneous, page 37

hp Heat pump, page 59

I Flow regime I during condensation defined by Shah (2016), page 40

i Inner, page 27

II Flow regime II during condensation defined by Shah (2016), page 40

ii Inner tube inside property/geometry, page 35

III Flow regime III during condensation defined by Shah (2016), page 40

io Inner tube outside property/geometry, page 35

L Liquid , page 36

o Outer, page 27

oi Outer tube inside property/geometry, page 35

oo Outer tube outside property/geometry, page 35

opt Optimum, page 48

ov Overall, page 63

p Pumps, page 57

$pred$ Predicted, page 32

r Refrigerant, page 27

s Surface, wall or properties at the surface temperature, page 33

sky sky, page 61

sup Superheat, page 61

t Tank, page 63

V Vapor , page 36

w Water, page 45

wd Wind, page 44

wf Water final property, page 58

wi Water inlet/initial property, page 57

wo Water outlet, page 57

LIST OF FIGURES

LIST OF TABLES

SUMMARY

1. INTRODUCTION

One of the main problems faced by humanity in the last decades are the climate change that impacts the environment, the society and the economy. Among these issues is the depletion of the ozone layer, which has strong consequences on people's health, and the global warming, which is a major cause of the increase frequency of climatic events such as severe storms, floods and droughts. In view of the scenario, the Montreal protocol was proposed, which, in general terms, established generic targets for the protection of the ozone layer. As the Brazilian Ministry of the Environment (MMA, 2017a), the last review, Beijing 1999, was approved by the Brazilian government by decree number 5.280, published on November 22, 2004, pledging to eliminate 100% of the use of Hydrofluorocarbons (HCFs) gases until 2040. The most commonly used HCF gas in Brazil nowadays is R22, which is widely used in stationary air conditioners.

Subsequently, at the 21st United Nations Climate Change Conference (COP21) of the UNFCCC (United Nations Framework Convention on Climate Change) was proposed the Paris Agreement establishing commitments to reduce emissions of gases which aggravate the greenhouse effect. The Brazilian Congress, in September of 2016, ratified this agreement making official targets. The Brazilian goal is to reduce emissions of greenhouse gases by 37% until 2025 and by 43% until 2030 (the reference value is the emissions in 2005) (MMA, 2017b). To reduce the greenhouse effect, some refrigerants which have high Global Warming Potential (GWP) are being banned by the European Parliament (EP, 2014).

The use of heat pumps instead of electric heaters and gas heaters is one way to reduce energy consumption and emissions of greenhouse gases. It is known that Solar Assisted Heat Pump (SAHP) and Ground Source Heat Pump (GSHP) have better season performance than Air Source Heat Pump (ASHP). Different types of SAHP can be found in the literature, a direct expansion solar assisted heat pump (DX-SAHP) is the setup with the lowest number of components thus the lowest cost. The coefficient of performance (COP) of a DX-SAHP using different refrigerants was investigated by Chaturvedi and Abazeri (1987) and Chata, Chaturvedi, and Almogbel (2005), but these authors only considered refrigerants with high GWP. They also did not consider the difference in the efficiency of the compressor, and they did not use any environmental metric to select the best refrigerant.

Experimental research comparing a DX-SAHP using different refrigerants may involve high costs for purchasing equipment, refrigerant, and require time for assembly, calibration and adjustment. An alternative way to research is the use of mathematical models which allows the simulation of the operation of various components of the refrigeration system at lower cost and time compared to the experimental set (KOURY; MACHADO; ISMAIL, 2001).

1.1 General objective

The general objective of this work is to present and validate experimentally a mathematical model to compare the energetic, environmental, and economical performances of a direct expansion solar assisted heat pump using refrigerant with low GWP.

1.2 Specific objectives

- Elaborate a mathematical model based in the assumptions widely used in the literature and correlations tested for different refrigerants;
- Calibrate the empirical and semi empirical components model using experimental data;
- Validate the model using the experimental data from a R134a DX-SAHP;
- Compare the Total Equivalent Warming Impact (TEWI) and COP of DX-SAHP running with different refrigerants;
- Perform an economical analysis of the DX-SAHP using the refrigerant with lower TEWI.

2. SOLAR ASSISTED HEAT PUMPS

Buker and Riffat (2016) presented 73 different studies on SAHP and they found three usual setups used to produce only Domestic Hot Water (DHW): (i) Parallel type indirect expansion SAHP, (ii) Series type indirect expansion SAHP, (iii) Direct expansion SAHP. In the parallel type IX-SAHP, the hot water is produced by a thermal solar collector in the sunny days, and by an ASHP, if the solar radiation is not enough to achieve the desired temperature. An example of an IX-SAHP parallel type is shown in Fig. 2.1.

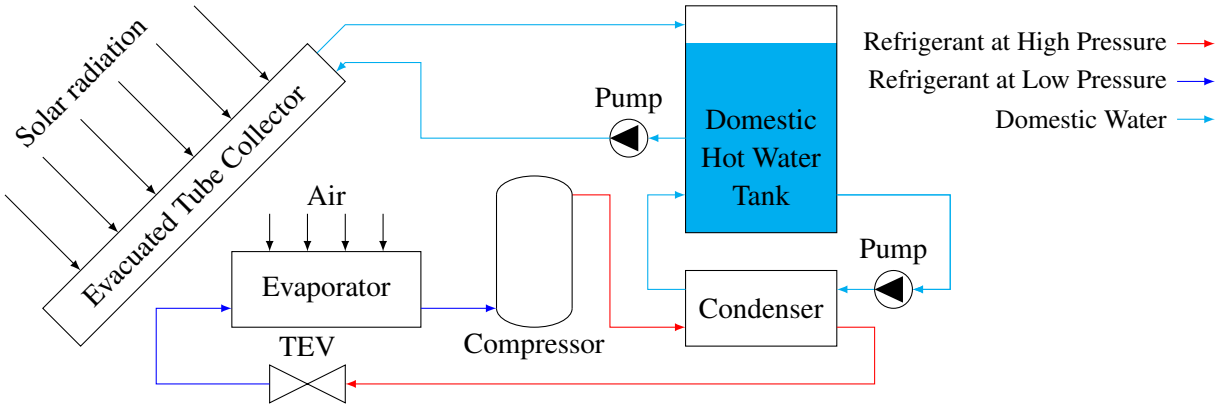

FIGURE 2.1: Example of Parallel type IX-SAHP
SOURCE: Adapted from Buker and Riffat (2016, p. 403)

Another configuration described by Buker and Riffat (2016) is show in Fig. 2.2. In this configuration, the heat pump is always running, but the evaporation temperature is higher than the one in the system of Fig. 2.1. In the results presented by Bertram, Pärisch, and Tepe (2012), considering the climate of Trabzon in Turkey, the heat pump in Fig. 2.2 has COP 25% higher than the ASHP in Fig. 2.1, but the parallel type system consumes 2% less energy during the year.

The third setup reported by Buker and Riffat (2016) is a direct expansion solar assisted heat pump (DX-SAHP) shown in Fig. 2.3. Although, there is no study comparing the IX-SAHP and DX-SAHP, a similar Coefficient of Performance (COP) was reported by Bertram, Pärisch, and Tepe (2012) for IX-SAHP and by Xiaolin Sun et al. (2015) for DX-SAHP. The cost of DX-SAHP is lower than the IX-SAHP because of the lower number of components.

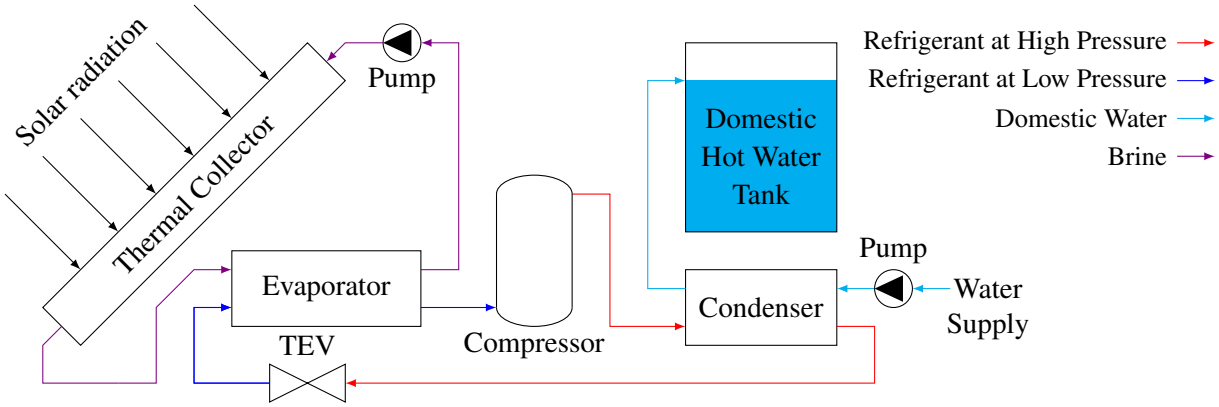

FIGURE 2.2: Example of Series type IX-SAHP
SOURCE: Adapted from Buker and Riffat (2016, p. 403)

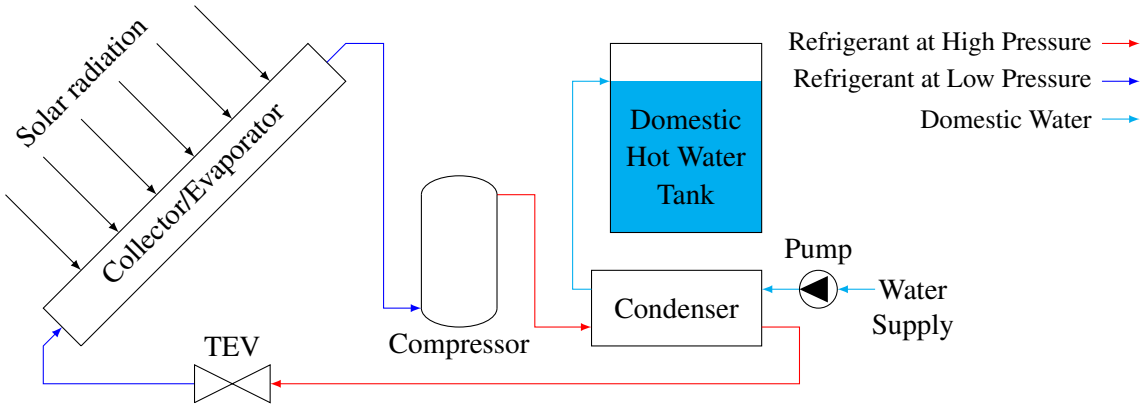

FIGURE 2.3: Example of DX-SAHP
SOURCE: Adapted from Buker and Riffat (2016, p. 403)

2.1 Studies on direct expansion solar assisted heat pump

Several studies using a DX-SAHP were found in the literature, most of them investigated the system energetic performance at different climate conditions, however, there are few investigations only on the exergetic performance (TORRES-REYES; NUÑEZ; GORTARI, 1998; CERVANTES; TORRES-REYES, 2002), in the component performance (OLIVEIRA et al., 2016; FARIA et al., 2016; SCARPA; TAGLIAFICO, 2016) and only two studies comparing the performance of DX-SAHP using different refrigerants (CHATURVEDI; ABAZERI, 1987; CHATA; CHATURVEDI; ALMOGBEL, 2005). The studies on energetic performance of DX-SAHP are summarized in Tab. 2.1. Four different types of evaporators/collector were found in these studies: uncovered bare flat plate (UBFP), covered bare flat plate (CBFP), Evacuated Tube U-Pipe (ETUP), and photovoltaic thermal hybrid solar collectors (PV-T) and two objective: producing domestic hot water (DHW) or space heating (SH).

TABLE 2.1
Studies on energetic performance of DX-SAHP

Authors	Collector		Refrigerant	COP	Type of study		Load	Location	Tank	Water
	Type	A (m^2)			Theo.	Exp.			(L)	Temp. (^oC)
Chaturvedi and Shen (1984)	UBFP	3.4	R12	2-3	✓	✓	DHW	Norfolk	-	-
Chaturvedi, DT Chen, and Kheireddine (1998)	UBFP	3.5	R12	2.5-4.5	✓	✓	SH	Norfolk	-	-
Ito, Miura, and K Wang (1999)	UBFP	3.2	R22	2-8	✓	✓	DHW	Japan	-	30-60
Torres-Reyes and Gortari (2001)	UBFP	4.5	R22	5.6-4.4	✓	✓	SH	Guanajuato	-	-
Hawlader, Chou, and Ullah (2001)	UBFP	3.0	R134a	4-9	✓	✓	DHW	Singapore	250	55
Chyng, C.P. Lee, and B.J. Huang (2003)	UBFP	1.9	R134a	1.7-2.5	✓	✓	DHW	Taiwan	-	52-56
Y. H. Kuang, Sumathy, and R. Z. Wang (2003)	UBFP	2.0	R22	4-6	✓	✓	DHW	Shangai	150	50
Ito, Miura, and Takano (2005)	PV-T	1.9	R22	4.5-6.5	✓	✓	SH, DHW	Japan	-	30-60
Y.H. Kuang and R.Z. Wang (2006)	UBFP	10.5	R22	2.6-3.3	✗	✓	SH, DHW	Shangai	150	50
Li et al. (2007)	UBFP	4.2	R22	5.21	✓	✓	DHW	Shangai	150	50
Guoying Xu et al. (2009)	PV-T	2.3	R22	4.9-5.1	✓	✗	DHW	Nanjing	150	50
Chow et al. (2010)	UBFP	12	R134a	6.5-10	✓	✗	DHW	Hong Kong	1500	50
Kong, D Zhang, et al. (2011)	UBFP	4.2	R22	5.2-6.6	✓	✓	DHW	Shangai	150	50
Moreno-Rodríguez et al. (2012)	UBFP	5.6	R134a	1.7-2.9	✓	✓	DHW	Madri	300	51
Fernández-Seara et al. (2012)	UBFP	1.6	R134a	2-4	✗	✓	DHW	Inside the lab.	300	55
Islam et al. (2012)	ETUP	-	R744	1.5-2.8	✓	✓	-	-	-	-
Xiaolin Sun et al. (2015)	UBFP	2	-	4-5.5	✓	✗	DHW	Shanghai	150	55
Deng and Yu (2016)	CBFP	2.5	R134a	3.9-6.2	✓	✗	DHW	-	150	55
Kong, Li, et al. (2017)	UBFP	4.2	R410A	5.2-6.6	✓	✗	DHW	-	150	50
Mohamed, Riffat, and Omer (2017)	UBFP	4.2	R407C	5.2-6.6	✓	✓	SH, DHW	Nottingham	200	50
Diniz (2017)	UBFP	1.6	R134a	2.1-2.9	✗	✓	DHW	Belo Horizonte	200	45
Kong, Penglong Sun, et al. (2018)	UBFP	2.1	R134a	3.6-5.6	✗	✓	DHW	Qingdao	200	60
Kong, Jiang, et al. (2018)	UBFP	1.6	R134a	2.8-4.3	✗	✓	DHW	Qingdao	195	42-60

Chaturvedi and Abazeri (1987) made a theoretical study comparing the performance of a DX-SAHP using the refrigerants R12 and R22. The system described by them is the same shown in Fig. 2.3, equipped with a 2m^2 copper UBFP collector and a 400 liters water tank. The evaporator/collector was modeled using the Hottel-Whilliar-Bliss model presented by Duffie and Beckman (2013). The energy balance in the evaporator is given by:

$$\dot{m}_r \Delta i_r = A_{ev} F' [I\tau a - U_{ev}(T_r - T_a)] \tag{2.1}$$

where A, a, F', i, $\dot{m}$, S, T, τ and U represents the area, solar absorptivity, collector efficiency factor, specific entalphy, solar irradiance, mass flow rate, temperature, transmissivity and overall heat transfer coefficient, respectively. The subscripts a, ev and r represent the ambient, evaporator and refrigerant properties/geometry. The collector efficiency factor is given by:

$$F' = \frac{1}{wU_{ev}} \left\{ \frac{1}{U_{ev}[D_o + F(w - D_o)]} + \frac{1}{\pi D_i h_i} + \frac{1}{\Gamma} \right\}^{-1} \tag{2.2}$$

where diameter, fin efficiency, heat transfer coefficient, colletor tube spacing and the bond conductance are represented by D, F, h, w and Γ, respectively. The subscripts i and o represent the inner and outer properties/geometry. For the condenser, an empirical polynomial expression using the condensation and water inlet temperatures were used. A better COP of DX-SAHP running with R12 than R22, considering the meteorological data from a typical year in the city of Norfolk US-VA, is shown in Fig. 2.4. These authors also investigate the effect of the water storage temperature, collector size and compressor speed control strategy in the COP and collector temperature. This work precedes the Montreal protocol and the refrigerant R12 and R22 were banished.

Chata, Chaturvedi, and Almogbel (2005) analyzed the performance of DX-SAHP using the refrigerants R134a, R404A, R410A and R407C for replacement of the refrigerants R22 and R12. The system chosen by them is similar of that one shown in Fig. 2.3. The evaporator was modeled using the Hottel-Whilliar-Bliss model, considering no superheat at exit of the evaporator and fixed temperature at the condenser (60^{o}C). The compressor was modeled using a semi-empirical model and the volumetric and overall efficiencies were assumed constant. The model was implemented using C++ language and the thermodynamics properties were ob-

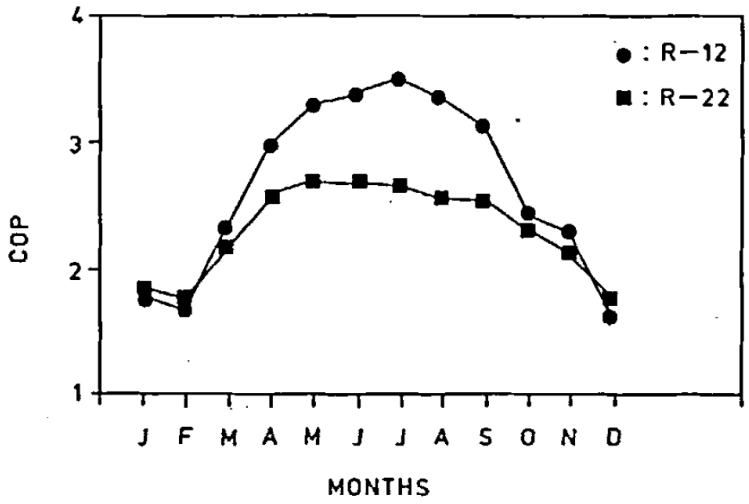

FIGURE 2.4: Average COP for a DX-SAHP in the cite of Norfolk
SOURCE: Chaturvedi and Abazeri (1987, p. 427)

tained from REFPROP. The COP of the selected refrigerants, considering the same evaporating temperatures (T_f), are shown in Fig. 2.5. These results demonstrate that the R134a is the best refrigerant of the group analyzed, since R12 and R22 have nonzero ODP (Ozone Depletion Potential). Chata, Chaturvedi, and Almogbel (2005) also present charts for sizing the collector and the compressor using R134a.

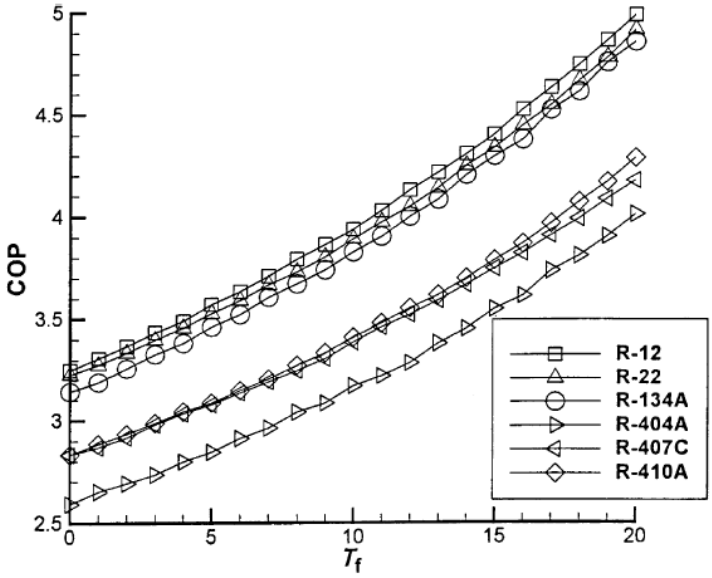

FIGURE 2.5: COP of DX-SAHP using the refrigerants R12, R22, R134a, R404A, R410A and R407C
SOURCE: Chata, Chaturvedi, and Almogbel (2005, p. 2619)

The two studies comparing the refrigerant for a DX-SAHP above mentioned analysed only the energetic performance and the refrigerants used have large GWP, as shown in

TABLE 2.2
Information of the refrigerants used in heat pumps.

Refrigerant	ODP	GWP	Normal Boiling Point (^{o}C) [1]	Critical Temp. (^{o}C)	Safety group	Refrigerating effect (kJ/m^3) [2]
R12	0.82	10900	-30	111.97	A1	2833
R22	0.04	1790	-41	96.145	A1	4529
R134a	0	1370	-26	101.6	A1	2972
R404A	0	3700	-46.6	72.046	A1	4797
R407C	0	1700	-43.8	86.034	A1	4215
R410A	0	2100	-51.6	74.67	A1	6729
R1234yf	0	<4.4	-29.4	94.7	A2L	2840
R1270	0	20	-48	91.061	A3	4653
R152a	0	133	-24	113.26	A2	2757
R290	0	20	-42	96.74	A3	3867
R600	0	20	0	151.98	A3	1143
R600a	0	20	-12	134.66	A3	1573
R717	0	<1	-33	132.25	B2L	5003
R744	0	1	-78	30.98	A1	14909

SOURCE: Adapted from ASHRAE handbook: Fundamentals, 2013 , p. 29.2 - 29.8.

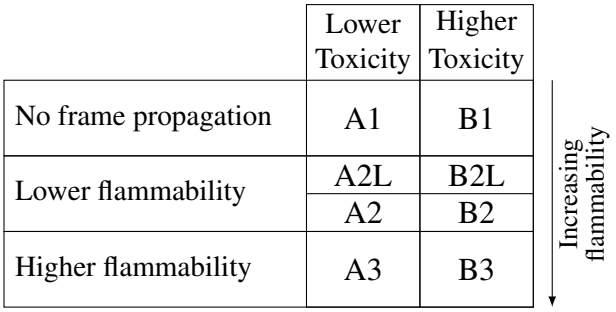

FIGURE 2.6: Safety groups defined by ASHRAE
SOURCE: ASHRAE handbook: Fundamentals, 2013, p. 29.9

Tab. 2.2. The recent studies in selection of refrigerant for other types of heat pump considered refrigerants with GWP lower than 150 and also listed in Tab. 2.2 (CHAICHANA; AYE; CHARTERS, W. W., 2003; MAKHNATCH; KHODABANDEH, 2014a; GHOUBALI et al., 2014; BOTTICELLA; VISCITO, 2015). This limit was settled by the the European Parlament (EP, 2014, 2006) for different system with different deadlines. The safety groups defined by ASHRAE are explained in Fig. 2.6.

Additionally, the setup described in most of the studies listed in Tab. 2.1 uses a naked tube condenser immersed at hot water tank, as shown in Fig. 2.7 instead of regular condenser shown in Fig. 2.3 and adopted by Chaturvedi and Abazeri (1987) and Chata, Chaturvedi,

[1] Normal bubble point for blends
[2] Data from EES, no subcool, zero superheat, no pressure loss, evaporating temperature at 7.2^{o}C and condensing temperature at 30^{o}C.

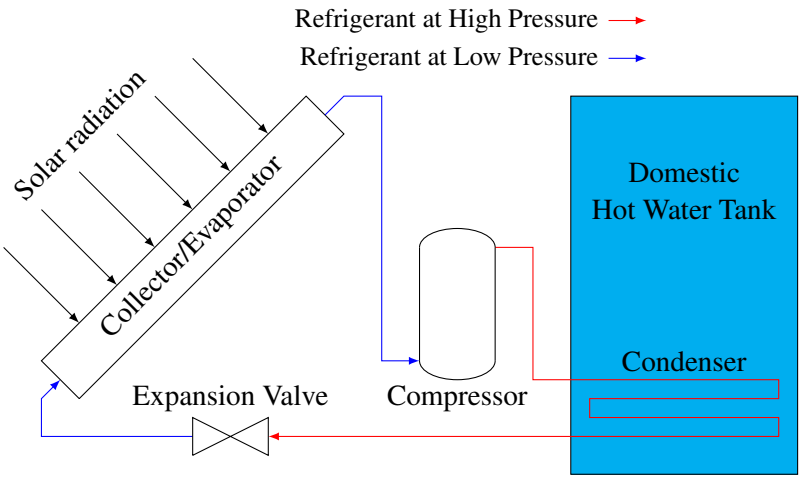

FIGURE 2.7: Example of DX-SAHP with immersed condenser
SOURCE: Adapted from Kong, D Zhang, et al. (2011, p. 6832)

and Almogbel (2005). Besides this, the model used by these authors are simplified compared to the most model listed in Tab. 2.1. In this work, refrigerants with low GWP, the immersed condenser and more detailed model are used.

2.2 Models of direct expansion solar assisted heat pump

Most of the models listed in Tab. 2.1 uses the Hottel-Whilliar-Bliss model for the collector and some articles can be highlighted in terms of model description: Y. H. Kuang, Sumathy, and R. Z. Wang (2003), Kong, D Zhang, et al. (2011), Kong, Li, et al. (2017), and Mohamed, Riffat, and Omer (2017). Y. H. Kuang, Sumathy, and R. Z. Wang (2003) developed quasi-steady model for DX-SAHP with immersed condenser using FORTRAN. The vertical solar collector was modeled using Hottel-Whilliar-Bliss model associated with the Watmuff, WWS Charters, and Proctor (1977) correlation for the air side and the correlation of Chaturvedi, Chiang, and Roberts (1982) for the refrigerant side. The compression process was assumed as polytropic and the hot water tank was assumed to be nonstratified. This model was validated experimentally to solar radiation between 50 to 290W/m^2 and ambient temperatures from 3 to 12^{o}C. These authors have analyzed the COP and collector efficiency during the year, furthermore they showed the effect of solar radiation, ambient temperature, collector area, hot water tank volume and compressor speed in COP and the collector efficiency.

The quasi-steady model presented by Kong, D Zhang, et al. (2011) and Kong, Li, et al. (2017) for a DX-SAHP uses the correlation of McAdams (1954) in the collector modeling and the collector efficiency factor proposed by Ito, Miura, and K Wang (1999) (EQ. 2.3). The

compression process was modeled as polytropic and the compressor efficiency assumed to be constant. The authors use the C++ language to implement the model with routines proposed by Cleland (1986) to obtain the R22 and R410A properties. The model was validated using 7 operating points obtained experimentally with a R22 heat pump with immersed condenser, which was operated in a range of ambient temperature from 20.5 to 29°C and solar radiation 663 to 955W/m^2. They presented the effect of solar radiation, ambient temperature, wind speed, compressor speed and refrigerant charge on COP and collector efficiency.

$$F' = F + \frac{D}{w}(1 - F) \tag{2.3}$$

A model of a DX-SAHP used for DWH and SH is presented by Mohamed, Riffat, and Omer (2017). These researchers implemented in MATLAB the Hottel-Whilliar-Bliss model to evaluate the efficiency of the evaporator and they used the correlation of Chaturvedi, Gagrani, and Abdel-Salam (2014) for the air, and the correlation of Gnielinski (1976) for the refrigerant. The compression process was modeled as polytropic and the compressor efficiency assumed to be constant. The model was validated using a heat pump with a tank of 200 liters, 4.22m^2 of solar collector and evaporator diameter of 13mm, two condensers (one for water and another for air) which, operated with solar radiation from 0 to 200W/m^2 and room temperature from 6.5 to 8.5°C. The results of COP found by them only for space heating were in the range of 2.7 to 3.9 and for both proposed they were in the range of 2.7 to 3.

3. CORRELATIONS REVIEW

In order to complete the set of equations from the mass, energy and momentum balances in the heat exchangers correlations for the heat transfer coefficient (HTC) and void fraction are necessary. Comparing the models presented in the previous chapter, different correlations have been used in each types of flow. Therefore, following it is presented a review of these correlations for different type of flow, focusing on those which are developed for many fluids or have experimental data of different refrigerants in the experimental validation.

For each type of flow, there are many correlations available in the literature, however, it is not the objective of this work to present all correlations available in the literature. So, in this chapter, it is presented only the correlation used or tested in the simulations.

In order to compare the accuracy of the correlation, the most used metrics are the Mean Absolute Deviation (MAD) and Mean Deviation (MD). For a correlation for heat transfer coefficient the MAD and MD are evaluated as following:

$$\text{MAD} = \frac{1}{n}\sum_{j=1}^{n}\left|\frac{h_{pred} - h_{exp}}{h_{exp}}\right| \tag{3.1}$$

$$\text{MD} = \frac{1}{n}\sum_{j=1}^{n}\left(\frac{h_{pred} - h_{exp}}{h_{exp}}\right) \tag{3.2}$$

where h is the heat transfer coefficient, n is the number of data points, the subscripts $pred$ and exp refer to predicted and experimental results. Some authors name MAD as mean absolute relative deviation and MD as mean relative deviation.

3.1 Internal single phase flow in ducts

3.1.1 Heat transfer coefficient

In horizontal circular section tubes, the Reynolds number (Re) is critical around 2300 and is considered fully turbulent flow to values above 10^4. The laminar flow can be considered fully developed (hydrodynamically and thermally) from the position z if $z/(DRePr) \geq$ 0.05 and in the turbulent regime for $z/D >$10 (INCROPERA et al., 2007). The Nusselt number (Nu) during laminar fully developed flow is 3.657 on walls with uniform temperature, and

4.364 on walls with uniform heat flux (ROHSENOW; HARTNETT; CHO, et al., 1998). For laminar developing flow Incropera et al. (2007) suggest the Sieder and Tate correlation shown in EQ. 3.3 recommended for $0.48 \leq Pr \leq 5$ and $0.0044 \leq \mu/\mu_s \leq 9.75$.

$$Nu = 1.86 \left(\frac{RePr}{L/D}\right)^{1/3} \left(\frac{\mu}{\mu_s}\right)^{0.14} \tag{3.3}$$

In this equation, Pr is the Prandtl number, L is the duct lenght, D is diameter, μ is dynamic viscosity. Properties evaluated in the film temperature are not subscripted and those marked with subscript s should be evaluated in surface temperature.

The correlation proposed by Gnielinski (1976) is the most used correlation for turbulent fully developed flow:

$$Nu = \frac{(f/8)(Re - 1000)Pr}{1 + 12.7(f/8)^{1/2}(Pr^{2/3} - 1)} \tag{3.4}$$

where f is the friction factor and the domain of this equation is $0.5 \leq Pr \leq 2000$ and $3000 \leq Re \leq 5 \cdot 10^6$.

For helically wound tubes, there is the formation of a secondary flow which increases turbulence and enhances heat transfer. For this configuration, the critical Reynolds number is given by EQ. 3.5. Correlation proposes by Reymon, Schmidt and Seban are shown in EQ. 3.6 to EQ. 3.8, respectively. The domain of Reymon equation is $0.0208 \leq D_i/D_{hel} \leq 0.08$ and $3 \cdot 10^4 \leq Re \leq 2 \cdot 10^5$, for Schmidt is $0.012 \leq D_i/D_{hel} \leq 0.2$ and $2 \cdot 10^4 \leq Re \leq 1.5 \cdot 10^5$ and for Seban is $0.096 \leq D_i/D_{hel} \leq 0.058$ and $6 \cdot 10^3 \leq Re \leq 6.5 \cdot 10^4$ (MACHADO, 1996).

$$Re_{crit} = 2100(1 + 12\sqrt{D_i/D_{hel}}) \tag{3.5}$$

$$Nu_{hel} = Nu_{circ} 0.965(1 + 1.37\sqrt{D_i/D_{hel}}) \tag{3.6}$$

$$Nu_{hel} = Nu_{circ} \left[1 + 3.6(1 - D_i/D_{hel})\sqrt{D_i/D_{hel}}\right] \tag{3.7}$$

$$Nu_{hel} = Nu_{circ}(1 - D_i/D_{hel})^{0.1} Re^{0.05} \tag{3.8}$$

To annular duct flow, the Reynolds number must be computed using the hydraulic

diameter (D_h) which is defined as the ratio of four times the area of the cross section and the perimeter. The critical Reynolds number flows in annular regions depends on the ratio between the inner tube outside diameter (D_{io}) and the outer tube inner diameter (D_{oi}) represented by r^*, as shown in FIG. 3.1. Rohsenow, Hartnett, Cho, et al. (1998) suggest, laminar flow in annular regions in the isolated outer surface, the Nusselt numbers presented in TAB. 3.1.

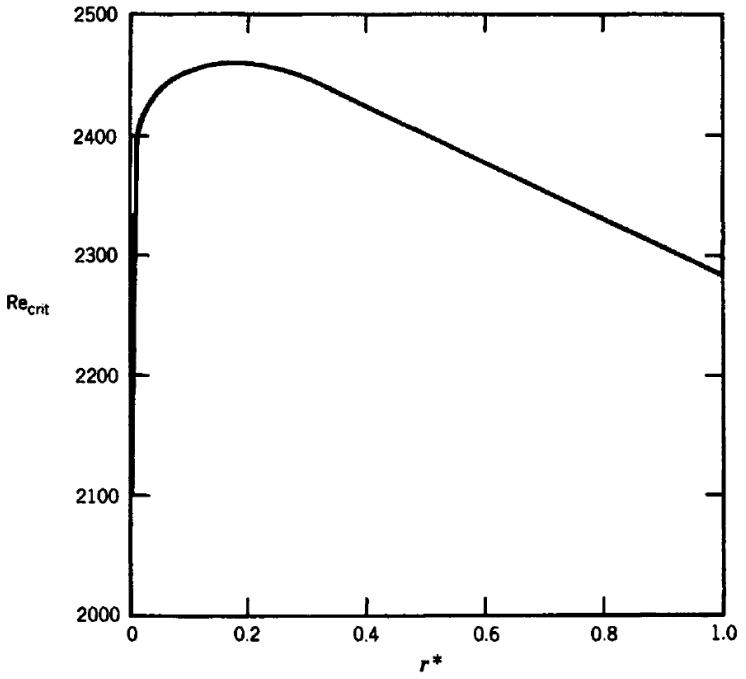

FIGURE 3.1: Critical Reynolds numbers for flow in concentric annular ducts.

SOURCE: Rohsenow, Hartnett, Cho, et al. (1998, p. 5-50)

TABLE 3.1
Nusselt number for fully developed laminar flow in annular regions.

	Uniform temperature		Uniform heat flux	
r^*	Nu_i	Nu_o	Nu_i	Nu_o
0.02	32.34	3.65	32.71	4.73
0.05	17.46	4.06	17.81	4.79
0.10	11.56	4.11	11.91	4.83
0.25	7.37	4.23	7.75	4.90
0.50	5.74	4.43	6.18	5.03

SOURCE: Rohsenow, Hartnett, Cho, et al. (1998, p. 5-38 to 5-59)

For turbulent flow in annular regions Machado (1996) suggest the Royzen correlation (EQ. 3.9), in order to obtain greater precision when using the correlations from circular duct.

$$Nu = 0.023Re^{0.8}Pr^{0.4}B_1\left(1 - \frac{0.45}{2.4 + Pr}\right)(r^*)^{B_2} \tag{3.9}$$

$$B_1 = \begin{cases} 1 & for: r^* > 0.2 \\ 1 + 7.5[(r^* - 5)Re^{-1}]^{0.6} & for: r^* \leq 0.2 \end{cases} \tag{3.10}$$

$$B_2 = 0.16Pr^{-0.15} \tag{3.11}$$

To calculate the friction factor (f) present in the Gnielinski's correlation, the correlation proposed by Churchill (1977) shown in EQ. 3.12 is the most used correlation for turbulent and laminar flow.

$$f = 2\left[\left(\frac{8}{Re}\right)^{12} + \frac{1}{B_1^{3/2}}\right]^{1/12} \tag{3.12}$$

$$B_1 = \left\{2.2088 + 2.457\ln\left[\frac{r}{D} + \frac{42.683}{Re^{0.9}}\right]\right\}^{16} + \left(\frac{37530}{Re}\right)^{16} \tag{3.13}$$

where r is the rugosity.

For flow into concentric annular regions, Rohsenow, Hartnett, Cho, et al. (1998) suggest the equation Natarajan and Lakshmanan (EQ. 3.14) for the laminar regime and for turbulent flow suggest the use of the same equations to circular ducts with the equivalent diameter described in EQ. 3.15.

$$f = \frac{24}{Re}(r^*)^{0.035} \tag{3.14}$$

$$D = (D_{oi} - D_{io})\frac{1 + (r^*)^2 + [1 - (r^*)^2]/ln(r^*)}{(1 - r^*)^2} \tag{3.15}$$

In this equation, D_{oi} is the outer tube inside diameter, and D_{io} is the inner tube outside diameter.

3.2 Internal two phase flow in Ducts

3.2.1 Void fraction

A generalized expression for six different classic correlations for void fraction (α) is shown in EQ. 3.16 and the constants for each correlation B_1 to B_4 are listed on TAB. 3.2 (ASHRAE, 2013).

$$\alpha = \left[1 + B_1 \left(\frac{1-x}{x}\right)^{B_2} \left(\frac{\rho_V}{\rho_L}\right)^{B_3} \left(\frac{\mu_L}{\mu_V}\right)^{B_4}\right]^{-1} \tag{3.16}$$

In this equation, x is vapor quality, ρ is density and subscripts L and V refer to liquid and vapor proprieties.

TABLE 3.2
Constants of generalized expression for void fraction correlations

Correlation	B_1	B_2	B_3	B_4
Homogeneous model	1.00	1.00	1.00	0.00
Lockhart and Martinelli (1949)	0.28	0.64	0.36	0.07
Baroczy (1963)	1.00	0.74	0.65	0.13
Thom (1964)	1.00	1.00	0.89	0.18
Zivi (1964)	1.00	1.00	0.67	0.00
Turner and Wallis (1965)	1.00	0.72	0.40	0.08

SOURCE: ASHRAE (2013, p. 5-11)

A comparison of 68 void fraction correlations was made by Woldesemayat and Ghajar (2007) using 2845 experimental data points from 8 different sources, different orientations and they indicate Toshiba and Rouhani–Axelsson as the best correlations. Another comparative study was presented by Godbole, Tang, and Ghajar (2011), considering 52 correlations and 1208 experimental data points from 10 sources. This study pointed out the Correlation of Rouhani–Axelsson as the best for higher accuracy. Rouhani and Axelsson (1970) correlation is given by:

$$\alpha = \frac{x}{\rho_V}\left\{[1 + 0.12\,(1-x)]\left(\frac{x}{\rho_V} + \frac{1-x}{\rho_L}\right) + \frac{1.18\,(1-x)\left[g\sigma'\left(\rho_L - \rho_V\right)\right]^{1/4}}{G\rho_L^{1/2}}\right\}^{-1} \tag{3.17}$$

where G is mass flux, g is gravitational acceleration and σ' is Surface tension.

Although the comparative studies presented by Woldesemayat and Ghajar (2007) and Godbole, Tang, and Ghajar (2011) were based on extensive databases, no refrigerants database are used. A comparison using refrigerants considering three different correlations is made by Machado, Haberschill, and Lallemand (1998), and considering eight correlations by Humia (2017). Both studies indicate Hughmark (1962) as the best correlation for void fraction. Indeed, Hughmark (1962) is also one of best five correlations listed by Woldesemayat and Ghajar (2007). Hughmark (1962) is calculated by the expression EQ. 3.18 and the values of B_1 is shown in TAB. 3.3 in function of B_2 calculated by EQ. 3.19, iteratively.

$$\alpha = B_1 \alpha_{hom} \tag{3.18}$$

$$B_2 = \left[\frac{D_i G}{\mu_L + \alpha(\mu_V - \mu_L)}\right]^{1/6} \left\{\frac{1}{gD_i}\left[\frac{Gx}{\rho_V \alpha_{hom}(1-\alpha_{hom})}\right]^2\right\}^{1/8} \tag{3.19}$$

TABLE 3.3
Parameters of Hughmark's correlation

B_2	B_1	B_2	B_1
1.3	0.185	8.0	0.767
1.5	0.228	10	0.780
2.0	0.325	15	0.808
3.0	0.490	20	0.830
4.0	0.605	40	0.880
5.0	0.675	70	0.930
6.0	0.720	130	0.980

SOURCE: Machado (1996, p. 36)

3.2.2 Heat transfer during boiling

Although there are correlations for boiling in solar evaporator, for example the correlation of Chaturvedi, Chiang, and Roberts (1982), these correlations were not tested with most of the refrigerants considered in this work and they will not be used in the model. Because of that, different correlations were tested for the evaporator model.

A correlation for boiling HTC was developed by Fang, Wu, and Yuan (2017) for various refrigerants and different flow directions. Fang, Wu, and Yuan (2017) used 17778 data point from 101 sources and 13 different fluids. After the fitting process, a second data base with 6664 others data points from 60 sources and 18 different fluids was used to evaluate the

correlation. The authors compared its new correlation with another 45 correlations available in the literature. The MAD of this new correlation, considering only the second data base, is 4.6%, the second best correlation was Fang, Zhou, and Hao Wang (2015) with MAD of 26%. The correlation proposed by Fang, Wu, and Yuan (2017) is given by:

$$h = \left(\frac{B_1 B_2 Fr_L^{0.48} Bo^{0.98} Bd^{0.72}}{M^{0.18}} \right) \left(\frac{\rho_L}{\rho_V} \right)^{0.29} \left[\ln \left(\frac{\mu_L}{\mu_{L,s}} \right) \right]^{-1} \frac{k_L}{D_i} \tag{3.20}$$

$$B_1 = \begin{cases} 1 & p \leq 0.43 \\ 1.38 - p^{1.15} & p > 0.43 \end{cases} \tag{3.21}$$

where M is the molecular weight, p is the reduced pressure, k is thermal conductivity, Bd is the bond number shown on EQ. 3.23, Bo is the boiling number shown on EQ. 3.22, and B_2 is a parameter listed in TAB. 3.4.

$$Bo = \frac{q}{G i_{lv}} \tag{3.22}$$

$$Bd = \frac{g \left(\rho_L - \rho_V \right) D_i^2}{\hat{\sigma}} \tag{3.23}$$

TABLE 3.4
Fluid-dependent parameter of Fang's correlation

Refrigerant	B_2	Refrigerant	B_2
R134a	1845	CO_2	2260
R22	1850	NH_3	1745
R245fa	1890	N_2	1715
R1234yf	1690	Water	2035
R236fa	1770	R29	1825
R410A	1790	R32	1435
R407C	2065	Other fluids	1850

SOURCE: Fang, Wu, and Yuan (2017, p. 976)

Shah (2017) presented an update on its previous correlation of 1982 and compared the results with another seven correlations, using 4852 experimental data points from 81 sources and 30 different fluids for a larger range of mass velocity than the one used by Fang, Wu, and Yuan (2017). Boiling heat transfer coefficient given by Shah's correlation is the largest value given by the EQ. 3.24.

$$h = \text{MAX} \begin{cases} 1.8 B_1^{-0.8} B_3 h_L \\ 230 Bo^{0.5} B_3 h_L \\ B_2 Bo^{0.5} \exp(2.74 B_1^{-0.1}) B_3 h_L \\ B_2 Bo^{0.5} \exp(2.74 B_1^{-0.15}) B_3 h_L \end{cases} \tag{3.24}$$

$$B_1 = \begin{cases} Co \quad \text{if horizontal with } Fr_L \geq 0.04 \text{ or vertical} \\ 0.38 Co Fr_L^{-0.3} \quad \text{if horizontal with } Fr_L < 0.04 \end{cases} \tag{3.25}$$

$$B_2 = \begin{cases} 14.7 \quad Bo \geq 0.0011 \\ 15.4 \quad Bo < 0.0011 \end{cases} \tag{3.26}$$

$$B_3 = \begin{cases} 2.1 - 0.008 We_V - 110 Bo \quad B_3 \geq 1 \\ 1 \quad B_3 < 1 \quad \text{or} \quad Fr_L < 0.01 \end{cases} \tag{3.27}$$

In these equations, h_L is the liquid heat transfer coefficient calculated by Dittus-Boelter equation (EQ. 3.28), the Froud number is calculated by EQ. 3.29, the convection number by EQ. 3.30, and the Weber number by 3.31.

$$Nu = \frac{h D_i}{k} = 0.023 Re^{0.8} Pr^{0.4} \tag{3.28}$$

$$Fr_L = \frac{G^2}{\rho_L^2 g D_i} \tag{3.29}$$

$$Co = \left(\frac{1-x}{x} \right)^{0.8} \left(\frac{\rho_V}{\rho_L} \right)^{0.5} \tag{3.30}$$

$$We_V = \frac{G^2 D_i}{\rho_V \sigma'} \tag{3.31}$$

Shah (2017) compared the experimental results with another seven correlations, the three best correlations were Shah (2017), Shah (1982) and Gungor and Winterton (1987) with MAD of 18.6%, 19.8% and 21.2%, respectively. A short comparison between the correlations presented in this section is shown in TAB. 3.5.

The correlation of Gungor and Winterton (1987) is one of best correlations in the comparison made by Shah (2017) and Fang, Wu, and Yuan (2017) and it is presented in EQ. 3.32.

TABLE 3.5
Summary of experimental validation of boiling HTC listed

	Fang, Wu, and Yuan (2017)	Shah (2017)
Data points	24442	4852
Data sources	161	81
Fluids	18	30
Reduced Pressure	0.0045-0.93	0.0046-0.787
Mass flux (kg/m^{2}s)	10-1782	15-2437
Diameter (mm)	0.207-32	0.38-27.1
MAD (%)	4.6	18.6

$$h = \left[1 + 3000Bo^{0.86} + 1.12\left(\frac{x}{1-x}\right)^{0.75}\left(\frac{\rho_L}{\rho_V}\right)^{0.41}\right] h_L B_1 \tag{3.32}$$

$$B_1 = \begin{cases} Fr_L^{(0.1-2Fr_L)} & \text{if horizontal and } Fr_L < 0.05 \\ 1 \quad \text{if horizontal with } Fr_L \geq 0.05 \text{ or vertical} \end{cases} \tag{3.33}$$

3.2.3 Heat transfer during condensation

Shah (2016) proposed the following equations for the flows regimes I, II and III:

$$h_I = h_L\left(1 + \frac{3.8}{B_1^{0.95}}\right)\left(\frac{\mu_L}{14\mu_V}\right)^{0.0058+0.557p} \tag{3.34}$$

$$h_{II} = h_I + h_{III} \tag{3.35}$$

$$h_{III} = 1.32Re_L^{-1/3}\left[\frac{\rho_L(\rho_L - \rho_V)gk_L^3}{\mu_L^2}\right]^{(1/3)} \tag{3.36}$$

$$B_1 = p^{0.4}\left(\frac{1}{x-1}\right)^{0.8} \tag{3.37}$$

where h_L is the is the liquid heat transfer coefficient calculated by Dittus-Boelter equation (EQ. 3.28) and Re_L is calculated by:

$$Re_L = \frac{G(1-x)D_i}{\mu_L} \tag{3.38}$$

The ranges that occurs the regime I and III are presented in TAB. 3.6. If the Regime

is neither I nor III by the criteria bellow, it is Regime II. The Weber number (We) and dimensionless vapor velocity (v) are calculated by EQ. 3.31 and 3.39, respectively.

TABLE 3.6
Flows regime of the correlation of Shah (2016)

	Horizontal Flow	Vertical Flow
Regime I	$We_V > 100$ and $v \geq 0.98(B_1 + 0.263)^{-0.62}$	$We_V > 100$ and $v \geq (0.73 + 2.4B_1)^{-1}$
Regime III	$We_V > 20$ and $v \leq 0.95(1.254 + 2.27B_1^{1.249})^{-1}$	$We_V > 20$ and $v \leq 0.89 - 0.93\exp(-0.087B_1^{-1.17})$

$$v = \frac{xG}{(gD\rho_V(\rho_L - \rho_V))^{0.5}} \tag{3.39}$$

For inclined channel with inclinations from 90^o upflow to 30^o downflow, Shah (2016) suggested the use of the correlation for horizontal channel. For inclinations (θ) from 30^o to 90^o downflow, the author proposed the following equation.

$$h = h_0 + (h_0 - h_{90})(30 - \theta)/60 \tag{3.40}$$

This correlation was compared with 4063 experimental data points from 67 different sources, and the MAD of this correlation is 17%. In these experimental data the range of diameter available is from 0.10 to 49 mm, the reduce pressure from 0.0008 to 0.946 and the mass velocity from 1.1 to 1400 kg/(m^{2}s).

3.3 Heat transfer coefficient in flat plates

The solar evaporator/collector changes heat with the environment by radiation, natural convection or/and forced convection. The forced convection occurs in the presence of wind. Combined free and forced (or mixed) convection regime in vertical plates occurs if $0.1 < Gr/Re^2 < 10$. The following sections present a brief review of the correlations for determining the coefficient convective flow in each configuration.

3.3.1 Natural convection

To determine the Nusselt number, and therefore heat exchange coefficient by natural convection in vertical flat plates, the Churchill and Chu (1975b) correlation is suggested by some authors (ASHRAE, 2013; INCROPERA et al., 2007; ÇENGEL; GHAJAR, 2015; NEILS; KLEIN, 2009; KARWA, 2017) and it is given by EQ. 3.41 and 3.42 for isothermal plat and by EQ. 3.43 for constant heat flux.

$$Nu = 0.68 + \frac{0.67Ra^{1/4}}{\left(1 + (0.492/Pr)^{9/16}\right)^{4/9}} \qquad 0.1 < Ra < 10^9 \tag{3.41}$$

$$Nu = \left[0.825 + \frac{0.387Ra^{1/6}}{\left(1 + (0.492/Pr)^{9/16}\right)^{8/27}}\right]^2 \qquad 10^9 < Ra < 10^{12} \tag{3.42}$$

$$Nu = \left[0.825 + \frac{0.387Ra^{1/6}}{\left(1 + (0.437/Pr)^{9/16}\right)^{8/27}}\right]^2 \qquad 0.1 < Ra < 10^{12} \tag{3.43}$$

In these equations, Ra is the Rayleigh number and it is determined by:

$$Ra = PrGr \tag{3.44}$$

$$Gr = \frac{g\beta\rho^2 \left|\Delta T\right| L_{ch}^3}{\mu^2} \tag{3.45}$$

where β is the coefficient of thermal expansion, ΔT is the temperature difference between the surface (T_s) and the quiescent fluid (T_∞) and L_{ch} is the characteristic length. All proprieties are evaluated at film temperature (Eq. 3.46), except β which is evaluated at T_∞ (ASHRAE, 2013).

$$T = \frac{T_s + T_\infty}{2} \tag{3.46}$$

For the horizontal flat plate, some authors pointed the correlation of Lloyd and Moran (1974), shown on EQ. 3.47 to 3.50, for downward-facing cooled plate and upward-facing heated plate (ASHRAE, 2013; INCROPERA et al., 2007; ÇENGEL; GHAJAR, 2015; NEILS; KLEIN, 2009; KARWA, 2017), and EQ. 3.51 for downward-facing heated plate and

upward-facing cooled plate (ASHRAE, 2013; ÇENGEL; GHAJAR, 2015; NEILS; KLEIN, 2009). For this flow configuration, the characteristic length is defined as the ratio between area and perimeter.

$$Nu = 0.96Ra^{1/6} \qquad 1 < Ra < 200 \tag{3.47}$$

$$Nu = 0.59Ra^{1/4} \qquad 200 < Ra < 10^4 \tag{3.48}$$

$$Nu = 0.54Ra^{1/4} \qquad 2.2 \cdot 10^4 < Ra < 8 \cdot 10^6 \tag{3.49}$$

$$Nu = 0.54Ra^{1/3} \qquad 8 \cdot 10^6 < Ra < 1.5 \cdot 10^9 \tag{3.50}$$

$$Nu = 0.27Ra^{1/4} \qquad 10^5 < Ra < 10^{10} \tag{3.51}$$

To inclined plates, top-cold and bottom-hot, Incropera et al. (2007) propose evaluate the convective coefficient for vertical plate, replacing the value of the gravity by the expression $g \cdot \sin(\theta)$ in the Rayleigh number. Subsequently, must repeat the process using the expression $g \cdot \cos(\theta)$ in the correlations for horizontal plate and adopting the highest value.

3.3.2 Forced convection

To calculated the average Nusselt number, some authors (ASHRAE, 2013; ROHSENOW; HARTNETT; CHO, et al., 1998; INCROPERA et al., 2007; ÇENGEL; GHAJAR, 2015; NEILS; KLEIN, 2009; KARWA, 2017) presented the EQ. 3.52 for turbulent regime and 3.53 for laminar regime. This equations can be used only if the Prandtl number is greater or equal to 0.6.

$$Nu = \left(0.037Re_z^{4/5} - 871\right) Pr^{1/3} \quad Re_z > 5 \cdot 10^5 \tag{3.52}$$

$$Nu = 0.664Re_z^{1/2}Pr^{1/3} \qquad Re_z \leq 5 \cdot 10^5 \tag{3.53}$$

$$Re = \frac{\rho V_\infty z}{\mu} \tag{3.54}$$

An empirical correlation was created by Test, Lessmann, and Johary (1981) considering the results from outdoor experiment in a tilted heated flat plate with 1 m^2, mean wind speed between 1.5 m/s and 5.6 m/s, and inclination of 40^o and 50^o, with respect to wind direc-

tion. The correlation proposed by them is given by:

$$h = 8.55 \pm 0.86 + (2.56 \pm 0.32)V_{wd} \tag{3.55}$$

3.3.3 Combined forced and natural convection

One of the first correlations in the literature was described by McAdams (1954) using experimental results obtained with a vertical heated copper plate, with an area of 0.5 m^2 mounted in a wind tunnel for wind velocity (V_{wd}) lower than 5 m/s. This correlation was used in a model of a R22 DX-SAHP with an tilted aluminum collector with 4.2 m^2 (KONG; ZHANG, D., et al., 2011). The correlation of McAdams is given by:

$$h = 5.7 + 3.8V_{wd} \tag{3.56}$$

Another correlation adjusted using data from experiments in wind tunnel was proposed by Watmuff, WWS Charters, and Proctor (1977), for wind speed between 0 and 7 m/s, is showed in EQ. 3.57. This correlation was also used in a mathematical model of R22 DX-SAHP with 2 m^2 aluminum vertical collector (KUANG, Y. H.; SUMATHY; WANG, R. Z., 2003).

$$h = 2.8 + 3V_{wd} \tag{3.57}$$

Sharples and Charlesworth (1998) adjusted an empirical correlation using 915 experimental data points obtained from a 1.81 m x 0.89 m flat plate mounted in a 35^o pitched roof of a domestic house. In these experiments, the wind velocity changed from 0.3 to 7.2 m/s. They proposed different equations for eight wind incidence angles, if the wind direction is parallel to lower side, the heat transfer coefficient is given by EQ. 3.58, and parallel to the larger size is given by EQ. 3.59.

$$h = 8.3 + 2.2V_{wd} \tag{3.58}$$

$$h = 6.5 + 3.3V_{wd} \tag{3.59}$$

Kumar and Mullick (2010) developed an empirical correlation using a 0.8 m^2 flat horizontal solar collector in outdoor conditions. In the experimental test, the solar radiation was around 960 W/m^2 and wind speed was in the range of 0 and 1.1 m/s. The correlation proposed by them is given by:

$$h = 6.90 \pm 0.05 + (3.87 \pm 0.13)V_{wd} \tag{3.60}$$

3.3.4 Dehumidification

When the evaporator operates without solar radiation, it is possible that the surface temperature reaches values below the dew temperature and the water vapor presented in the air condenses on the evaporator. Some experimental studies (LI, C.; LI, J., 2011; DANILO; DOMINIQUE; FRÉDÉRIC, 2016) indicate that for moist air, condensation occurs by two processes: dropwise condensation (DWC) and filmwise condensation (FWC). The heat transfer coefficient of DWC is superior to that of FWC. Figure 3.2 shows the variation in a surface temperature during different relative humidity step and the time zones where occur only convection, DWC and FWC observed experimentally.

Jian Huang, Junxia Zhang, and Li Wang (2015) enumerated 22 experimental and theoretical studies of condensation heat and mass transfer in the presence of non-condensable gas. These studies were performed considering the presence of 0.02 to 80% of non-condensable gas, but the interest range of this work is 96-100% of non-condensable gas.

A theoretical and experimental study of heat transfer mechanism in the evaporator or solar collector of a DX-SAHP was performed by Scarpa and Tagliafico (2016). The heat transfer due condensation is given by:

$$Q_{cond} = h_{cond} A_{col} (P_V - P_{sat}) i_{lv} \tag{3.61}$$

$$h_{cond} = \frac{h_{air} P_{atm}}{R_w (C\rho T)_{air} (P_V - P_{sat})} \ln\left(\frac{P_{atm} - P_{sat}}{P_{atm} - P_V}\right) \tag{3.62}$$

$$h_{air} = 4 + 4V_{wd} \tag{3.63}$$

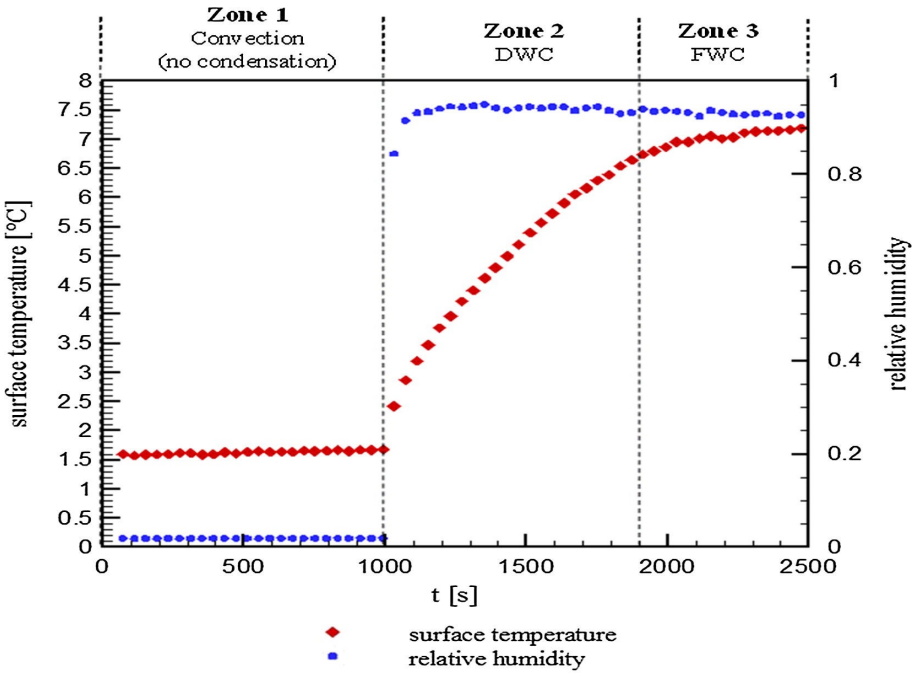

FIGURE 3.2: Temperature response of relative humidity steps

SOURCE: Sakay *et al* (DANILO; DOMINIQUE; FRÉDÉRIC, 2016), p. 851.

where R_w is water vapor gas constant 461.5 J/kgK (SONNTAG et al., 2003), C is the specific heat at constant pressure, P_V is the partial pressure of water vapor, A_{col} is the collector area, h_{air} is the convective coefficient given by EQ. 3.63 (ISO, 2007), and P_{sat} is the water saturation pressure at film surface temperature, which is calculated by the following empirical equation:

$$T_{flm,s} = T_{col,s} - 5.491 \cdot 10^{-2}(T_{air} - T_{col,s})\ln\left(\frac{P_{air}}{P_{atm}}\right) \tag{3.64}$$

where P_{air} is the partial pressure of dry air. These authors presented experimental results obtained with three tests with ambient temperatures 5.3, 16.5, and 33.2^{o}C, and wind speed 4; 7.75 and 3 m/s. The difference between experimental and theoretical results was 20%.

3.4 Natural convection in horizontal cylinders

The heat transfer between the immersed condenser tube and the water of a DX-SAHP occurs by natural convection. Many authors (ROHSENOW; HARTNETT; CHO, et al., 1998; NEILS; KLEIN, 2009; ÇENGEL; GHAJAR, 2015; INCROPERA et al., 2007; ASHRAE, 2013; KARWA, 2017) suggest the correlation of Churchill and Chu (1975a) for natural convec-

tion in a horizontal cylinder, if $10^9 < Ra < 10^{13}$. This correlation is given by:

$$Nu = \left\{ 0.6 + \frac{0.387 Ra^{1/6}}{[1 + (0.559/Pr)^{9/16}]^{8/27}} \right\}^2 \tag{3.65}$$

3.5 Optimum pressure for R744 heat pump

In the simulations using R744 the DX-SAHP, the model is running with transcritical cycle due the low critical point of R744 (31^{o}C). In many studies about heat pump using R744 available in the literature, the authors demonstrated that there is a high pressure that maximize the COP. Some correlations have been developed to predict this optimum pressure. In the few studies of SAHP using R744 (ISLAM et al., 2012; FARIA et al., 2016; OLIVEIRA et al., 2016) the optimum pressure was not investigated, thus the correlation for R744 ASHP was used in this work.

The correlations of Liao, Zhao, and Jakobsen (2000), Sarkar, Bhattacharyya, and Gopal (2006), Aprea and Maiorino (2009), Sung Chul Kim, Won, and Min Soo Kim (2009), Shouguo Wang et al. (2013), and Yang et al. (2015) were selected and are presented in EQ. 3.66 to 3.71, respectively. Each correlation was tested in the range listed in TAB. 3.7.

TABLE 3.7
Domain of the correlation for optimum pressure

EQ.	T_a (^{o}C)	T_{gco} (^{o}C)	T_{ev} (^{o}C)	T_{wi} (^{o}C)	T_{wo} (^{o}C)	P_{opt} (bar)
3.66	-	30 to 60	-10 to 20	-	-	71 to 120
3.67	-	-	-	20 to 40	-	-
3.68	-	30 to 60	-10 to 20	-	-	71 to 120
3.69	25 to 45	-	-	-	-	75 to 135
3.70	-15 to 35	-	-	-	55 to 80	-
3.71	-	30 to 60	-10 to 20	-	55 to 80	-

$$P_{opt} = (2.788 - 0.0157 T_{ev}) T_c + 0.381 T_{ev} - 9.34 \tag{3.66}$$

$$P_{opt} = 85.45 + 0.77 T_{wi} \tag{3.67}$$

$$P_{opt} = (2.788 - 0.0157 T_{ev}) T_c + 0.381 T_{ev} - 9.34 - 0.003 T_c + 0.174 \tag{3.68}$$

$$P_{opt} = 1.938T_c + 9.872 \tag{3.69}$$

$$P_{opt} = 10.97995 + 1.06442T_{wo} + 1.01404T_a - 0.012 \tag{3.70}$$

$$P_{opt} = 2.918T_{gco} + 0.471T_e - 0.018T_eT_{gco} - 13.955 \tag{3.71}$$

In these equations, T_a, T_{gco}, T_{ev}, T_{wi}, T_{wo} are the ambient, gas cooler outlet, evaporating, water inlet and water outlet temperatures, and P is the pressure.

4. EXPERIMENTAL SETUP USED IN THE MODEL VALIDATION

The R134a DX-SAHP installed at the laboratory of the Cooling and Heating Group (GREA) in UFMG is shown in FIG. 4.1, and it was used to validate the mathematical model, to be presented in the next section.

FIGURE 4.1: Photo of the R134a DX-SAHP installed at GREA of UFMG.

SOURCE: Diniz (2017, p. 72)

This heat pump has an inclined solar evaporator and a finned coil evaporator below the static evaporator. Indeed, this equipment was designed by Reis (2012) to operate as a parallel type IX-SAHP (FIG. 2.1) to produce domestic hot water for a single family house. The COP and the season performance of the system were investigated by Reis (2012). In the results presented by Reis (2012), the COP of system using the static evaporator was 9.7% bigger than using the finned coil evaporator.

Lately, Diniz (2017) made some modifications in this heat pump to operate as DX-SAHP, with two types of condensers and the static evaporator was used as a solar evaporator. Diniz (2017) reported the same COP using a coaxial condenser and an immersed condenser either in the ASHP mode or in the SAHP mode. In this work, the model validation was performed using the geometrical parameter described by Reis (2012) and Diniz (2017) and experimental results presented by Diniz (2017). In the following section, it is described the main components of this DX-SAHP.

4.1 Description of the components

The plate of solar evaporator has length of 1.6 m, width of 1.03 m, thickness of 1 mm and is made of aluminum. The emissivity of the collector is 0.95, and it was obtained using a thermographic camera. The copper evaporator tube shown in FIG. 4.2 has length of 17.28 m and inner and outer diameters of 8.73 and 9.53 mm, respectively. The inclination of the evaporator is 30^o, and it was determined to maximize the incidence of solar radiation in Belo Horizonte. The details of the design of the solar evaporator were presented by Reis (2012).

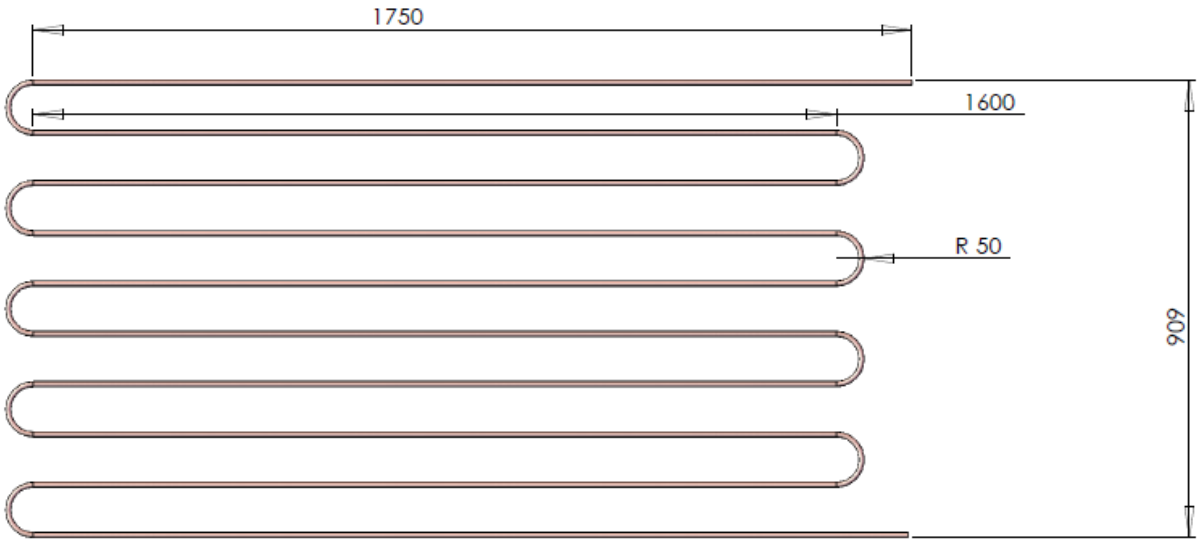

FIGURE 4.2: Evaporator tube of the R134a DX-SAHP.
SOURCE: Reis (2012, p. 64)

The finned coil evaporator of the heat pump is a commercial component manufactured by Elgin model CDE2777. The evaporator tube has 6.6 m and the same diameter of the solar evaporator. The power of the fan is 0.016 hp and the diameter of the blades is 260 mm. In the experiments made by Diniz (2017), the finned coil evaporator was not used and will not be represented in the following diagrams.

The immersed condenser is basically a 4.5 m horizontal copper tube, without fin, folded into tank bottom, as shown FIG. 4.3. The diameters of the tube in this condenser are the same of the solar evaporator. The tank volume is 200 liters and the thickness of the thermal insulation is 40 mm. The details of the design of this condenser were presented by Reis (2012).

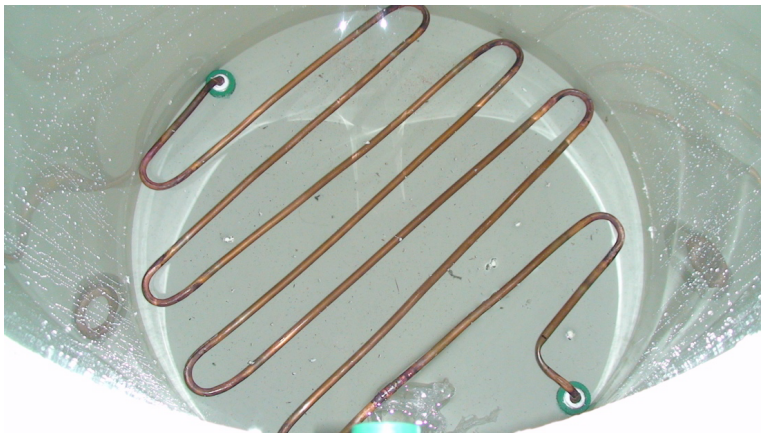

FIGURE 4.3: Immersed condenser of the R134a DX-SAHP.
SOURCE: Rodriguez (2015, p. 65)

The coaxial condenser is a counterflow heat exchanger where the water flows in a annular region, and R134a flows in the inner tube. Both tubes are made of copper and the diameters and thickness of the walls are shown in FIG. 4.4. The thickness of the thermal insulation is 9 mm. This condenser has length of 5.5 m and it is mounted in helical format with mean diameter of 0.65 m. The design of the condenser was describe by Diniz (2017).

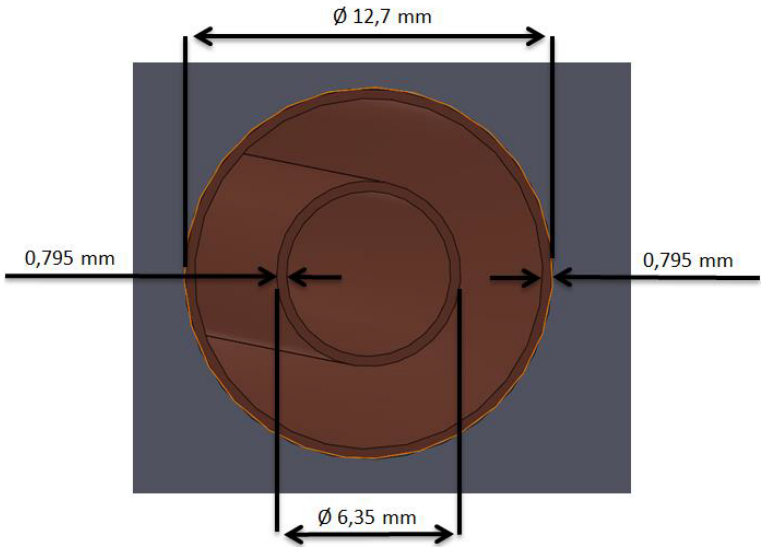

FIGURE 4.4: Geometry of the coaxial condenser
SOURCE: Diniz (2017, p. 111)

The DX-SAHP has a hermetic compressor model FFU100HAK, manufactured by

Embraco, with 7.95 cm^3 of displacement, and it is driven by two poles asynchronous electric motor powered in 127V and 60Hz. The performance map available in the website of Embraco has results of cooling capacity, power and current consumption and mass flow rate for condensing temperatures of 35, 45 and 55^{o}C and seven evaporating temperatures, from -5 to -35^{o}C with uncertainty of 5%. The Thermostatic Expansion Valve (TEV) was manufactured by Danfoss, model TEN2-NR0X, and it was used to control the superheat.

4.2 Instrumentation

The thermocouples are K-type, with 1,5 mm of diameter and standard uncertainty of 1^{o}C. They were installed at the inlet and outlet of each component of DX-SAHP to measure the temperature of R134a and water. These thermocouples were connected to NI9213 module, manufactured by National Instruments for reading thermocouples signal. Pressure gauge was installed in the positions 1 to 4, shown in FIG. 4.5. The uncertainty of the sensor 1 and 4 is 0.1 bar and of the sensor 2 and 3 is 0.35 kgf/cm^2 (DINIZ, 2017).

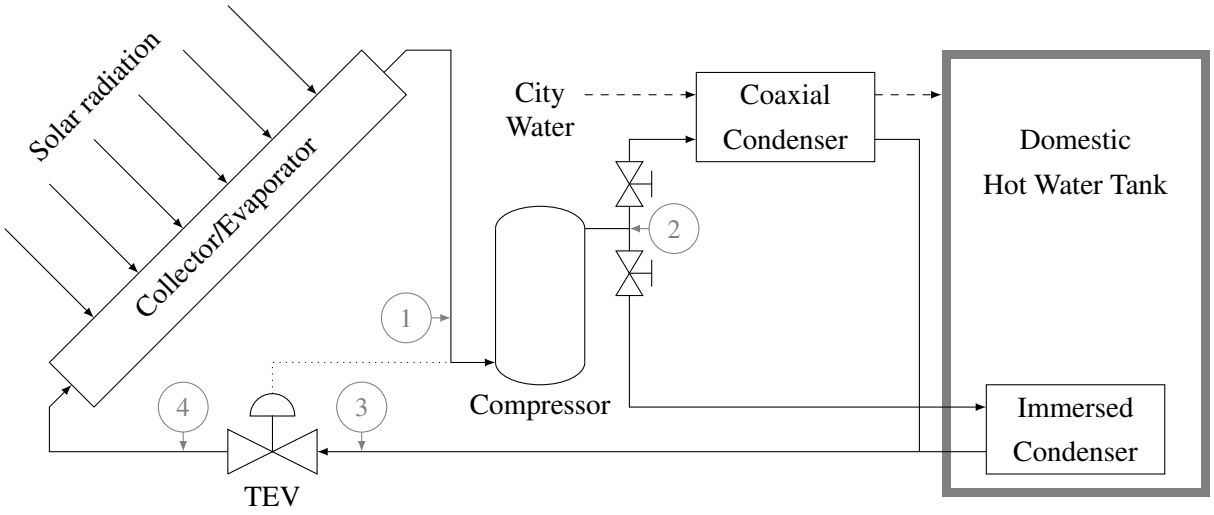

FIGURE 4.5: Scheme of R134a DX-SAHP used in the validation.

Two pyranometers have 5% of uncertainty and were used to measure the solar radiation perpendicular to the ground and perpendicular to the solar evaporator, as can be seen in FIG. 4.1. The pyranometers data were collected by USB-6211 board also manufactured by National Instruments. The consumption of the compressor was measured using a wattmeter with uncertainty of 1%. The wind velocity was measured by a digital vane anemometer, with range of 0 to 30 m/s and uncertainty of 3%. The direction of wind was checked using a windsock and the anemometer pointed into the direction of the wind. A digital psychrometer was

used to measure dew point temperature ($\pm 2^{o}$C) and ambient temperature ($\pm 1^{o}$C). To measure volumetric water flow of the coaxial condenser, in the range of 0.5 to 1 liter per minute, it was used 1 liter graduated container with resolution of 50 milliliters and a timer (DINIZ, 2017).

4.3 Experimental results

Diniz (2017) made 20 experimental tests using the DX-SAHP to heat 200 liters of water from ambient temperature to approximately 45^{o}C, considering indoor and outdoor environments. These tests were made to compare the system using both condensers. Diniz (2017) concluded that since the average COP is equal, regarding the uncertainties, the system with immersed condenser should be used due the lower cost of installation. Diniz (2017) also discusses that the subcooling remains approximately constant if the coaxial condenser is used and the subcooling increases in time, if immersed condenser is used as shown in FIG. 4.6 and 4.7. Although these two figures are in different scale, the water temperature in 4.7 increases linearly with time.

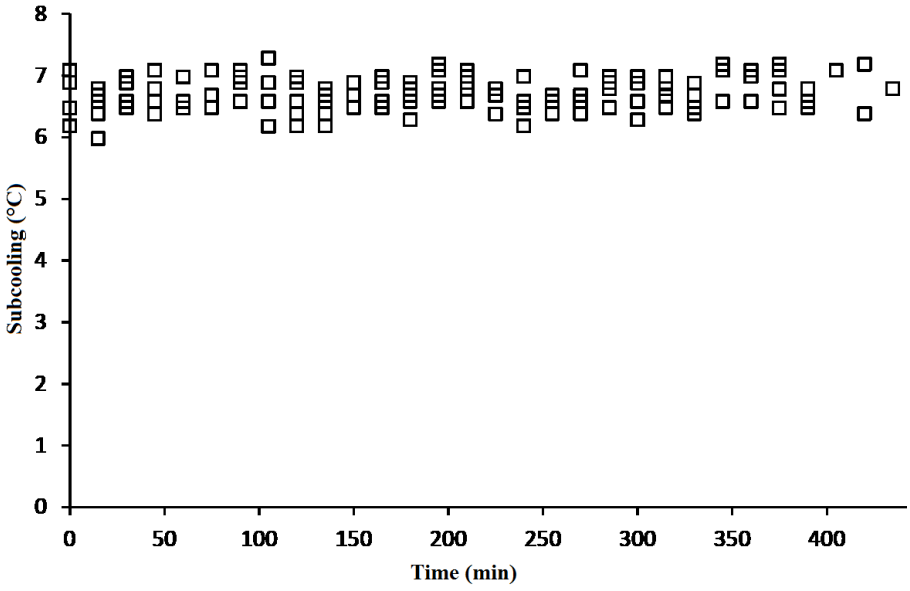

FIGURE 4.6: Subcooling of the DX-SAHP running with coaxial condenser
SOURCE: Diniz (2017, p. 126)

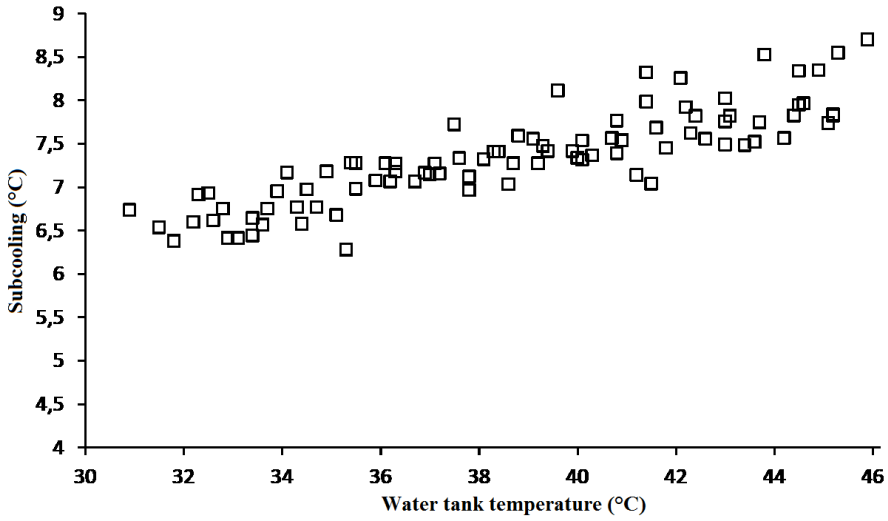

FIGURE 4.7: Subcooling of the DX-SAHP running with immersed condenser
SOURCE: Diniz (2017, p. 135)

For each test Diniz (2017) reported the measurements on a frequency of four samples per hour. The mean values of the environmental variable, the final water temperature, the time of operation, and the COP for each test is listed in TAB. 4.1 and TAB. 4.2 for the immersed condenser and for the coaxial condenser, respectively.

TABLE 4.1
Experimental results obtained using the immersed condenser

Test #	Date dd/mm/yyyy	$\overline{T}_a$ ^{o}C	$\overline{\phi}$ %	$\overline{I}$ W/m^2	$\overline{V}_{wd}$ m/s	T_{wi} ^{o}C	T_{wf} ^{o}C	Time h	$\overline{COP}$
1	07/01/2017	28.2	48	0	0	32.8	44.9	3.75	2.31± 0.12
2	14/01/2017	26.1	74	0	0	32.6	45.3	4.0	2.27± 0.11
3	18/01/2017	26.0	59	0	0	31.5	45.2	4.5	2.29± 0.11
4	20/01/2017	26.6	47	0	0	30.9	45.9	5.0	2.30± 0.11
5	24/01/2017	27.3	56	0	0	32.2	45.2	4.25	2.27± 0.11
6	04/02/2017	29.8	51	482	0.72	29.6	44.8	3.0	2.88± 0.14
7	11/02/2017	26.4	58	346	0.86	28.1	45.3	4.25	2.58± 0.12
8	16/02/2017	33.2	30	520	0.99	29.8	46.1	3.75	2.64± 0.13
9	17/02/2017	32.6	32	671	1.53	29.3	44.8	3.0	2.80± 0.14
10	18/02/2017	31.6	39	807	1.25	29.4	45.5	3.0	2.91± 0.15

SOURCE: Adapted from Diniz (2017, p. 130, 131, 139 and 198 to 208)

TABLE 4.2
Experimental results obtained using the coaxial condenser

Test #	Date dd/mm/yyyy	$\overline{T}_a$ ^{o}C	$\overline{\phi}$ %	$\overline{I}$ W/m^2	$\overline{V}_{wd}$ m/s	T_{wi} ^{o}C	T_{wo} ^{o}C	Time h	COP
11	12/01/2017	27.1	55	0	0	27.3	44.8	5.5	2.37± 0.12
12	13/01/2017	26.6	68	0	0	26.3	45.3	6.05	2.25± 0.12
13	16/01/2017	24.9	72	0	0	25.0	46.0	7.05	2.26± 0.11
14	17/01/2017	26.1	58	0	0	25.1	46.0	6.83	2.36± 0.12
15	19/01/2017	26.5	61	0	0	25.8	45.5	6.45	2.32± 0.12
16	23/01/2017	29.7	42	421	0.52	27.6	46.7	4.78	2.56± 0.13
17	25/01/2017	32.9	37	709	0.86	28.7	47.4	3.88	2.72± 0.14
18	25/01/2017	32.7	38	758	0.95	29.3	47.3	3.78	2.64± 0.14
19	27/01/2017	32.5	32	629	1.16	29.0	45.9	3.67	2.69± 0.14
20	28/01/2017	31.2	34	811	1.36	29.0	47.8	4.33	2.48± 0.13

SOURCE: Adapted from Diniz (2017, p. 130, 131, 139 and 198 to 208)

In this table, T_a, ϕ, I, V_{wd}, T_{wi}, T_{wo}, T_{wf} and Time represent the ambient temperature, relative humidity, solar radiation, wind speed, initial or inlet water temperature, final water temperature and time of operation, respectively.

5. METHODOLOGY

5.1 Pre selection of refrigerants

The refrigerants with low GWP selected for this work are the refrigerants R290, R600a, R744 and R1234yf. Although, there are other refrigerants with GWP lower than 150 listed in Tab. 2.2, some studies demonstrate that these refrigerants have teh worst environmental performance compared with the refrigerants R290, R600a, R744 and R1234yf.

The R290 was selected because of the best results of season performance, COP and TEWI than other refrigerants presented by Sarbu (2014), Makhnatch and Khodabandeh (2014a), Ghoubali et al. (2014), and Botticella and Viscito (2015). In addition, the R290 is used by many heat pump manufactures (PALM, 2008) and it can work at high evaporating temperature (CHAICHANA; AYE; CHARTERS, W. W., 2003). Despite of the flammability of the R290, the DX-SAHPWH of this work is a small equipment and it will be installed in an open ventilated location.

Selection of the refrigerant R600a is due to the small circuit of the refrigerant, equivalent to a domestic refrigerator (UNEP, 2015). Furthermore, the R600a presents a lower noise level, which is important for domestic products, and the compressor for this refrigerant has a good efficiency (PALM, 2008).

The selection of the R744 is based on the utilization of the SAHP, as presented by Islam et al. (2012), Oliveira et al. (2016) and Faria et al. (2016). In addition, the use of the R744 in a heat pump for heating water is highlighted in Ma, Liu, and Tian (2013) by the good match between the water temperature profile in applications with conventional heaters.

Finally, the choice of R1234yf is based on analyses presented in Makhnatch and Khodabandeh (2014a), Ghoubali et al. (2014), Botticella and Viscito (2015) for different points of operation of the system. In addition, the R1234yf is always an ecological alternative (SARBU, 2014). Also, the R1234yf has been used as a drop-in replacement of the R134a in different systems (LEE, Y.; JUNG, 2012; BELMAN-FLORES et al., 2017) and the COP values are quite similar, but the R134a COP is slightly better.

Despite of the studies pointing out R717 as a good refrigerant (CHAICHANA; AYE; CHARTERS, W. W., 2003), ammonia will be not included in this work due the high toxicity and lack of commercial components for the heating capacity discussed in this work.

5.2 Mathematical modelling

The first step to prepare the DX-SAHP model is define what are the input and output variables of the model. The list of input and output variables are shown in FIG 5.1 and 5.2. The main difference in these models are the subcooling and refrigerant charge. These two variables are connected, if the subcooling is known, the charge can be calculated and vice versa. The choice of the subcooling as the input of the model with coaxial condenser and output in the mode with the immersed condenser are based in the experimental observations made by Diniz (2017).

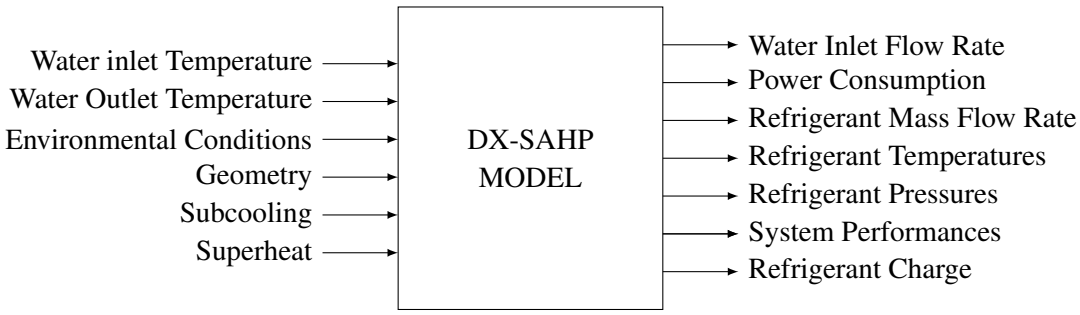

FIGURE 5.1: Input and output variables of DX-SAHP model operating with a coaxial condenser

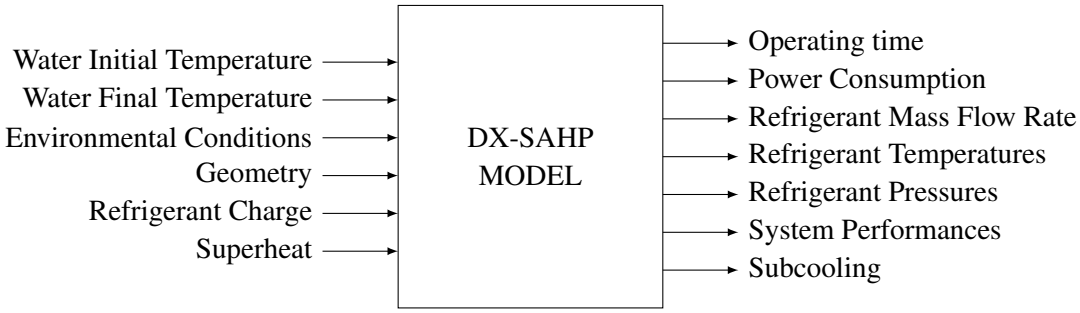

FIGURE 5.2: Input and output variables of DX-SAHP model operating with a immersed condenser

In these figures, the environment conditions are the ambient temperature, the wind speed, the solar radiation, the sky temperature, the relative humidity, the atmospheric pressure, and the gravitational acceleration. The system performances are the energetic, economical and environmental indicators. The indicator of energetic performance is the COP. The COP of DX-SAHP using a coaxial condenser is given by:

$$\text{COP} = \frac{\dot{\forall}_w \rho_w C_w (T_{wo} - T_{wi})}{\dot{W}_{cmp}} \tag{5.1}$$

where $\dot{\forall}_w$ is the water volumetric flow rate, ρ_w is the water density, C_w is the water heat capacity at constant pressure, T_{wo} water outlet temperature, T_{wi} water inlet/initial temperature, and $\dot{W}_{cmp}$ compressor electric power consumption. For of DX-SAHP equipped with an immersed condenser is given by:

$$\text{COP} = \frac{\forall_w \rho_w C_w (T_{wf} - T_{wi})}{W_{cmp}} \tag{5.2}$$

where $\forall_w$ is the water volume at the tank and W_{cmp} is the compressor energy consumption. The collector efficiency (η_{col}) proposed by (KONG; ZHANG, D., et al., 2011; KONG; LI, et al., 2017) and (KUANG, Y. H.; SUMATHY; WANG, R. Z., 2003) is defined as follow:

$$\eta_{col} = \frac{\dot{Q}_{ev}}{A_{ev} I} \tag{5.3}$$

In this work, the environmental performance is evaluated by the TEWI given by:

$$\text{TEWI} = \text{GWP}\lambda N' + \frac{E\Phi N'}{COP} \tag{5.4}$$

where GWP is the value of Global Warming Potential, λ is the annual refrigerant leakage rate, N' is the system lifetime, E is the annual energy heating demand and Φ is the emission factor to the producing electricity. Some authors (DAVIES; CARETTA, 2004; TSAMOS et al., 2017; XU, X.; HWANG; RADERMACHER, 2013) prefer to use the TEWI to analyze the environment impact of refrigerating system, because it is simpler to use it than LCCP (Life-cycle climate performance), and it take into account many other factors than GWP (MAKHNATCH; KHODABANDEH, 2014b).

The economical performance is evaluated by payback period (P') of the DX-SAHP over an electrical heater. Payback period is given by:

$$P' = \frac{I'}{s(1 + \text{IR})^{(P'-1)}} \tag{5.5}$$

where I' is the difference of initial investment between DX-SAHP and an electrical heater, IR

is the annual inflation rate and the annual savings (s) which is given by:

$$s = E\left(\frac{T'_{ele}}{\eta_{ele}} - \frac{T'_{hp}}{COP}\right) \tag{5.6}$$

where T'_{hp} is the electricity tariff during heat pump running hours, T'_{ele} is the electricity tariff during electrical heater utilization period, and η_{ele} is the efficiency of the electrical heater.

The difference of initial investment is divided in three parts: (i) the fixed cost, in a DX-SAHP comprises the cost with compressor, DHW tank, expansion valve and electrical components, in an instantaneous electrical heater is the all initial investment; (ii) the variable cost which comprises the collector cost, the piping of condenser cost, the refrigerant charge cost; and (iii) the service of installation and assembling cost, estimated as a percentage of materials costs.

The model of DX-SAHP is based on the following assumptions which are also made by many authors listed in TAB. 2.1:

- The heat pump system is at quasi-steady-state;
- The refrigerant kinetic and potential energies are negligible;
- Pressure drop at heat exchanges and in the tubes between components is negligible;
- Constant superheat;
- Water is an incompressible fluid.

The following sections describe the model of each component of the heat pump.

5.2.1 Solar evaporator/collector model

The solar evaporator model is developed to predict the thermal performance of the solar evaporator, based on the following assumptions:

- Thermal resistance of the wall evaporator tube due conduction is zero;
- Heat transfer at the edges of evaporator is negligible;
- Thermal resistance of bond tube/fin is zero;
- Thermal resistance of the walls tube due conduction is zero;

- Vapor quality varies linearly with length in the boiling region.

The energy balance in the refrigerant circulating inside the duct is given by:

$$Q_{ev} = \dot{m}_r(i_1 - i_4) \tag{5.7}$$

In this equation, $\dot{m}_r$ is refrigerant mass flow rate, i is specific entalphy, and the subscripts from 1 to 4 are related to the points shown in FIG. 4.5.

The heat transfer hate between the refrigerant and the environment is given by:

$$Q_{ev} = A_{ev}F'[S - U_{ev}(\overline{T}_r - T_a)] \tag{5.8}$$

where A_{ev} is the collector/evaporator area, S is the difference between the solar radiation absorbed by the collector per unit area and the total radiation heat loss from the collector surface, T_a is the air temperature, F' is the collector efficiency factor that is evaluated using the Hottel-Whilliar-Bliss model described by Duffie and Beckman (DUFFIE; BECKMAN, 2013) and tested in solar evaporators models of DX-SAHP by many authors (KUANG, Y. H.; SUMATHY; WANG, R. Z., 2003; KONG; ZHANG, D., et al., 2011; FARIA et al., 2016; MOHAMED; RIFFAT; OMER, 2017; KONG; LI, et al., 2017). The collector efficiency factor is given:

$$F' = \frac{1}{wU_{ev}}\left\{\frac{1}{U_{ev}[D_o + F(w - D_o)]} + \frac{1}{\pi D_i \overline{h}_r}\right\}^{-1} \tag{5.9}$$

where w, D_i,D_o, F, U_{ev} and $\overline{h_r}$ represents the distance between tubes, inner diameter, outer diameter, fin efficiency, collector overall loss coefficient, and the mean inner heat transfer coefficient, respectively. These geometric parameter are shown in Fig. 5.3. The collector overall loss coefficient for DX-SAHP and the fin efficiency are given by EQ. 5.10 and EQ. 5.11 (KONG; ZHANG, D., et al., 2011).

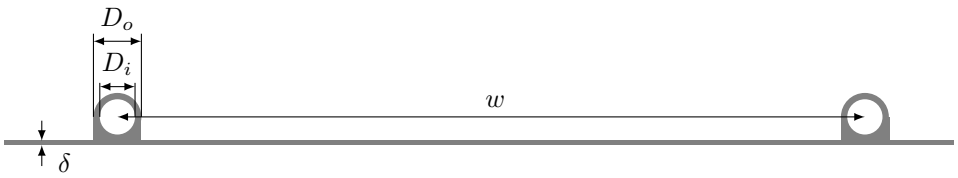

FIGURE 5.3: Geometric parameters of the evaporator

$$U_{ev} = h_a + 4\varepsilon\sigma T_a^3 \tag{5.10}$$

$$F = \frac{\tanh\left[(w - D_o)/2\sqrt{U_{ev}/(k\delta)}\right]}{(w - D_o)/2\sqrt{U_{ev}/(k\delta)}} \tag{5.11}$$

In these equation, the collector thickness shown in Fig. 5.3 is δ, the emissivity is ε, the Stefan-Boltzmann constant is σ which value is, in SI units, $5,670367(13) \cdot 10^{-8} W/(m^2 K^4)$ (MOHR; NEWELL; TAYLOR, 2016). The net radiation absorbed by the collector can be approximated by the following equation proposed by Kong, D Zhang, et al. (2011):

$$S = aI - \varepsilon\sigma(\overline{T}_r^4 - T_{sky}^4) \tag{5.12}$$

where a is the absorptivity and T_{sky} is the sky temperature. The average properties ($\overline{h_r}$ and $\overline{T}_r$) are calculated using the weighted arithmetic mean using the boiling length (L_{bo}), the superheat length (L_{sup}), and the evaporator tube length (L_{ev}):

$$L_{bo} = L_{ev}\frac{i_V - i_4}{i_1 - i_4} \tag{5.13}$$

$$L_{sup} = L_{ev} - L_{bo} \tag{5.14}$$

$$\overline{h}_r = \frac{\overline{h}_{bo}L_{bo} + \overline{h}_{sup}L_{sup}}{L_{ev}} \tag{5.15}$$

$$\overline{T}_r = \frac{T_4 L_{bo} + \overline{T}_{sup}L_{sup}}{L_{ev}} \tag{5.16}$$

$$\overline{T}_{sup} = \frac{T_4 + T_1}{2} \tag{5.17}$$

where i_V is the vapor entalphy, $\overline{h}_{sup}$ is the convective heat transfer coefficient calculated using

a correlation for single phase flow in the temperature $\overline{T}_{sup}$, and $\overline{h}_{bo}$ is calculated by .

$$\overline{h}_{bo} = \frac{1}{L_{bo}} \int h_{bo} dL \tag{5.18}$$

The wall temperature (T_s) required to use the correlation of Fang, Wu, and Yuan (2017) is evaluated by:

$$T_s = \frac{T_r h_r + T_a h_a}{h_r + h_a} \tag{5.19}$$

5.2.2 Compressor model

In a refrigeration machine or heat pump, the suction and discharge pressures are imposed by the secondary fluid in the hot source and cold source, respectively, and the compressor does not have direct influence on these variables. The compressor model is a gray box model and it is based on the following assumptions:

- No refrigerant leakage;
- Compression process is adiabatic;
- Compression process is isentropic;
- Compressor rotational speed is constant.

The mass flow rate of compressor is given by:

$$\dot{m}_{cmp} = \rho_1 \forall_d N \eta_{vol} \tag{5.20}$$

where $\forall_d$ is the compressor displacement volume, N is the rotational speed, ρ_1 is the suction density, and η_{vol} is the volumetric efficiency. The electric consumption ($\dot{W}_{cmp}$) is evaluated by:

$$\dot{W}_{cmp} = \frac{\dot{m}_r (i_2 - i_1)}{\eta_{ov}} \tag{5.21}$$

The volumetric efficiency (η_{vol}) and overall isentropic efficiency (η_{ov}) are given by EQ. 5.22 and 5.23, the constants B_1 to B_5 fitted using the performance data provided by manufacture, as made by Minetto (2011).

$$\eta_{vol} = B_1 + B_2 \left(\frac{P_2}{P_1} \right) \tag{5.22}$$

$$\eta_{ov} = B_3 + B_4 \left(\frac{P_2}{P_1} \right) + B_5 \left(\frac{P_2}{P_1} \right)^2 \tag{5.23}$$

5.2.3 Immersed condenser

The balance of energy in the hot water tank, assuming that there is no stratification, is given by:

$$Q_t = \rho_w \forall_w C_w \frac{\Delta T_w}{\Delta t} \tag{5.24}$$

where $\forall_w$ is the volume of water in the tank and ΔT_w is the the increase of temperature in the tank during a time interval Δt. The ΔT_w is given by:

$$\Delta T_w = \frac{T_{wf} - T_{wf}}{n} \tag{5.25}$$

where n is a number of division in the transient process of heating the water tank.

The condenser was dived into three regions to apply the balance of energy: ($C1$) vapor flow region, ($C2$) condensation flow region, and ($C3$) liquid flow region. The balance of energy in the refrigerant in each region is given by:

$$Q_{C1} = \dot{m}_r (i_2 - i_V) \tag{5.26}$$

$$Q_{C2} = \dot{m}_r (i_V - i_L) \tag{5.27}$$

$$Q_{C3} = \dot{m}_r (i_L - i_3) \tag{5.28}$$

where the L, and V represent the liquid and vapor properties, respectively. If the thermal resistance of the wall of the tube is negligible, the balance of energy in the wall for region $C1$ is given by EQ. 5.29 and the inner and outer area are calculated by EQ. 5.30 and 5.31. For the other two regions, the equations are similar and omitted.

$$Q_{C1} = A_{i;C1}\overline{h}_{r;C1}(\overline{T}_{r;C1} - \overline{T}_{s;C1}) = A_{o;C1}\overline{h}_{w;C1}(\overline{T}_{s;C1} - T_w) \tag{5.29}$$

$$A_{i;C1} = \pi D_i L_{C1} \tag{5.30}$$

$$A_{o;C1} = \pi D_o L_{C1} \tag{5.31}$$

The refrigerant temperature in each region is defined in EQ. 5.32 to 5.34. The mean HTC in the side of refrigerant ($\overline{h}_r$) and in the region $C1$ and $C3$ is calculated using the correlation of Gnielinski (1976) considering the average temperatures $\overline{T}_{r;C1}$ and $\overline{T}_{r;C3}$, and in the region $C2$, it is calculated using the EQ. 5.18, assuming that the vapor quality varies linearly with length and using the correlation of Shah (2016). The mean HTC in the side of water ($\overline{h}_W$) is determined using a correlation of Churchill and Chu (1975a) using the wall temperature ($\overline{T}_s$), for each region.

$$\overline{T}_{r;C1} = \frac{T_{cond} + T_2}{2} \tag{5.32}$$

$$\overline{T}_{r;C2} = T_{cond} \tag{5.33}$$

$$\overline{T}_{r;C3} = \frac{T_{cond} + T_3}{2} \tag{5.34}$$

In order to consider the heat loss at the water tank and in the connecting tubes before and after the condenser, Kong, D Zhang, et al. (2011) propose a heat leakage coefficient of 95% given by:

$$\zeta = \frac{Q_t}{Q_{cond}} \tag{5.35}$$

$$Q_{cond} = Q_{C1} + Q_{C2} + Q_{C3} \tag{5.36}$$

5.2.4 Coaxial condenser

During the operation with coaxial condenser, the hot water tank is filled with hot water, so the energy balance in the hot water tank is given by:

$$Q_t = \rho_w T_w C_w \frac{\Delta \forall_w}{\Delta t} \tag{5.37}$$

The balance of energy in the refrigerant at the condenser is evaluated as follow:

$$Q_{cond} = \dot{m}_r (i_2 - i_3) \tag{5.38}$$

Assuming no heat loss in the coaxial condenser, the balance of energy in the water is given by:

$$Q_{cond} = \dot{m}_w C_w (T_{wo} - T_{wi}) \tag{5.39}$$

The heat transfer rate in the condenser is calculated using the effectiveness-NTU method. The effectiveness (ξ) of a concentric heat exchanger is evaluated as follows (INCR-OPERA et al., 2007):

$$\xi = \frac{Q_{cond}}{\dot{C}_{min}(T_2 - T_{wi})} \tag{5.40}$$

$$\xi = \frac{1 - \exp[-\mathbf{NTU}(1 - \dot{C}_{min}/\dot{C}_{max})]}{1 - \exp[-\mathbf{NTU}(1 - \dot{C}_{min}/\dot{C}_{max})]\dot{C}_{min}/\dot{C}_{max}} \tag{5.41}$$

where $\dot{C}_{min}$ and $\dot{C}_{max}$ is the equal to $\dot{C}_r$ or $\dot{C}_w$, whichever is smaller and bigger, respectively. The refrigerant and water heat capacity rate are given by:

$$\dot{C}_r = \dot{m}_r \overline{C}_r \tag{5.42}$$

$$\dot{C}_w = \dot{m}_w C_w \tag{5.43}$$

In these equations, the mean specific heat of the refrigerant ($\overline{C}_r$) is evaluated by EQ. 5.44 and the Number of Transfer Units (NTU) by EQ. 5.45.

$$\overline{C}_r = \frac{i_2 - i_3}{T_2 - T_3} \tag{5.44}$$

$$\text{NTU} = \frac{UA}{\dot{m}_w C_w} \tag{5.45}$$

The UA value is determined by:

$$UA = \left(\frac{1}{\overline{h}_r \pi D_{ii} L_{cond}} + \frac{ln(D_{ii}/D_{io})}{2\pi k L_{cond}} + \frac{1}{\overline{h}_w \pi D_{oi} L_{cond}} \right)^{-1} \tag{5.46}$$

where the diameters D_{ii} and D_{oi} are shown in FIG. 5.4, the mean water HTC ($\overline{h}_w$) is calculated using the correlations described in section 3.1.1 for flow in annular regions, and the mean refrigerant HTC ($\overline{h}_r$) is calculated by EQ. 5.18, and assuming that the entalphy varies linearly with length and using the correlation of Gnielinski (1976) for h_r if $i \geq i_V$ or $i \leq i_L$ and the correlation of Shah (2016) if $i_L < i < i_V$.

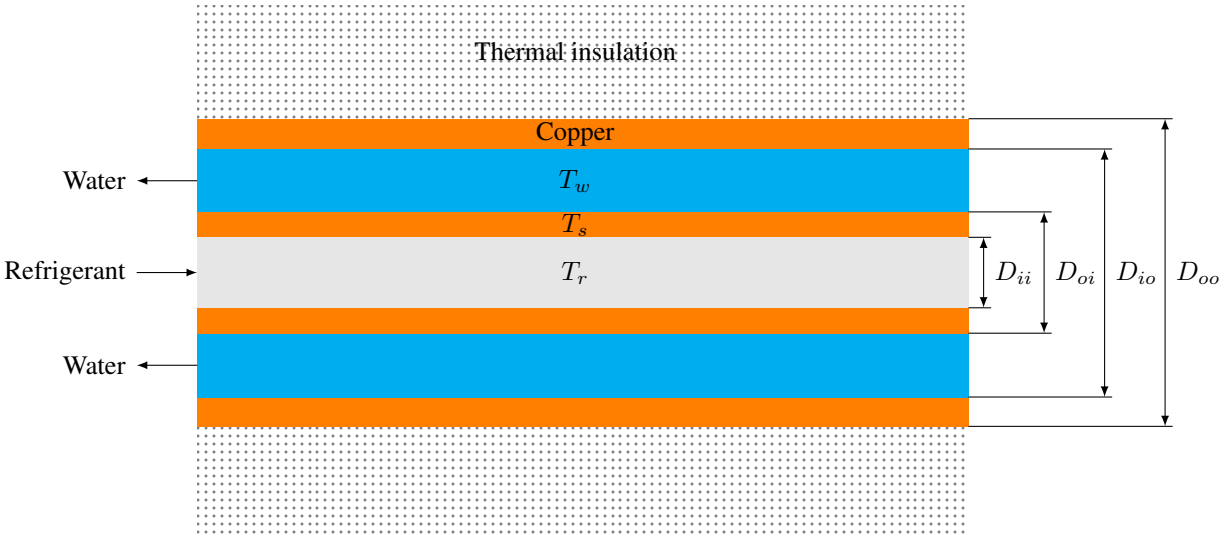

FIGURE 5.4: Concentric condenser geometric parameters

5.2.5 *Expansion device*

The expansion device required for a DX-SAHPWH is the electronic valve or a thermostatic valve, because of the large variations in solar radiation. The expansion valve is used to control the superheat at evaporator outlet, and it is modeled as isenthalpic and the mass flow rate can be calculated as follows:

$$\dot{m}_r = c_{ed} A_{ed} \sqrt{2\rho_3 (P_3 - P_4)} \tag{5.47}$$

where A_{ed} is the area of the orifice valve, and c_{ed} is the flow coefficient or flow factor calculated by equation 5.48 proposed by Kong, D Zhang, et al. (2011).

$$c_{ed} = 0.02005\sqrt{\rho_3} + \frac{0.634}{\rho_4} \tag{5.48}$$

5.2.6 *Refrigerant charge*

The charge of the refrigerant is evaluated by the EQ. 5.49 for single phase flow and by the EQ. 5.50 for two-phase flow using the correlation of Hughmark (1962) for void fraction (α).

$$m_r = \overline{\rho}_r \frac{\pi D_i^2}{4} \tag{5.49}$$

$$m_r = \int \left[\alpha \rho_V + (1-\alpha)\rho_L\right] dV \tag{5.50}$$

5.3 Numerical procedure

To solve the set of equations previously presented, the platform chosen was the Equation Engineering Solver (EES). The library of EES has many functions to calculate the thermophysical properties of pure refrigerants, blends, humid air, solids, ideal gases, etc. Furthermore, some correlations for heat transfer coefficient, frictional drop pressure and void fraction are available in the library. The EES can check units to avoid fail in the programming

process. Finally, EES automatically identifies and groups equations that must be solved simultaneously. For this last reason, a flow chart describing the sequence for solving the equations is not presented. In fact, this feature allows to change easily an input variable for an output variable and vise versa. The interface to operate the model is shown in FIG. 5.5.

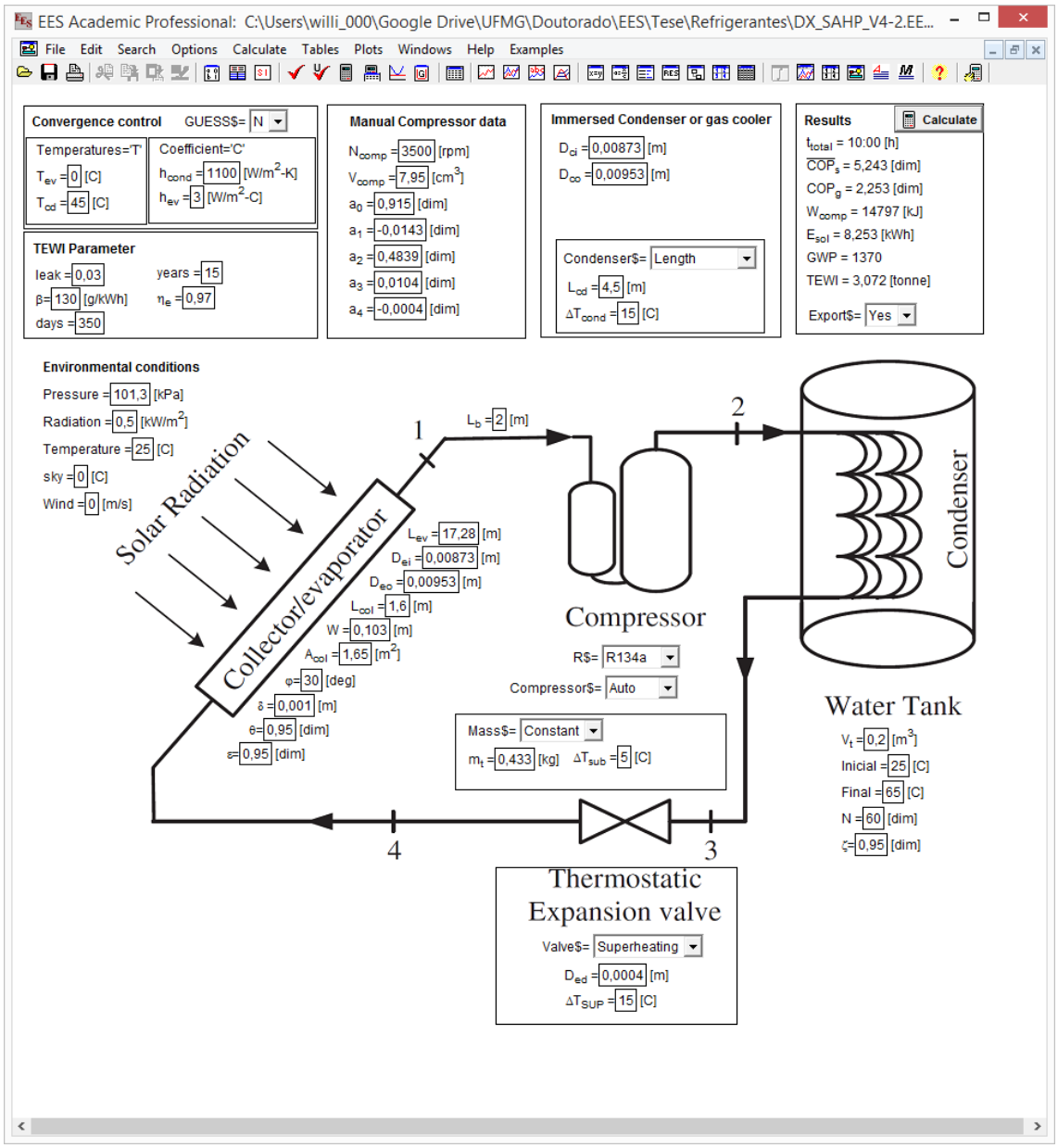

FIGURE 5.5: Interface to operate the model with an immersed condenser

6. MODEL CALIBRATION AND VALIDATION

In this chapter, it is presented the calibration and the experimental validation of a complete model of DX-SAHP. For the black or gray box model, the calibration process is the adjustment of the constant parameters introduced in the mathematical equations.

6.1 Compressor model calibration

The 18 data points of a volumetric and global efficiency, calculated using the performance map provided by the compressor manufacturer, are shown in FIG. 6.1 with their respective uncertainty (5%). The equation 6.1 and 6.2 were fitted to the data using a standard tool available in EES and plotted in FIG. 6.1. The fitted curves pass through the uncertainty range of all data points.

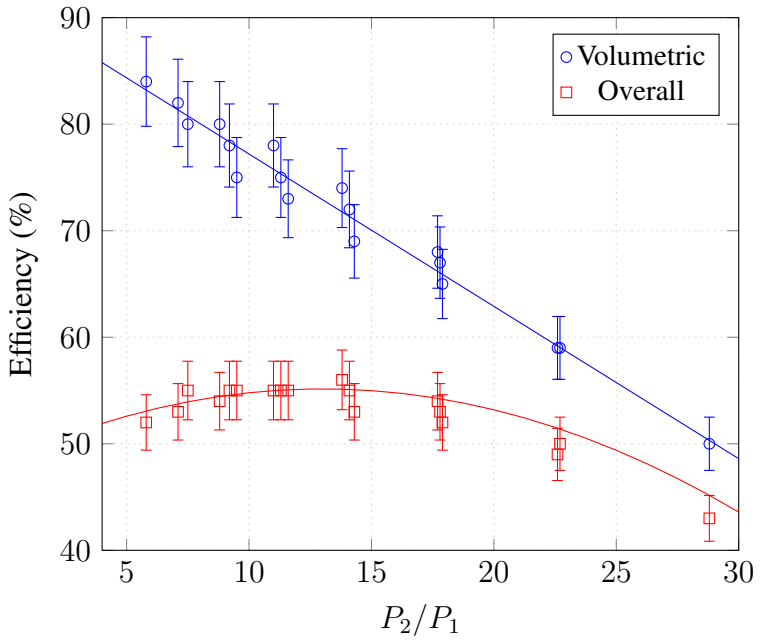

FIGURE 6.1: Volumetric and global efficiency of the R134a compressor

$$\eta_{vol} = 0,915 - 0,0143\frac{P_2}{P_1} \tag{6.1}$$

$$\eta_{ov} = 0,4839 + 0,0104\frac{P_2}{P_1} - 0,0004\left(\frac{P_2}{P_1}\right)^2 \tag{6.2}$$

Additionally, some other metrics are presented in TAB. 6.1. The r^2 is the coefficient of correlation which the best value is 100%. The results in TAB. 6.1 demonstrate that these equations represent with accuracy the efficiencies of the compressor.

TABLE 6.1
Metrics on the adjustment of compressor efficiencies curves

	r^2 (%)	MD (%)	MAD (%)
Volumetric efficiency	97.6	0.05	1.5
Overall efficiency	94.4	-0.41	1.4

6.2 DX-SAHP model validation

To validate the model, the results obtained from simulation were compared with the experimental results. In the simulations of this chapter, the superheat was assumed constant at 7.4^{o}C. The values of solar radiation, ambient temperature, atmospheric pressure, relative humidity and wind speed were kept constant at the mean value obtained from experimental tests. This value is the average value obtained from experimental results. For the acceleration of gravity, it was used the value of 9.7838550(5) m/s^2 measured at UFMG (SOARES, 2011). The value of solar absorptivity was assumed the same of measured emissivity (0.95). To evaluate the atmospheric pressure, it was used the data from Pampulha weather station which is located 1.7 km distant from the laboratory. The historical and real time weather data are available in INMET (2017). The mean atmospheric pressure for the test listed in TAB. 4.2 and 4.1 are presented in TAB. 6.2.

TABLE 6.2
Mean atmospheric pressure during the experimental tests

Test #	1	2	3	4	5	6	7	8	9	10
Pressure (kPa)	91.9	91.8	91.8	91.9	91.8	91.8	91.8	92.2	91.8	92.0
Test #	11	12	13	14	15	16	17	18	19	20
Pressure (kPa)	91.5	91.5	91.7	91.5	91.7	91.9	92.0	92.0	92.1	92.1

The sky temperature was fixed constant and the value used (0^{o}C) was estimated by the method proposed by Gliah et al. (2011), the correlation of Angstrom presented by Berdahl and Fromberg (1982) for sky emissivity, the annual average ambient temperature, average atmospheric pressure and average humidity in Belo Horizonte (INMET, 2017). For the simulation

for the tests made at an indoor environment, the sky temperature was assumed the same of the ambient temperature. The geometrical parameters are those described in chapater 4.

6.2.1 Immersed condenser

In the model of DX-SAHP using the immersed condenser, the refrigerant charge is an input variable, but the experimental device described in chapter four has two evaporators and two condensers, thus the charge of refrigerant used when the heat pump operate with the immersed condenser is difficult to measure. To determine the charge of the refrigerant needed the model was used to calculate the charge in the most critical condition. The charge of refrigerant was calculated with the heat pump operating without solar radiation and wind, ambient temperature of 0^{o}C, water temperature of 10^{o}C, and subcooling of 5^{o}C. The value of refrigerant charge found was 0.445 kg. To solve the integral of EQ. 5.18 and 5.50, the increase of quality (Δx) used was 1%. The heating process in the water tank was divide in 15 divisions with constant ΔT_w.

Firstly, it was checked which correlations have more accuracy to calculate the HTC in the solar evaporator. The correlation for the air side was tested first using the correlation of Shah (2017) for the refrigerant side. For each correlation the COP of the DX-SAHP was calculated and compared with the experimental results from TAB. 4.1. The maximum deviation, Mean Deviation (MD) and Mean Absolute Deviation (MAD) of each correlation are presented in TAB. 6.3, in the order in which they were tested.

TABLE 6.3
Test of the HTC correlations for air in the solar evaporator

Correlation	MAD	MD	Maximum
McAdams (1954)	6.4	3.0	10.4
ASHRAE (2013)	3.9	3.0	6.9
ISO (2007)	4.9	5.2	9.9
Sharples and Charlesworth (1998)	7.9	7.9	10.7
Test, Lessmann, and Johary (1981) and Kumar and Mullick (2010)	7.2	7.2	10.8
Watmuff, WWS Charters, and Proctor (1977)	3.9	3.5	8.7
Scarpa and Tagliafico (2016)	21.6	21.6	30.6

In this table, the correlation of Test, Lessmann, and Johary (1981) and Kumar and Mullick (2010) was tested together, because of the domain of the first is from wind speed from 1.5 to 5.6 m/s, and the domain of the second is 0 to 1.1 m/s. In the second row, the correlations

used are those described in EQ. 3.41 to 3.53 which are listed in ASHRAE (2013).

Using the correlations presented in ASHRAE (2013), the correlation of Shah (2017) was compared to the correlation of Fang, Wu, and Yuan (2017) and Gungor and Winterton (1987). The correlation of Fang, Wu, and Yuan (2017) did not converge for 70% of the tests listed in TAB. 4.1 and the results found in the converged simulations were worst than the results using the correlation of Shah (2017). The maximum deviation, MD and MAD using the correlation of Gungor and Winterton (1987) was 7.1. 4.1 and 4.9%, respectively. Therefore, the correlations of Shah (2017) and ASHRAE (2013) were selected for this work.

After choosing the correlations, a sensitivity study on the number of division in the transient process of the tank was performed. The results of this study are presented in TAB. 6.4 and 6.4. In the simulations of the TAB. 6.4, the DX-SAHP was used to heat water from 25 to 45^{o}C assuming the ambient temperature of 25^{o}C, sky temperature of 0^{o}C, atmospheric pressure of 101.3 kPa, without solar radiation or wind. In table 6.5, to heat water from 25 to 65^{o}C, assuming the ambient temperature of 15^{o}C, sky temperature of 15^{o}C, atmospheric pressure of 90 kPa, solar radiation of 500 W/m^2 and wind speed of 5 m/s.

TABLE 6.4
Results of the sensitivity study of the number of division in the transient process

ΔT_w (^{o}C)	2	1.54	1.18	0.91	0.69	0.53	0.41
COP	2.402	2.356	2.323	2.298	2.279	2.265	2.255
ΔCOP (%)	-	-2.0	-1.4	-1.1	-0.8	-0.6	-0.4
TEWI (tonne CO_2-eq)	1.317	1.343	1.362	1.376	1.388	1.397	1.403
ΔTEWI (%)	-	1.9	1.4	1.0	0.9	-0.6	-0.4

TABLE 6.5
Results of the sensitivity study of the number of division in the transient process

ΔT_w (^{o}C)	2	1.54	1.18	0.91	0.69
COP	2.367	2.354	2.344	2.337	2.331
ΔCOP (%)	-	-0.6	-0.4	-0.3	-0.3
TEWI (tonne CO_2-eq)	2.672	2.687	2.698	2.706	2.715
ΔTEWI (%)	-	0.6	0.4	0.3	0.3

In this tables, if ΔT_w is lower than 0.69 ^{o}C, the changes in the value of COP and TEWI are lower than $\pm 1\%$. Finally, the charge of the refrigerant was recalculated using the correlations of Shah (2017), ASHRAE (2013) and the simulation was remade with ΔT_w lower or equal to 0.69 ^{o}C. The new values of refrigerant charge, MAD, MD and maximum deviation found were 0.433kg, 2.7%, 1.7% and 5,2%, respectively. The comparison between experimental

and calculated COP are shown in FIG. 6.2. The average uncertainty of the experimental COP is 4,9% which is higher than the MD and MAD.

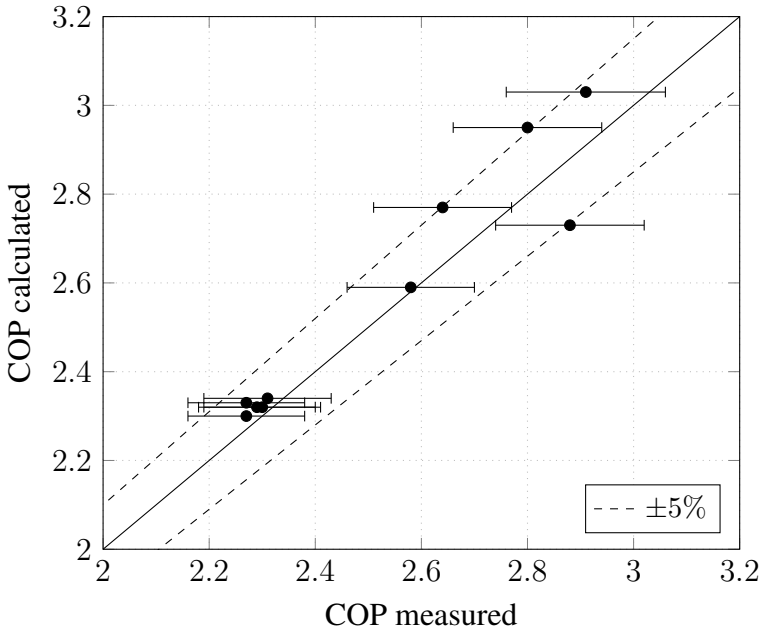

FIGURE 6.2: Comparison between the experimental and theoretical results using the immersed condenser

To evaluate if the quasi-stead-state model represents transient process of the heat of water tank, the variations of water temperature in the tank in time is shown in FIG. 6.3 and 6.4 for the experimental tests 4 and 7. These were the longest tests in a indoor and outdoor environment, so these tests have more measures of the water tank temperature. In the tests 4 and 7, the model underestimated the time need to heat the water in 4% and 2%, respectively. In these two figures, most of the values obtained from simulation are in the range of the uncertainty of the experimental values.

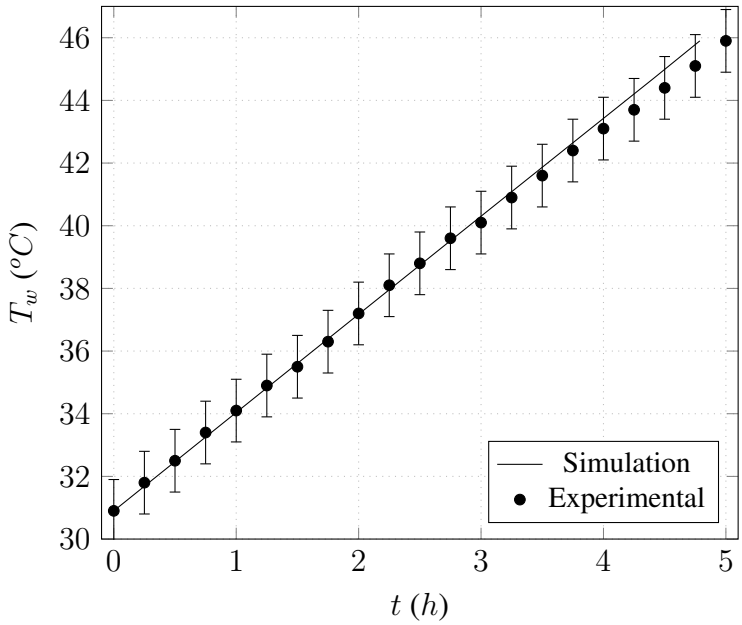

FIGURE 6.3: Comparison between the experimental and theoretical water tank temperature for experimental test # 4

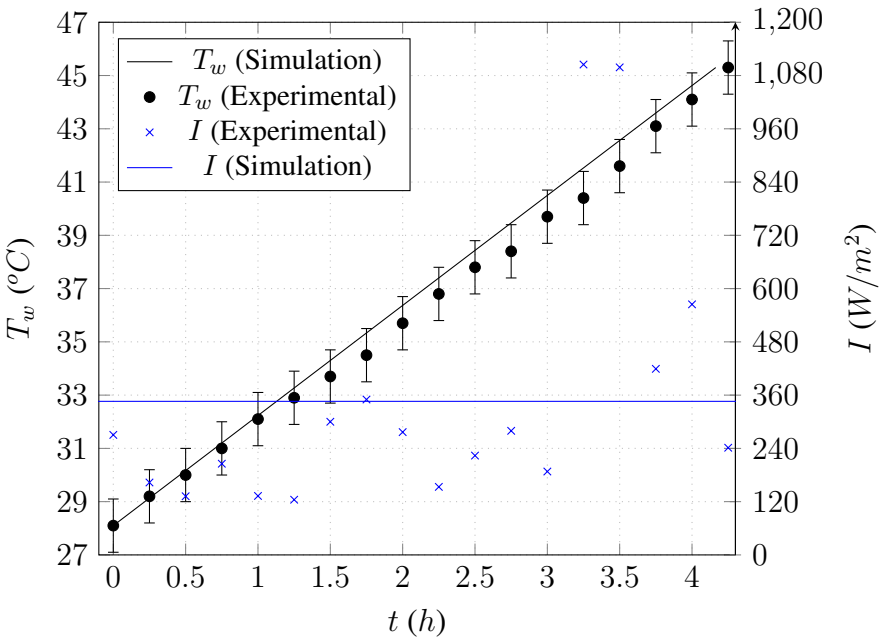

FIGURE 6.4: Comparison between the experimental and theoretical water tank temperature for experimental test # 7

The variations of instantaneous COP are shown in FIG. 6.5 and 6.6 for the experimental tests 4 and 7, respectively. The reduction of COP with the increase of the water tank temperature shown in these figures was discussed by many authors (KUANG, Y. H.; SUMATHY; WANG, R. Z., 2003; KONG; ZHANG, D., et al., 2011; KONG; LI, et al., 2017; DINIZ, 2017; KONG; SUN, P., et al., 2018). The instruments used in this DX-SAHP were optimized to calculate the average COP with low uncertainty and not to calculate the instantaneous COP, due

this reason, there are some large variation on instantaneous COP.

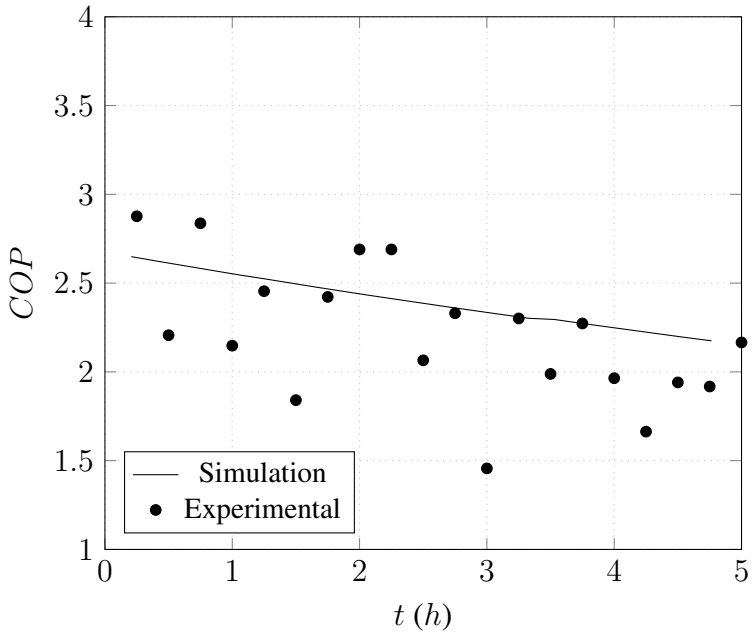

FIGURE 6.5: Comparison between the COP experimental and COP theoretical experimental test # 4

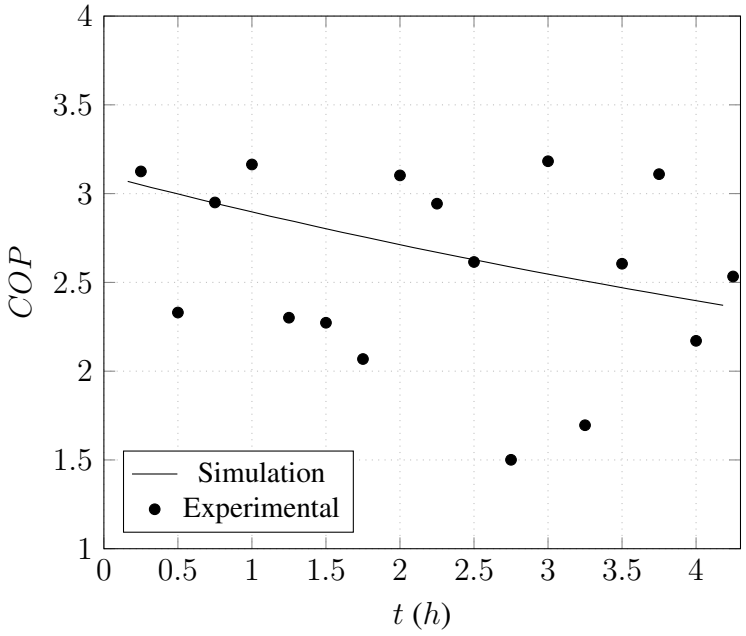

FIGURE 6.6: Comparison between the COP experimental and COP theoretical experimental test # 7

6.2.2 Coaxial condenser

To model of DX-SAHP using the coaxial condenser, it was validate using the same correlations selected for the solar evaporator using the model for immersed condenser. The subcooling was assumed fixed in 6.5^{o}C, which represents the average value in FIG. 4.7. To solve the integral of EQ. 5.18 and 5.50, the increase of specific entalphy (Δi) used was 0.75 kJ/kg.

The graphical comparison of measured COP and calculated COP of the DX-SAHP is presented in FIG. 6.7. Only one point in FIG. 6.7 is outside of the range of $\pm 5\%$, this point represents the experimental test number 20. Comparing the experimental results, in the test number number 20, the solar radiation, ambient temperature, wind speed are higher than test 16 and the difference of outlet and inlet water temperature are lower than test number 16, so the COP found experimentally in test number 20 should be bigger than the COP of test 16. This large difference of experimental and theoretical COP of this point is probably due to a fail in the equipment or the measures during the experimental test, but is not detected by Diniz (2017). The MD, MAD and maximum deviation of COP in FIG. 6.7 are 2.6, 2.9, and 11.6%, respectively. If the experimental test number 20 is excluded, the MD, MAD and maximum deviation reduces to 1.6, 2.0, and 4.2%, respectively.

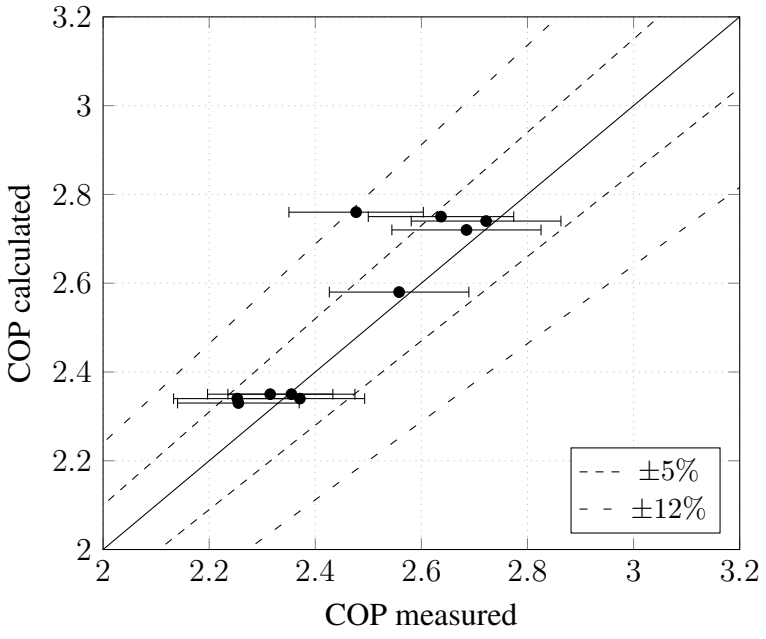

FIGURE 6.7: Comparison between the experimental and theoretical results using the coaxial condenser

The MD and MAD of comparing all 20 experiments are 2.1 and 2.8% which are

lower than the uncertainty of all test which are 5%.

7. ENVIRONMENTAL ANALYSIS

In this chapter, the environmental and energetic performance of the DX-SAHP are presented to guide the choice of one of refrigerant in the list of pre-selected to substitute the R134a. In this work it is assumed that a new heat pump can be build or components can be changed. A similar study considering the change only of the refrigerant and the oil of the compressor is presented by Duarte, Diniz, et al. (2018).

In the following results the simulations were done considering the geometrical parameters described in chapter 4 and the parameters listed in TAB. 7.1. The value of final water temperature was chosen based in the guideline of ASHRAE (2000) to minimize the risk of Legionellosis bacteria formation in the water. The superheat was set to 15 ^{o}C due the need of R600a to work with higher superheat to avoid the presence of liquid drops at the outlet of compressor. The value of system life time and annual leakage rate were recommended by Makhnatch and Khodabandeh (2014a) and the emission factor for producing electricity, by Rees (2016).

TABLE 7.1
Simulation parameters list of enviromental analysis

Parameter	Value	Parameter	Value
Atmospheric Pressure	101.3 kPa	Wind speed	0 m/s
Ambient temperature	25^{o}C	Annual leakage rate	3% of charge
Sky temperature	0 ^{o}C	Solar radiation	500 W/m^2
System life time	15 years	Heating demand	350 days/year
Emission factor	130 g/kWh	Superheat	15 ^{o}C
Solar absorptivity	0.95	Emissivity	0.95
Initial water temperature	25 ^{o}C	Final water temperature	65 ^{o}C

TABLE 7.2
Compressors selected

Ref.	Model	Manufacturer	$\forall_c$ (cm^3)
R1234yf	AE4430HFZ	Tecumseh	8.02
R134a	FF85HBK	Embraco	7.95
R290	NEK2121U	Embraco	6.2
R600a	NEK6170Y	Embraco	14.28
R744	SRADB	Sanden	1.75

The commercial compressors for the selected refrigerants were chosen considering the refrigeration capacity of R134a compressor described in chapter 4 at 20^{o}C. The selected

compressors are listed in TAB. 7.2. The model of the compressor of R134a was changed because the compressor used by Diniz (2017) was not tested for the condensing temperature of the simulations made in this chapter. The volumetric and overall efficiencies equations fitted in to manufacturers performance data for each compressor are listed in EQ. 7.1 to 7.10 and plotted in the Figures 7.1 and 7.2.

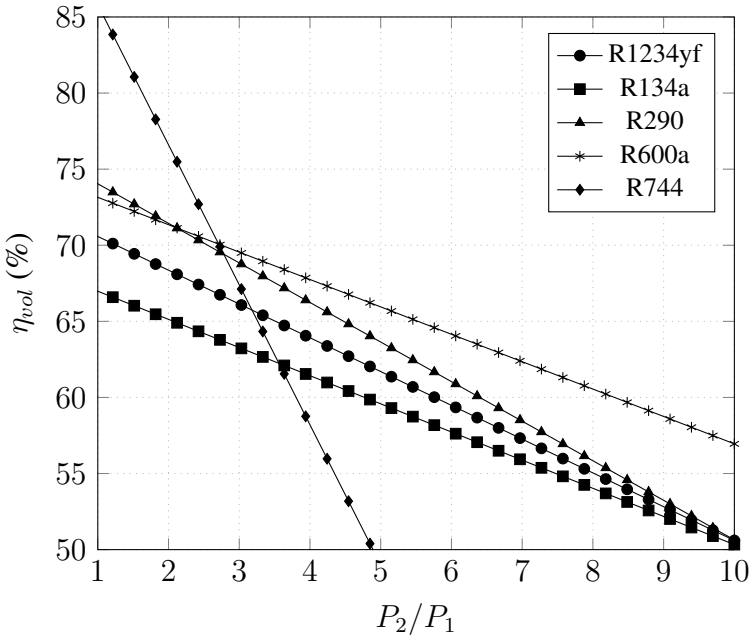

FIGURE 7.1: Volumetric efficiency function of pressure ratio

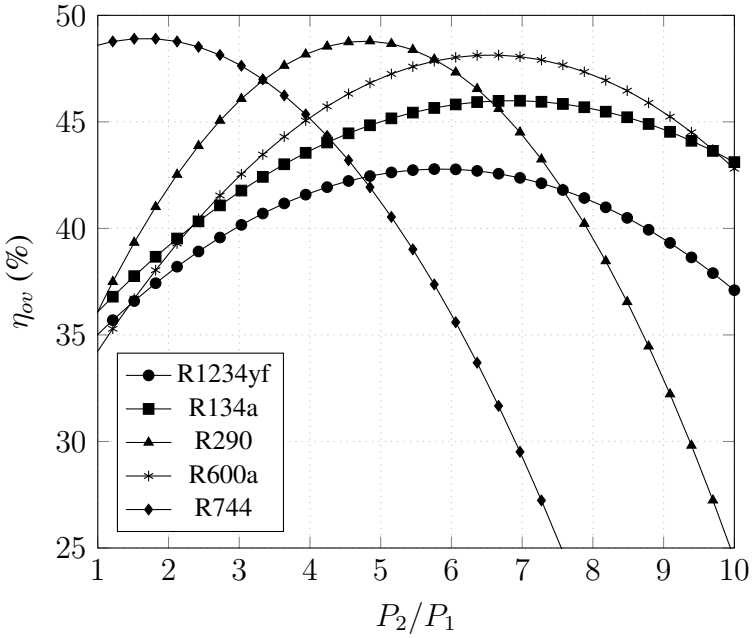

FIGURE 7.2: Overall efficiency function of pressure ratio

$$\eta_{vol} = -2,2(P_2/P_1) + 73 \quad \text{(R1234yf)} \tag{7.1}$$

$$\eta_{vol} = -1,9(P_2/P_1) + 69 \quad \text{(R134a)} \tag{7.2}$$

$$\eta_{vol} = -2,6(P_2/P_1) + 77 \quad \text{(R290)} \tag{7.3}$$

$$\eta_{vol} = -1,8(P_2/P_1) + 75 \quad \text{(R600a)} \tag{7.4}$$

$$\eta_{vol} = -9,2(P_2/P_1) + 95 \quad \text{(R744)} \tag{7.5}$$

$$\eta_{ov} = -0,33(P_2/P_1)^2 + 3,9(P_2/P_1) + 32 \quad \text{(R1234yf)} \tag{7.6}$$

$$\eta_{ov} = -0,29(P_2/P_1)^2 + 4,0(P_2/P_1) + 32 \quad \text{(R134a)} \tag{7.7}$$

$$\eta_{ov} = -0,89(P_2/P_1)^2 + 8,5(P_2/P_1) + 28 \quad \text{(R134a)} \tag{7.8}$$

$$\eta_{ov} = -0,45(P_2/P_1)^2 + 5,9(P_2/P_1) + 29 \quad \text{(R600a)} \tag{7.9}$$

$$\eta_{ov} = -0,69(P_2/P_1)^2 + 2,3(P_2/P_1) + 47 \quad \text{(R744)} \tag{7.10}$$

The performance data provided by the manufacturers have an uncertainty from 5 to 7%. The performance data of the selected compressors was obtained for evaporating temperatures from -15^{o}C to 15^{o}C and condensing temperatures from 35^{o}C to 65^{o}C, or from 80 bar to 100 bar for R744. The maximum global efficiency (η_g) for refrigerants R290, R600a and R744 is approximately the same and the refrigerant R1234yf has the lowest maximum efficiency.

The following sections presented the COP and TEWI of DX-SAHP using the immersed condenser and after for the coaxial condenser.

7.1 Immersed condenser

Since none study using an immersed gas cooler was found in the literature researched in this work, so for the R744 was considered only a coaxial heat exchanger. The charge of the refrigerant, for operation with immersed condenser, was calculated in the same way as made in the previous chapter. The charge used in each refrigerant is listed in TAB. 7.3

TABLE 7.3
Charge of refrigerants

Parameter	Value	Parameter	Value
R1234yf charge	408 g	R134a charge	433 g
R290 charge	205 g	R600a charge	184 g

Figure 7.3 shows the solar radiation effect on the COP of the DX-SAHP equipped with an immersed condenser for all refrigerants. There is an expressive improvement in the COP with the increase in the solar radiation. For example, considering the R290, the COP increases of 44% when the solar radiation grows from 0 to 700 W/m2. The linear increase of COP with the solar radiation for R134a is similar to those described by Deng and Yu (2016) and shown on FIG. 7.4. In figure 7.4 the results identified by DX represent the COP if only the solar evaporator is used and M-DX if the both solar evaporator and a finned coil evaporator are used at same time.

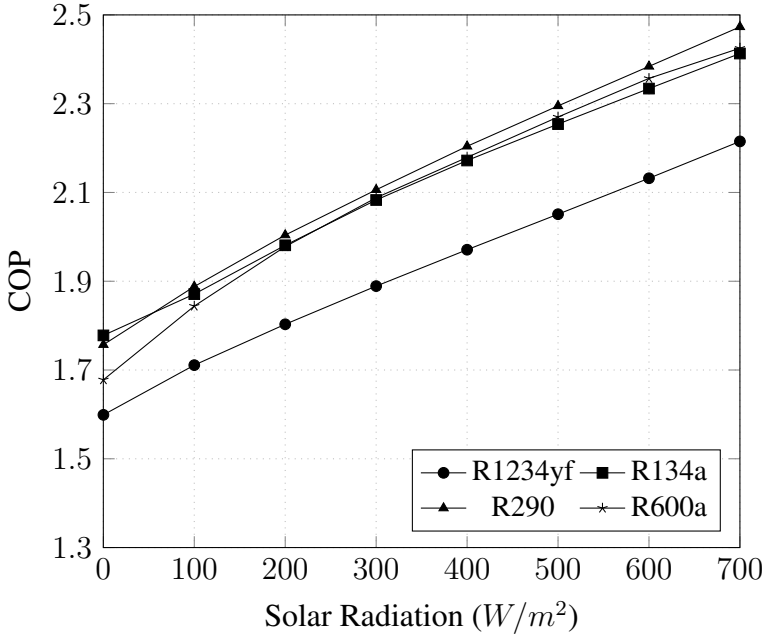

FIGURE 7.3: COP in function of solar radiations

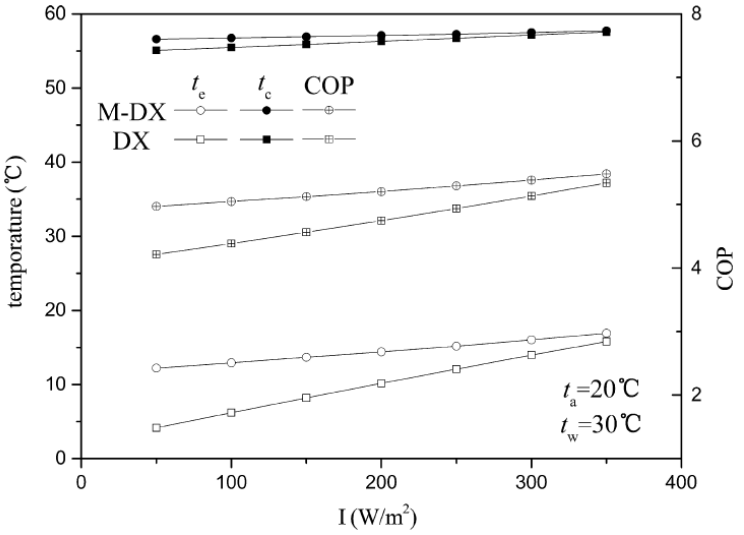

FIGURE 7.4: COP for a R134a DX-SAHP analyzed by Deng and Yu (2016)

SOURCE: Deng and Yu (2016, p. 384)

In figure 7.3, R134a has the best COP for solar radiation lower than 50 W/m^2 and R290 has the best COP for solar radiation greater than 50 W/m^2. The COP of R290 is in average of 1.2% better than R134a, 1.9% better than R600a and 11.3% better than R1234yf.

Figure 7.6 shows the variation of the COP with the wind speed for all refrigerants (fixed values for solar radiation and ambient temperature). The results of the COP with ambient temperature and wind velocity in a DX-SAHP were similar with those observed by Kong, D Zhang, et al. (2011) and shown in FIG. 7.5. The maximum performance improvement is around 1% for any refrigerant. The variation of COP with the environment temperature is shown in the Figure 7.7. For the R134a, the COP increased 8% when the temperature changed from 10^{o}C to 35^{o}C, while for the other refrigerants, the increase was 9%.

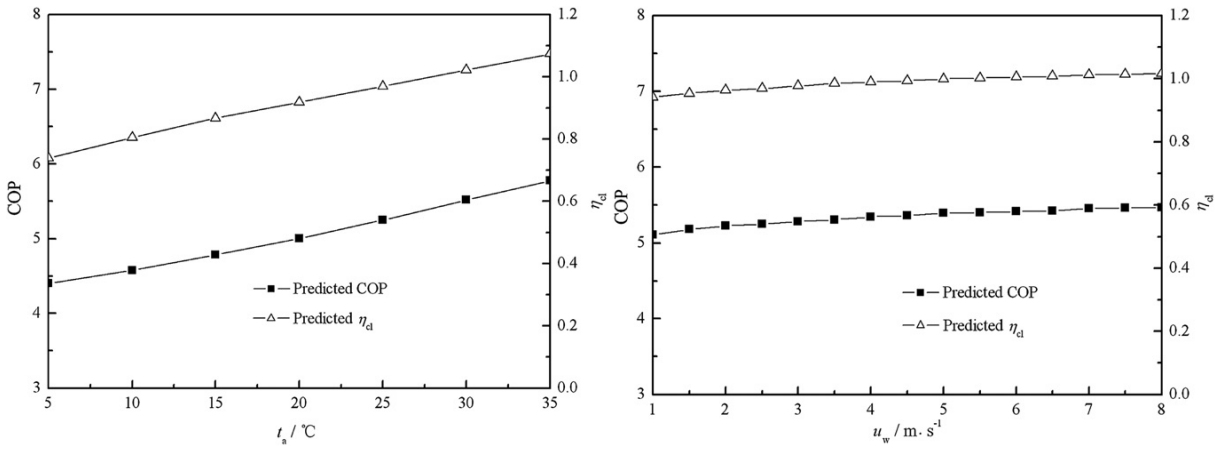

FIGURE 7.5: COP in function of ambient temperature and wind speed of R22 DX-SAHP

SOURCE: Kong, D Zhang, et al. (2011, p. 6836 and 6837)

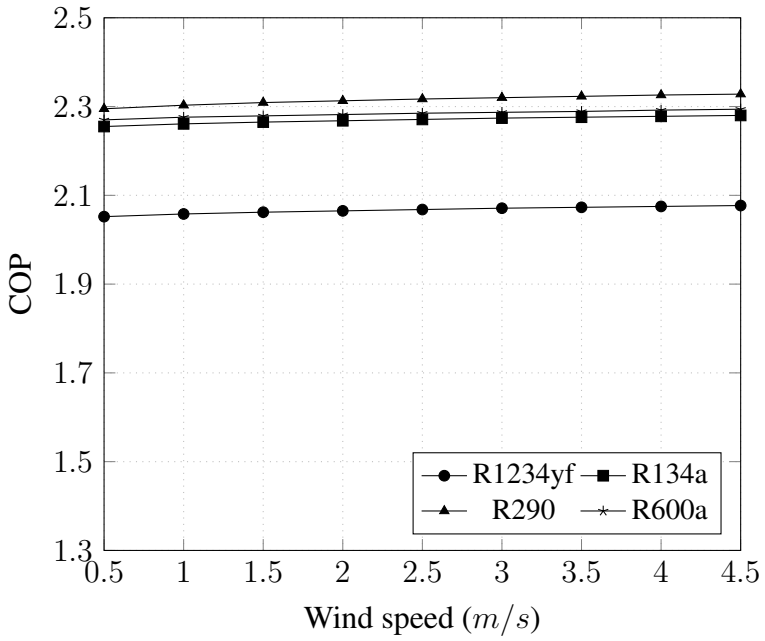

FIGURE 7.6: COP in function of wind speed

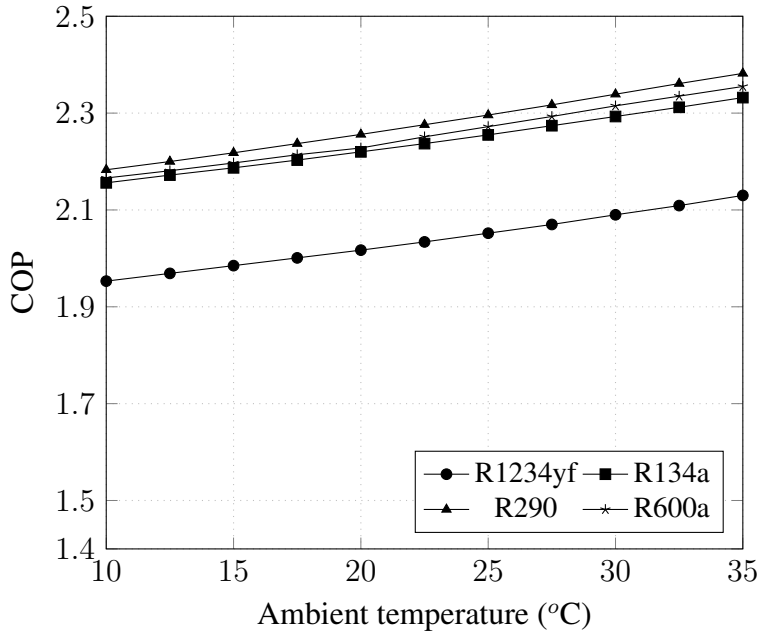

FIGURE 7.7: COP in function of ambient temperature

The TEWI for different solar radiation is shown in Figure 7.8. The refrigerant with lowest TEWI is the R290. For the R134a, its contribution of direct emissions represents 7% to 9.2% of the TEWI value and for the other refrigerants, the direct emissions are lower then 0.1%. To compare the environmental metrics, the TEWI of an electric heater with 97% of efficiency in the same conditions is 6.52 t CO_2-eq, and for the electrical heater there is no direct emissions. Therefore, between the refrigerants with GWP lower than 150, the one with higher COP will

have the lowest environmental impact.

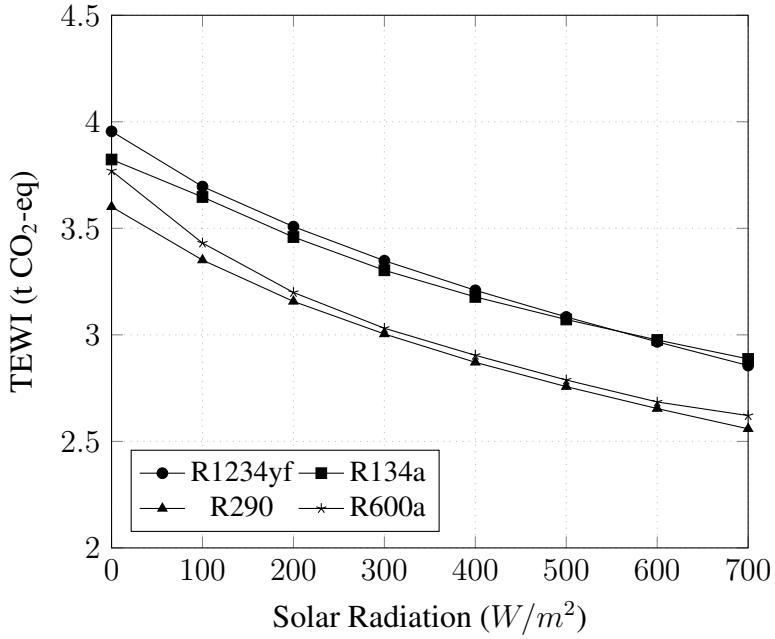

FIGURE 7.8: TEWI in function of solar radiation

7.2 Coaxial Condenser

In this study, R744 operates with transcritical cycle and a correlation for the high pressure in order to maximize the COP is required. As there are no correlations for DX-SAHP operating with CO_2, seven correlations for different systems available in the literature were tested (LIAO; ZHAO; JAKOBSEN, 2000; SARKAR; BHATTACHARYYA; GOPAL, 2004; APREA; MAIORINO, 2009; KIM, S. C.; WON; KIM, M. S., 2009; QI et al., 2013; WANG, S. et al., 2013; YANG et al., 2015). The best results were found by the correlation presented by Aprea and Maiorino (2009).

The same methodology used to model the coaxial condenser was used by Islam et al. (2012) to model a coaxial gas cooler. In this work, the correlation of Gnielinski (1976) was used to calculate the HTC of R744 for a single phase flow including the transcritical region as made by some authors (JIN; CHEN, J.; CHEN, Z., 2011; ISLAM et al., 2012; OLIVEIRA et al., 2016). The simulations with this type of condenser and the refrigerants R134a, R1234yf, R290, and R600a were done considering a subcooling of 6.5^{o}C.

The COP of the heat pump with coaxial condenser in function of solar radiation is presented in Figure 7.9. The improvement in the COP was 46% for R1234yf when the solar radiation grows from zero to 700 W/m^2. The average COP of the R290 was 0.1%, 6.3%, 20.5%

and 21.5% better than the COP of R134a, R600a, R744 and R1234yf, respectively. Again, R290 has the best COP for high solar radiation.

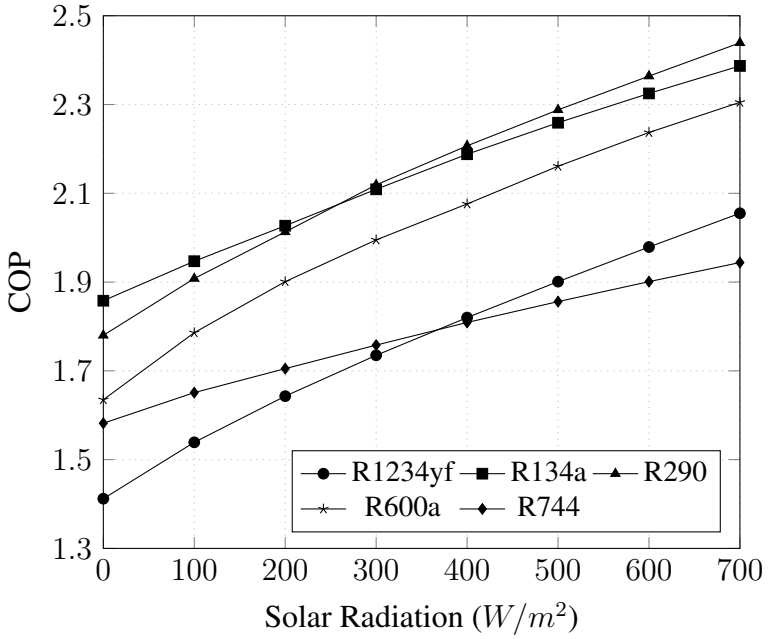

FIGURE 7.9: COP in function of solar radiation

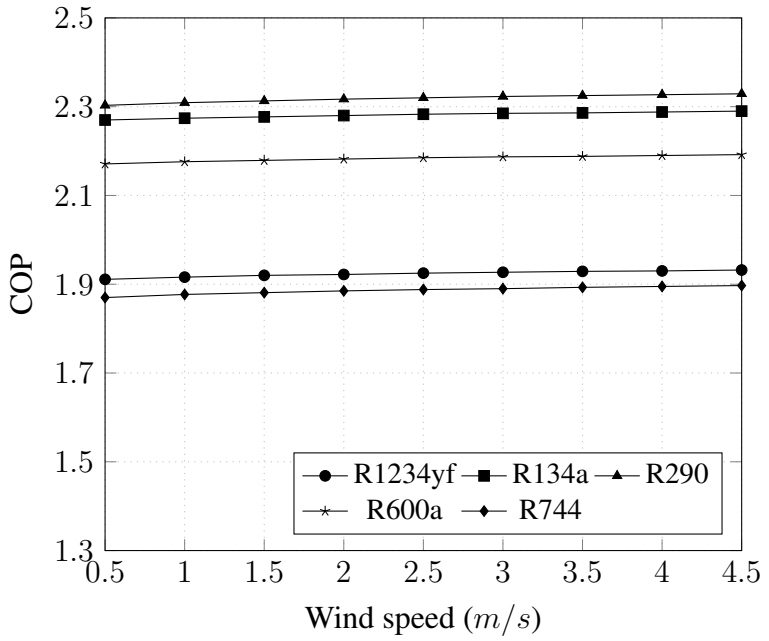

FIGURE 7.10: COP in function of wind speed

Figure 7.10 and 7.11 show the increase of the COP with the wind speed and ambient temperature. The COP of DX-SAHP increased from 1.9% to 3% when the wind speed increases from 0 m/s to 4.5 m/s, and from 4.5% to 7% when the ambient temperature changed from 10^{o}C to 35^{o}C. The COP of R134a and R290 with the immersed condenser are in average the same

with the coaxial condenser, but for R1234yf and R600a the COP is 9.3% and 4.3% better with the immersed condenser.

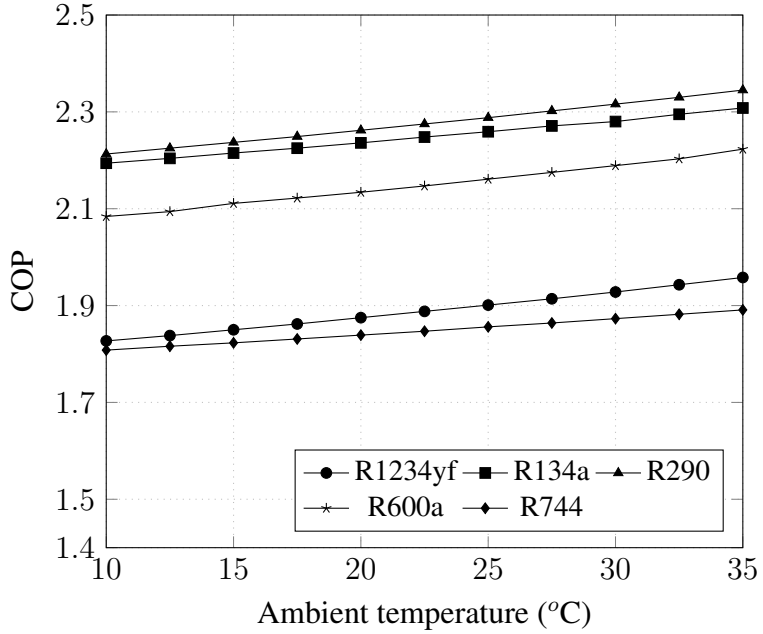

FIGURE 7.11: COP in function of ambient temperature

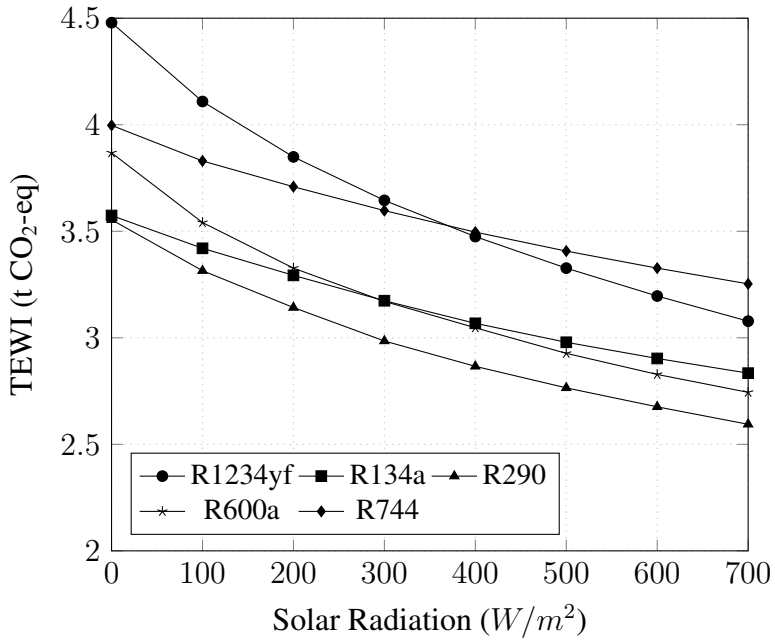

FIGURE 7.12: TEWI in function of solar radiation

The refrigerant with the lowest TEWI for a coaxial condenser is also the R290 as shown in Figure 7.12. In this case, the contribution of direct emissions in the TEWI is from 5% to 6.5% for R134a and it is lower than 0.1% for the other refrigerants. Because of the lower diameter of this heat exchanger, the maximum charge required by R134a, R1234yf and R290

is around 30% lower than that required with immersed condenser, and of 52% lower for the R600a. For higher solar radiation, the worst TEWI was that of the one from R744, and for lower solar radiations was that one for R1234yf. The TEWI for R1234yf, R134a and R600a are 8.5%, 4.3% and 4.2% lower for the immersed condenser than for the coaxial condenser, respectively. The average TEWI for R290 is the same with both condensers.

It is interesting to change some fixed parameters in the previous results, and check the results variance. For this parametric analysis the model with coaxial condenser was used because of the lower computational effort and the similar results between the two types of condensers. The first important parameter is the CO_2 emission factor for producing electricity since each country or region keeps different values. The variation of TEWI for different emission factor is shown in Figure 7.13. In places with lower emission factors, around 20 g/kWh, the TEWI of R290 is 0.43 t CO_2-eq. The worst TEWI is from R134a (0.617 t CO_2-eq). In places with higher emission factor, the refrigerant with the best COP has the best TEWI.

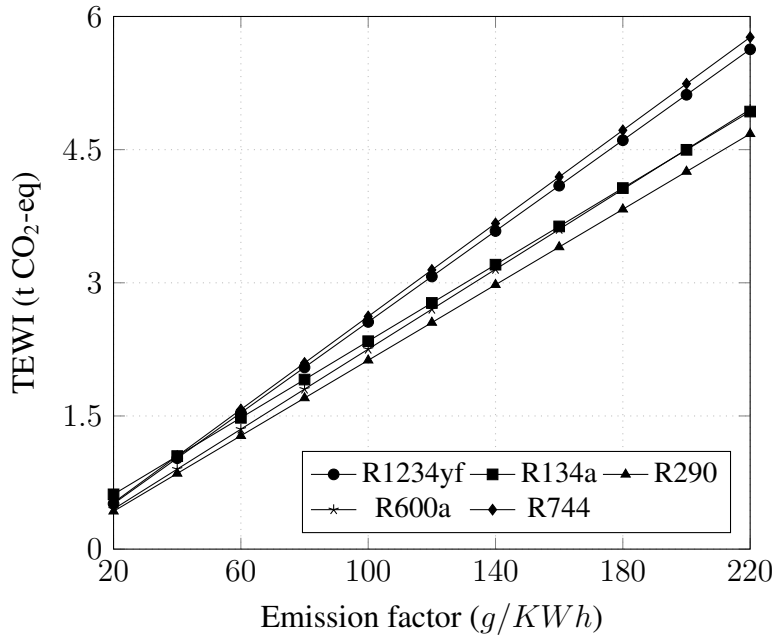

FIGURE 7.13: TEWI in function of emission factor

Another important parameter is the length of the condenser (or gas cooler in the case of R744). It is known that the heat transfer coefficient for a gas is lower than the heat transfer coefficient in condensation region for the same mass flux rate. Figures 7.14 and 7.15 show the variation of COP and TEWI in function of the gas cooler/condenser length. For the CO_2, the sudden change in the inclination of COP and TEWI curves happens in the transition between transcritical and sub-critical cycle. For a length higher than 18.5 m, the COP increase

and TEWI decrease rates are very low for all refrigerants. Besides of that, for this length, the COP of the R290 is 3% higher than the COP of the R744. Based in these facts R290 is selected for economical analysis in next chapter.

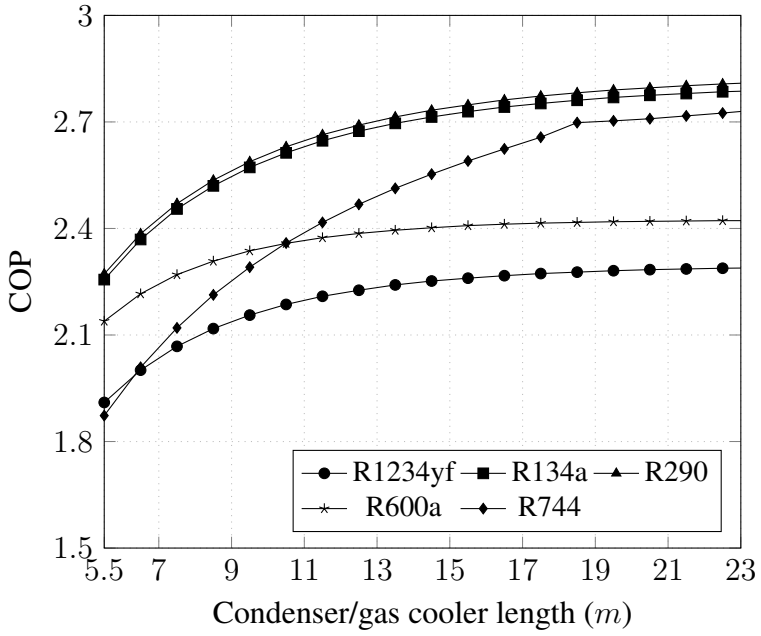

FIGURE 7.14: COP in function of condenser/gas cooler length

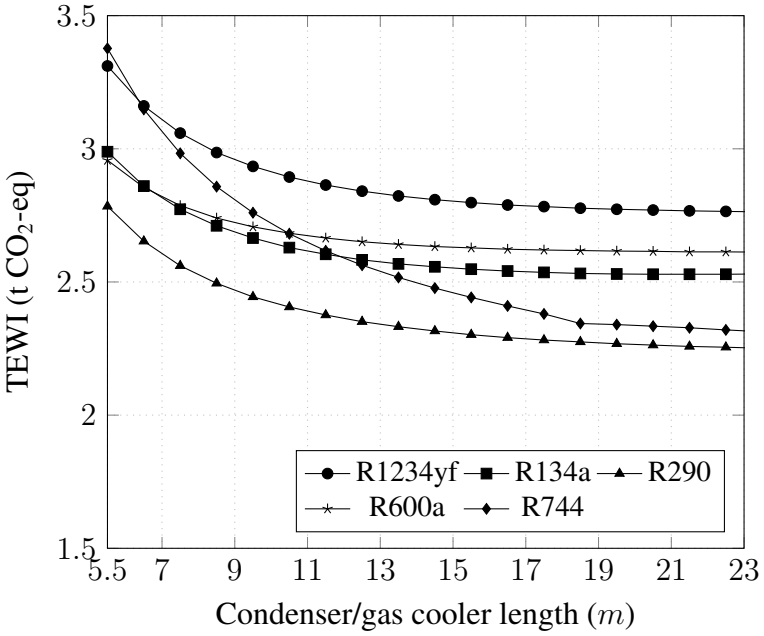

FIGURE 7.15: The in function of condenser/gas cooler length

8. ECONOMIC ANALYSIS

The model of DX-SAHP using the coaxial condenser has 139 equations and the model of DX-SAHP using the immersed condenser has 6625 equations. This large difference in the number of equation is due to the discretization of the transient process at the tank. The time need to run a simulation using the model with the immersed condenser is 16 times higher than the time to run the model with the coaxial condenser. This economic analysis was made using the model with coaxial condenser because of the lower computational effort, the similar results between the two types of condensers for R290, and the possibility of increase of the condenser size and improvement of COP as shown in FIG. 7.14.

In the following simulations, the collector length was fixed in 1.65 m and the width was changed, but the distance between the tubes in the collector was kept constant. The evaporator tube length was calculated considering linear proportion with the collector area. For each collector area, a new design for immersed condenser was made considering a fixed effectiveness. The other geometrical parameters listed in chapter 4 was considered constant. A list of other parameters used in the simulations is presented in Tab. 8.1. The costs in Tab. 8.1 are based in the Brazilian market in March of 2018. For the inflation rate, it was chosen the INPC (National Consumer Price Index), and the value in Tab. 8.1 was measured between 2013 to 2017. Electricity tariff used was the value for households in Belo Horizonte during March of 2018, obtained from Brazilian Electricity Regulatory Agency (ANEEL) website.

TABLE 8.1
Simulation parameters list of economic analysis

Parameter	Value	Parameter	Value
Atmospheric Pressure	101,3 kPa	Condenser effectiveness	0,8
Outlet water temperature	65 ^{o}C	Inlet water temperature	25 ^{o}C
Emissivity	0,95	Solar absorptivity	0,95
Subcooling	5 ^{o}C	Ambient temperature	25 ^{o}C
Superheating	10 ^{o}C	Solar radiation	700 W/m^2
Sky temperature	0 ^{o}C	Electricity tariff	0,494 R$/kWh
Heating demand	350 days/year	Inflation rate	6.34 %
Fixed cost	3000 R$	Collector cost	300 R$/m^2
R290 cost	100 R$/kg	Condenser tubing cost	20 R$/m
Service cost	30 %	Electric heater efficiency	97%

8.1 Analysis of the evaporator size

The coefficient of performance for different collector size is shown in Fig. 8.1. It can be observed that the increase of collector size increases the COP for any solar radiation in the range of area from 1,3 to 5,9 m^2. The shape of these curves are similar to that ones found by Ito, Miura, and K Wang (1999) for a R22 DX-SAHP and shown in FIG. 8.2. A similar curve was also presented by Chaturvedi and Abazeri (1987). Considering the solar radiation of 700W/m^2 the increase of the COP is 74% if the collector area is increased from 1,3 to 5,8 m^2.

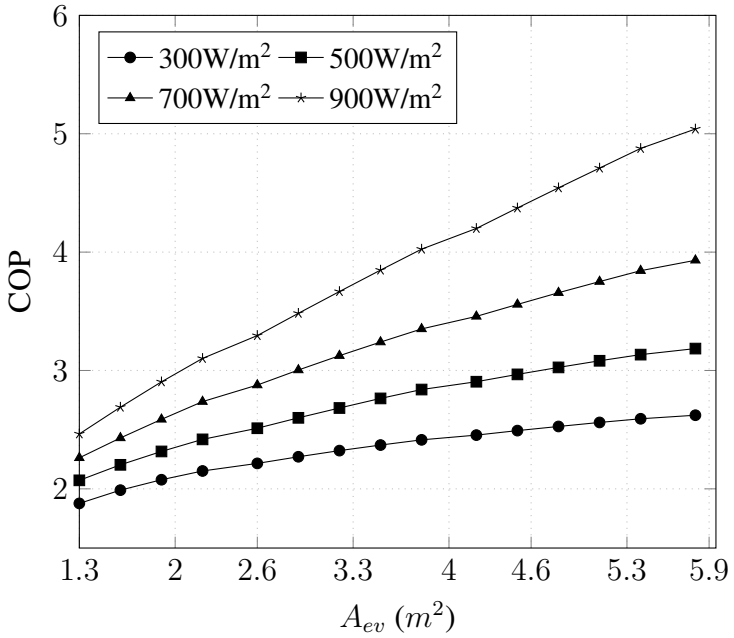

FIGURE 8.1: COP in function of collector area

The collector efficiency for different collector size is shown in Fig. 8.3. The decrease of the collector efficiency with the increase of solar energy in a DX-SAHP, with uncovered collector and a fixed area, has been discussed by some authors (KONG; ZHANG, D., et al., 2011; KONG; LI, et al., 2017; KUANG, Y. H.; SUMATHY; WANG, R. Z., 2003). For high solar radiation the difference between of the ambient temperature and the evaporation temperature is positive and there is a heat loss for the ambient in the collector. On the other hand, if the solar radiation reduces, the evaporation temperature decrease and there is less heat loss at the collector. If the evaporation temperature is lower than the ambient temperature, a certain heat is gained from the ambient and the collector efficiency can be higher than one.

In fact, the increase of the collector area increases the COP and reduces the cost with electricity but increase also the cost of the collector, the refrigerant charge and the condenser,

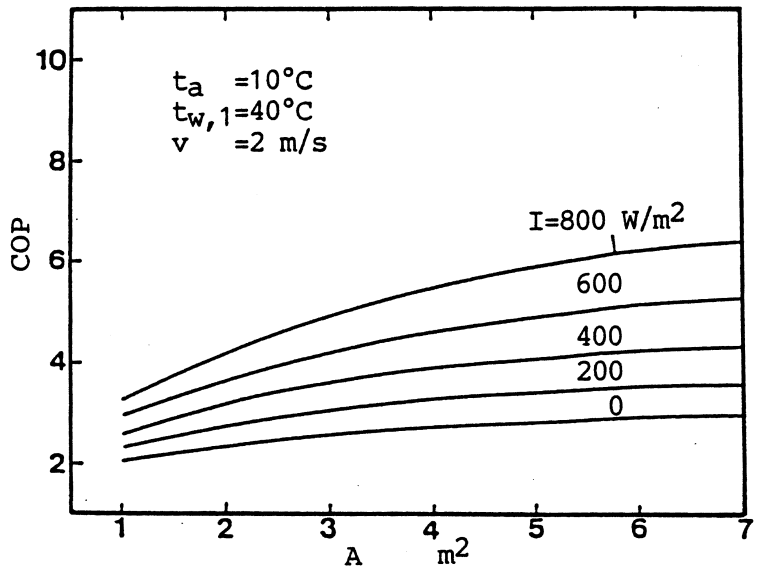

FIGURE 8.2: COP in function of collector area for a R22 DX-SAHP
SOURCE: Ito, Miura, and K Wang (1999, p. 195)

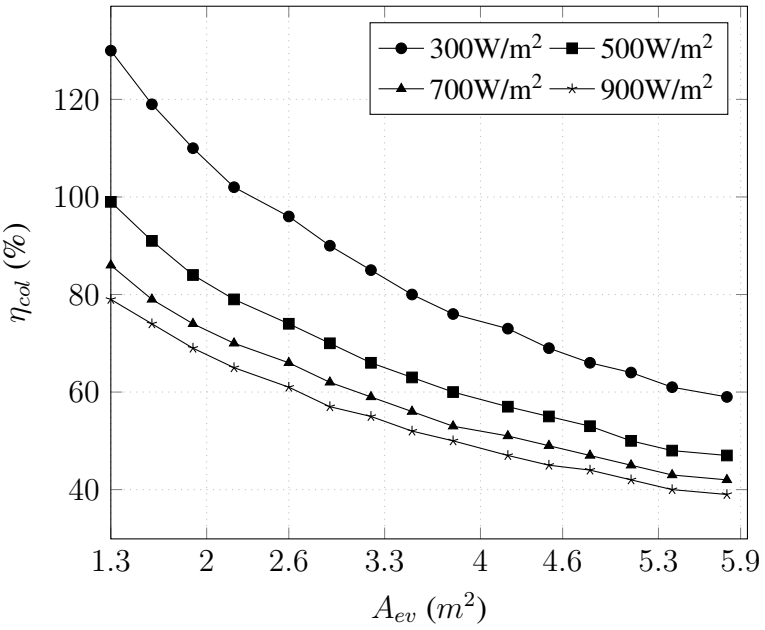

FIGURE 8.3: Collector efficiency in function of collector area

therefore, an economic analysis should be made. The payback time in function of the collector size is shown in Fig. 8.4 for different solar radiations. There is a collector area that minimizes the payback period, approximately 2.2 m^2 for any solar radiation and ambient temperature. The payback time is lower in condition with high solar radiation. In the sensitive analysis conducted by Duarte, Rabelo, et al. (2018), the parameters that strongly influenced the collector area that minimizes the payback time were the fixed initial invest cost and the collector cost.

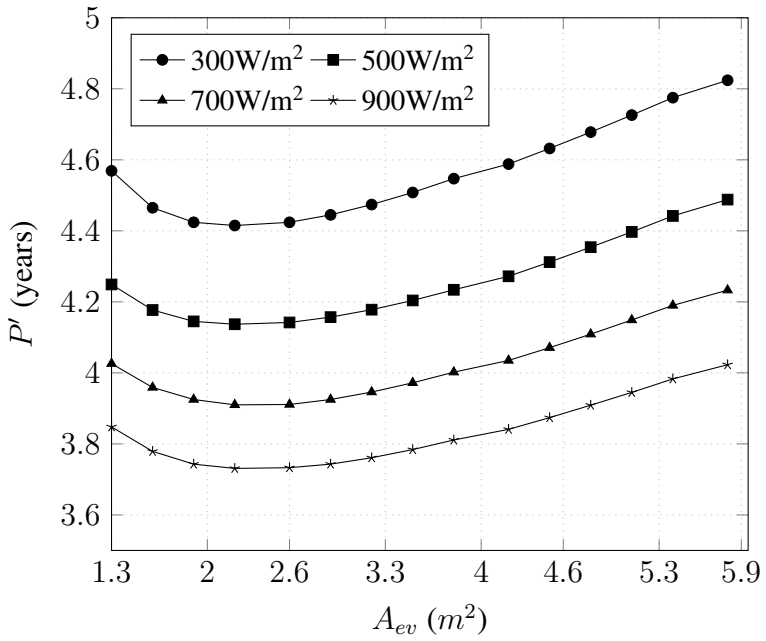

FIGURE 8.4: Payback time in function of collector area

8.2 Analysis of the condenser size

The variation of COP in function of the condenser size is shown in FIG. 8.5 considering a collector area of 2.24 m^2. For a solar radiation of 700 W/m^2 the increase of COP is 56% if the condenser length is increased from 4 to 25 m. The payback time in function of the condenser size is shown in FIG. 8.6. The condenser length that minimizes the payback increases with the increase of solar radiation. The minimum points of FIG. 8.6 are listed in TAB. 8.2.

TABLE 8.2
Optimum points of condenser length

I (W/m^2)	L_{cond} (m)	COP	P'	m (g)	ξ (%)
300	11,5	2,44	4,20	160	94,9
500	13	2,77	4,99	170	94,8
700	13	3,12	3,80	177	94,6
900	14,5	3,62	3,64	189	92,9

In fact, if the length of evaporator or condenser is increased, a new diameter for the tubes should be determined to maintain the levels of pressure dropping in the accepted level. The increase of diameter also increases the cost of the tubing and change the optimum length. A sensitive analysis was made increasing the cost of tubing in 100% and the optimum length reduces approximately 10%. In the range of diameter used in the condenser, to cost increment when the diameter is doubled, it is approximately 25%.

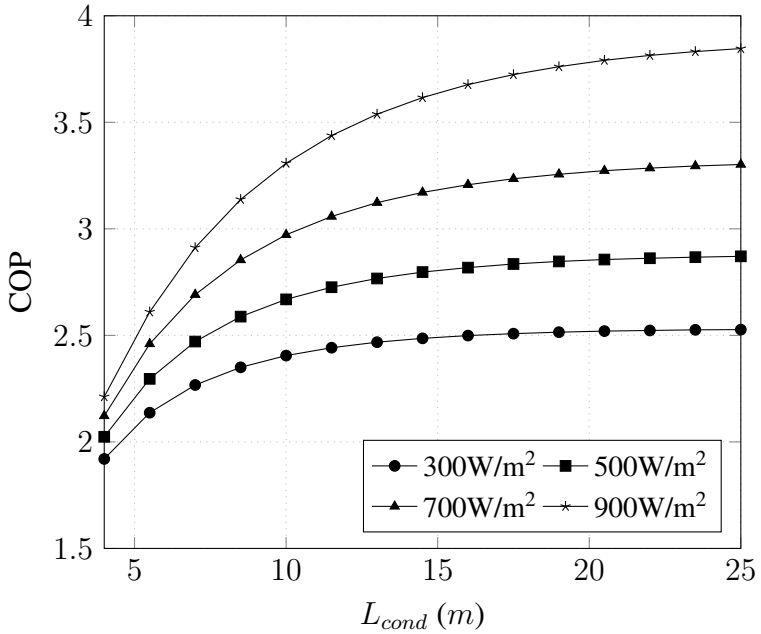

FIGURE 8.5: COP in function of condenser length

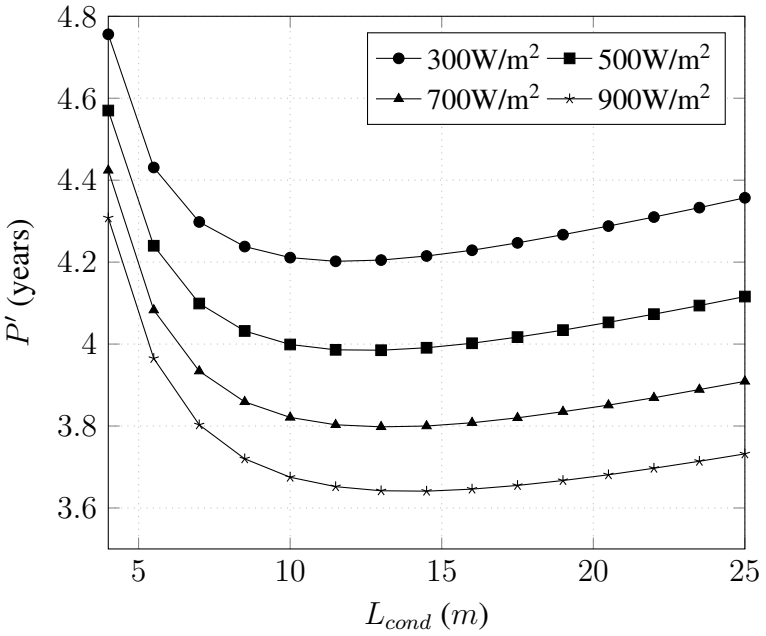

FIGURE 8.6: Payback time in function of condenser length

8.3 A new design of R290 DX-SAHP for Belo Horizonte

In fact, a larger collector reduces the time of operation need to heat the water than the heat pump can be programmed to operate during the hours with higher solar radiation and a better COP and payback can be found. To carry out this analysis, the annual mean solar radiation for Belo Horizonte (MG) was obtained using the weather data from meteorological institute of Brazil (INMET) considering that at noon, the heat pump is in the half time to heat

the water. Figure 8.7 shows the solar radiation available, and the solar radiation required and payback period for different collector area.

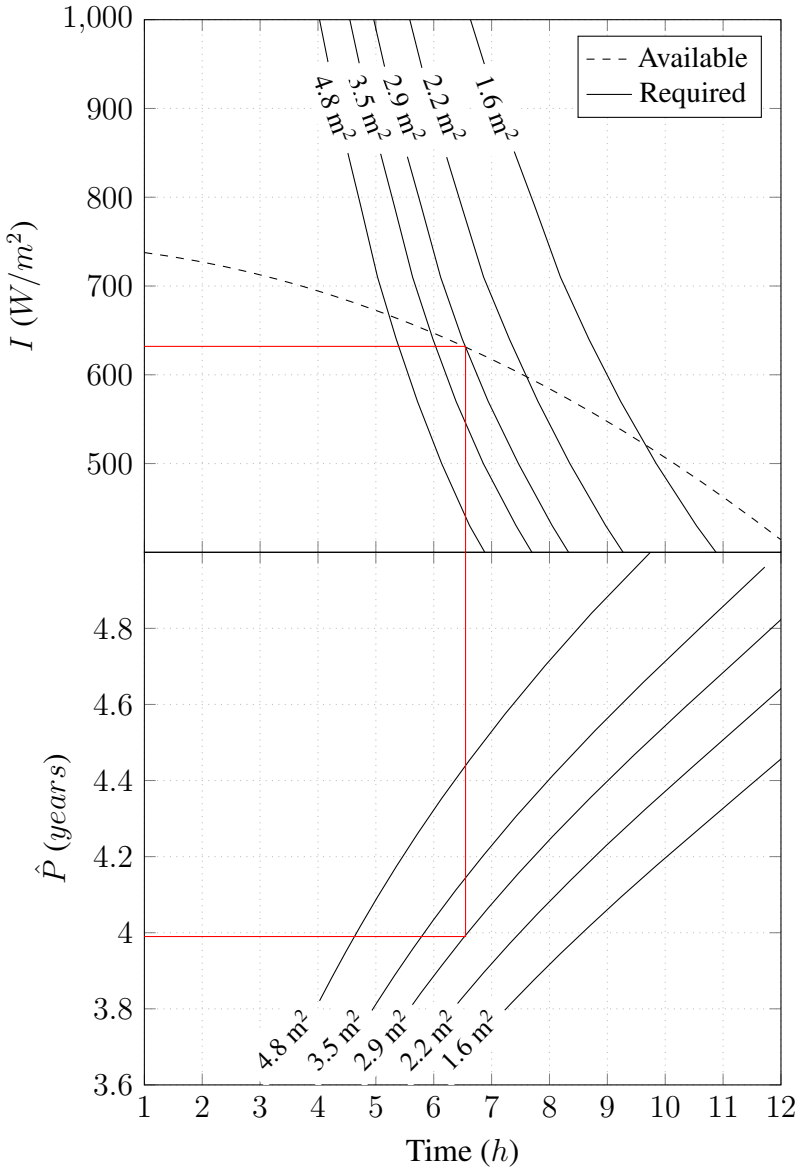

FIGURE 8.7: Required and available solar radiation and payback in function of time of operation

The interception of the curve of solar radiation required by a collector of 1,6 m^2 and the solar radiation available is the point of 520 W/m^2 and 9.8 hours, for that time, the payback is 4.15 years. Following this procedure, the payback for the collector sizes of 2.2, 2.9, 3.5 and 4.8 m_2 are 4.03, 3.98, 4,03 and 4.18 years. The collector of 2.9 m^2 was selected and the variation of the payback time is shown on FIG. 8.8. The minimum point was obtained with a length of 14,5 m. For this geometry, the average COP, TEWI and payback expected are 3.38, 1.9 tonne of CO^2 and 3.9 years. This payback time value is 13% bigger than that one found by Duarte,

Rabelo, et al. (2018) for a DX-SAHP using R134a.

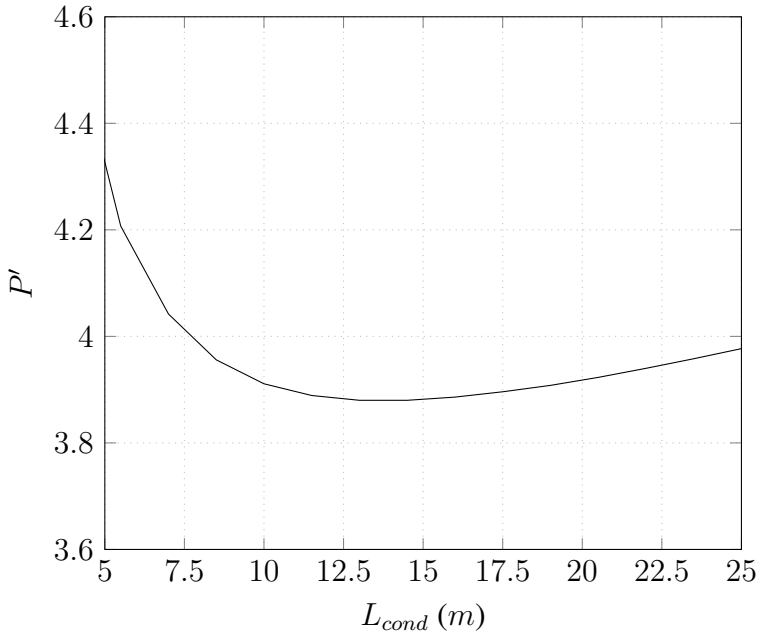

FIGURE 8.8: Payback time in function of condenser length for a collector area of 2.9 m^2 and average solar radiation of 630W/m^2

9. CONCLUSION

In this work a numeric model for a DX-SAHP equiped with a coaxial and immersed condenser is presented and experimentally validated. The model is based in the assumptions widely used in the literature. The condensers and the solar evaporator was modeled using a lumped model and the compressor were modeled using a gray box model. Results from a R134a DX-SAHP obtained under solar radiation from 0 to 1100 W/m^2, ambient temperature between 24.8 and 34.5^{o}C, final water temperature around 45^{o}C and wind velocity between 0 and 2.4 m/s were used to validate the model. The model used was validated in terms of COP with the mean differences between the experimental COP and the theoretical COP of 2%.

A comparison of refrigerants for a DX-SAHP has been carried out in terms of thermal performance and environmental impact. The thermal performance parameter used in this work was the COP of a DX-SAHP, and the environmental impact parameter was the TEWI. The refrigerants with low GWP selected were the R290, R600a, R744 and R1234yf. The analyses were performed with the solar radiation between 0 W/m^2 and 700 W/m^2, the ambient temperature between 10^oC and 35^oC and the wind speed between 0 and 4.5 m/s. Among the refrigerants compared, the R290 has better COP than the other refrigerants for solar radiation between 300 W/m^2 and 700 W/m^2, as well as, for ambient temperature between 10^{o}C and 35^{o}C. On the other hand, for solar radiation less than 50 W/m^2, the R134a has better COP than the other refrigerants. The influence of length of the high pressure heat exchanger was analyzed, it was observed that this value significantly interferes in the COP and TEWI of the heat pump. For a length higher than 18.5 meters for the gas cooler/condenser, the COP of R290 is 3% higher than the COP of R744.

Since R290 has the lowest environmental impact among the refrigerants pre-selected, an economic analysis was made considering this refrigerant. In this analysis the influence of the collector area and condenser length in the COP and payback time were investigated. The simulation showed that there is a collector area and condenser length that minimizes the payback time. The optimum size of condenser is affected by the changes in solar radiation and the optimum collector size is not affected. The payback time of a R290 DX-SAHP is 3.9 years and it is similar to the payback time available in the literature for R134a.

The suggestions for future work are following summarized:

- Exergetic analysis of the DX-SAHP considering different refrigerants;
- Optimization of the geometry of the heat pump in order to minimize the TEWI;
- Economical analysis considering different size of compressor of the DX-SAHP;
- Comparative study between IX-SAHP and DX-SAHP to produce domestic hot water.

BIBLIOGRAPHY

APREA, C.; MAIORINO, A. Heat rejection pressure optimization for a carbon dioxide split system: An experimental study. **Applied Energy**, Elsevier, v. 86, n. 11, p. 2373–2380, 2009.

ASHRAE. ASHRAE Guideline 12-2000: Minimizing the risk of Legionellosis associated with building water systems. **Atlanta (GA): ASHRAE**, 2000.

_____. **Handbook - Fundamentals (SI Edition)**. Atlanta, GA: American Society of Heating, Refrigerating and Air-Conditioning Engineers, Inc., 2013.

BAROCZY, C. **Correlation of liquid fraction in two-phase flow with application to liquid metals**. Canoga Park, Calif., 1963.

BELMAN-FLORES, J. M. et al. Experimental study of R1234yf as a drop-in replacement for R134a in a domestic refrigerator. **International Journal of Refrigeration**, Elsevier, v. 81, p. 1–11, 2017.

BERDAHL, P.; FROMBERG, R. The thermal radiance of clear skies. **Solar Energy**, v. 29, n. 4, p. 299–314, 1982.

BERTRAM, E.; PÄRISCH, P.; TEPE, R. Impact of solar heat pump system concepts on seasonal performance-Simulation studies. In: PROCEEDINGS of the EuroSun 2012 Conference. Rijeka: International Solar Energy Society, 2012.

BOTTICELLA, F.; VISCITO, L. Seasonal Performance Analysis of a Residential Heat Pump Using Different Fluids with Low Environmental Impact. **Energy Procedia**, Elsevier, v. 82, p. 878–885, 2015.

BUKER, M. S.; RIFFAT, S. Solar assisted heat pump systems for low temperature water heating applications: A systematic review. **Renewable and Sustainable Energy Reviews**, Elsevier, v. 55, p. 399–413, 2016.

ÇENGEL, Y. A.; GHAJAR, A. J. **Heat and mass transfer (a practical approach, SI version)**. 5. ed. New York: McGraw-Hill Education, 2015.

CERVANTES, J.; TORRES-REYES, E. Experiments on a solar-assisted heat pump and an exergy analysis of the system. **Applied Thermal Engineering**, v. 22, n. 12, p. 1289–1297, 2002.

CHAICHANA, C.; AYE, L.; CHARTERS, W. W. Natural working fluids for solar-boosted heat pumps. **International Journal of refrigeration**, Elsevier, v. 26, n. 6, p. 637–643, 2003.

CHATA, F. G.; CHATURVEDI, S. K.; ALMOGBEL, A. Analysis of a direct expansion solar assisted heat pump using different refrigerants. **Energy Conversion and Management**, v. 46, n. 15, p. 2614–2624, 2005.

CHATURVEDI, S. K.; ABAZERI, M. Transient simulation of a capacity-modulated, direct-expansion, solar-assisted heat pump. **Solar Energy**, v. 39, n. 5, p. 421–428, 1987.

CHATURVEDI, S. K.; CHEN, D.; KHEIREDDINE, A. Thermal performance of a variable capacity direct expansion solar-assisted heat pump. **Energy Conversion and Management**, v. 39, n. 3, p. 181–191, 1998.

CHATURVEDI, S. K.; CHIANG, Y.; ROBERTS, A. Analysis of two-phase flow solar collectors with application to heat pumps. **Journal of Solar Energy Engineering**, American Society of Mechanical Engineers, v. 104, n. 4, p. 358–365, 1982.

CHATURVEDI, S. K.; GAGRANI, V.; ABDEL-SALAM, T. Solar-assisted heat pump–a sustainable system for low-temperature water heating applications. **Energy Conversion and Management**, Elsevier, v. 77, p. 550–557, 2014.

CHATURVEDI, S. K.; SHEN, J. Y. Thermal performance of a direct expansion solar-assisted heat pump. **Solar Energy**, v. 33, n. 2, p. 155–162, 1984.

CHOW, T. T. et al. Modeling and application of direct-expansion solar-assisted heat pump for water heating in subtropical Hong Kong. **Applied Energy**, Elsevier, v. 87, n. 2, p. 643–649, 2010.

CHURCHILL, S. W. Friction-factor equation spans all fluid-flow regimes. **Chemical engineering**, MCGRAW HILL INC, NEW YORK, v. 84, n. 24, p. 91–92, 1977.

CHURCHILL, S. W.; CHU, H. H. S. Correlating equations for laminar and turbulent free convection from a horizontal cylinder. **International journal of heat and mass transfer**, Elsevier, v. 18, n. 9, p. 1049–1053, 1975.

_____. Correlating equations for laminar and turbulent free convection from a vertical plate. **International Journal of Heat and Mass Transfer**, v. 18, n. 11, p. 1323–1329, 1975.

CHYNG, J.; LEE, C.; HUANG, B. Performance analysis of a solar-assisted heat pump water heater. **Solar Energy**, v. 74, n. 1, p. 33–44, 2003.

CLELAND, A. Computer subroutines for rapid evaluation of refrigerant thermodynamic properties. **International Journal of Refrigeration**, Elsevier, v. 9, n. 6, p. 346–351, 1986.

DANILO, S.; DOMINIQUE, C.; FRÉDÉRIC, P. Experimental dropwise condensation of unsaturated humid air – Influence of humidity level on latent and convective heat transfer for fully developed turbulent flow. **International Journal of Heat and Mass Transfer**, v. 102, p. 846–855, 2016.

DAVIES, T. W.; CARETTA, O. A low carbon, low TEWI refrigeration system design. **Applied Thermal Engineering**, Elsevier, v. 24, n. 8, p. 1119–1128, 2004.

DENG, W.; YU, J. Simulation analysis on dynamic performance of a combined solar/air dual source heat pump water heater. **Energy Conversion and Management**, v. 120, p. 378–387, 2016.

DINIZ, H. A. G. **Estudo comparativo da eficiência energética de uma bomba de calor assistida por energia solar operando com condensadores por imersão e coaxial**. 2017. MA thesis – UFMG. Available from: ¡`http:` `//www.bibliotecadigital.ufmg.br/dspace/handle/1843/BUOS-8YHPE2`¿.

DUARTE, W. M.; DINIZ, H. A. G., et al. Performance comparison of direct expansion solar assisted heat pump working with R1234yf as a drop-in replacement for R134a. In: 17TH Brazilian Congress of Thermal Sciences and Engineering (to appear). Águas de Lindóia-SP: ABCM, 2018.

DUARTE, W. M.; RABELO, S. N., et al. Economic and energetic analysis of solar collector size of a direct expansion solar assisted heat pump. In: 17TH Brazilian Congress of Thermal Sciences and Engineering (to appear). Águas de Lindóia-SP: ABCM, 2018.

DUFFIE, J. A.; BECKMAN, W. A. **Solar engineering of thermal processes**. New Jersey: John Wiley & Sons, 2013.

EP. Directive 2006/40/EC of the European Parliament and of the Council of 17 May 2006 relating to emissions from air-conditioning systems in motor vehicles and Amending Council Directive 70/156/EEC. **Official Journal of the European Union**, v. 1, 2006.

_____. Regulation (EU) No 517/2014 of the European Parliament and of the Council of 16 April 2014 on fluorinated greenhouse gases and repealing regulation (EC) No 842/2006 Text with EEA relevance. **Official Journal of the European Union**, v. 57, n. L 150, p. 195–230, 2014.

FANG, X.; WU, Q.; YUAN, Y. A general correlation for saturated flow boiling heat transfer in channels of various sizes and flow directions. **International Journal of Heat and Mass Transfer**, Elsevier, v. 107, p. 972–981, 2017.

FANG, X.; ZHOU, Z.; WANG, H. Heat transfer correlation for saturated flow boiling of water. **Applied Thermal Engineering**, v. 76, p. 147–156, 2015.

FARIA, R. N. et al. Dynamic modeling study for a solar evaporator with expansion valve assembly of a transcritical CO_2 heat pump. **International Journal of Refrigeration**, Elsevier, v. 64, p. 203–213, 2016.

FERNÁNDEZ-SEARA, J. et al. Experimental analysis of a direct expansion solar assisted heat pump with integral storage tank for domestic water heating under zero solar radiation conditions. **Energy Conversion and Management**, v. 59, p. 1–8, 2012.

GHOUBALI, R. et al. Simulation study of a heat pump for simultaneous heating and cooling coupled to buildings. **Energy and buildings**, Elsevier, v. 72, p. 141–149, 2014.

GLIAH, O. et al. The effective sky temperature: an enigmatic concept. **Heat and mass transfer**, Springer, v. 47, n. 9, p. 1171–1180, 2011.

GNIELINSKI, V. New equations for heat and mass transfer in turbulent pipe and channel flow. **Int. Chem. Eng.**, v. 16, n. 2, p. 359–368, 1976.

GODBOLE, P. V.; TANG, C. C.; GHAJAR, A. J. Comparison of void fraction correlations for different flow patterns in upward vertical two-phase flow. **Heat Transfer Engineering**, Taylor & Francis, v. 32, n. 10, p. 843–860, 2011.

GUNGOR, K. E.; WINTERTON, R. H. S. Simplified general correlation for saturated flow boiling and comparisons of correlations with data. **Chemical engineering research & design**, v. 65, p. 148–156, 1987.

HAWLADER, M.; CHOU, S.; ULLAH, M. The performance of a solar assisted heat pump water heating system. **Applied Thermal Engineering**, v. 21, n. 10, p. 1049–1065, 2001.

HUANG, J.; ZHANG, J.; WANG, L. Review of vapor condensation heat and mass transfer in the presence of non-condensable gas. **Applied Thermal Engineering**, v. 89, p. 469–484, 2015.

HUGHMARK, G. Holdup in gas liquid flow. **Chemical Engineering Progress**, n. 58, p. 62–65, 1962.

HUMIA, G. M. **Estudo experimental e modelo de simulação para a determinação do inventário em sistemas de refrigeração carregados com os fluidos R134a e HFO-1234yf**. 2017. MA thesis – UFMG.

INCROPERA, F. P. et al. **Fundamentos da Transferência do Calor e massa**. 6. ed. Rio de Janeiro: Editora LTC, 2007.

INMET. **National Institute of Meteorology: Automatic station**. 2017. Available from: ¡https://goo.gl/bEnRpf¿. Visited on: 15 Feb. 2017.

ISLAM, M. R. et al. Performance study on solar assisted heat pump water heater using CO_2 in a transcritical cycle. In: INTERNATIONAL Conference on Renewable Energies and Power Quality. Santiago de Compostela, Spain: [s.n.], 2012.

ISO. **ISO 6946: 2007 Building components and building elements—Thermal resistance and thermal transmittance—Calculation method**. [s.l.]: British Board of Agrément tel, 2007.

ITO, S.; MIURA, N.; WANG, K. Performance of a heat pump using direct expansion solar collectors. **Solar Energy**, Elsevier, v. 65, n. 3, p. 189–196, 1999.

ITO, S.; MIURA, N.; TAKANO, Y. Studies of heat pumps using direct expansion type solar collectors. **Journal of solar energy engineering**, American Society of Mechanical Engineers, v. 127, n. 1, p. 60–64, 2005.

JIN, J.; CHEN, J.; CHEN, Z. Development and validation of a microchannel evaporator model for a CO_2 air-conditioning system. **Applied Thermal Engineering**, Elsevier, v. 31, n. 2, p. 137–146, 2011.

KARWA, R. **Heat and Mass Transfer**. Singapore: Springer eBooks, 2017.

KIM, S. C.; WON, J. P.; KIM, M. S. Effects of operating parameters on the performance of a CO_2 air conditioning system for vehicles. **Applied Thermal Engineering**, Elsevier, v. 29, n. 11, p. 2408–2416, 2009.

KONG, X.; JIANG, K., et al. Control strategy and experimental analysis of a direct-expansion solar-assisted heat pump water heater with R134a. **Energy**, v. 145, p. 17–24, 2018.

KONG, X.; SUN, P., et al. Experimental performance analysis of a direct-expansion solar-assisted heat pump water heater with R134a in summer. **International Journal of Refrigeration**, v. 91, p. 12–19, 2018.

KONG, X.; LI, Y., et al. Modeling evaluation of a direct-expansion solar-assisted heat pump water heater using R410A. **International Journal of Refrigeration**, Elsevier, v. 76, p. 136–146, 2017.

KONG, X.; ZHANG, D., et al. Thermal performance analysis of a direct-expansion solar-assisted heat pump water heater. **Energy**, Elsevier, v. 36, n. 12, p. 6830–6838, 2011.

KOURY, R.; MACHADO, L.; ISMAIL, K. Numerical simulation of a variable speed refrigeration system. **International journal of refrigeration**, Elsevier, v. 24, n. 2, p. 192–200, 2001.

KUANG, Y. H.; SUMATHY, K.; WANG, R. Z. Study on a direct-expansion solar-assisted heat pump water heating system. **International Journal of Energy Research**, Wiley Online Library, v. 27, n. 5, p. 531–548, 2003.

KUANG, Y.; WANG, R. Performance of a multi-functional direct-expansion solar assisted heat pump system. **Solar Energy**, v. 80, n. 7, p. 795–803, 2006.

KUMAR, S.; MULLICK, S. Wind heat transfer coefficient in solar collectors in outdoor conditions. **Solar Energy**, Elsevier, v. 84, n. 6, p. 956–963, 2010.

LEE, Y.; JUNG, D. A brief performance comparison of R1234yf and R134a in a bench tester for automobile applications. **Applied Thermal Engineering**, Elsevier, v. 35, p. 240–242, 2012.

LI, C.; LI, J. Laminar Forced Convection Heat and Mass Transfer of Humid Air across a Vertical Plate with Condensation. **Chinese Journal of Chemical Engineering**, v. 19, n. 6, p. 944–954, 2011.

LI, Y. et al. Experimental performance analysis and optimization of a direct expansion solar-assisted heat pump water heater. **Energy**, v. 32, n. 8, p. 1361–1374, 2007.

LIAO, S.; ZHAO, T.; JAKOBSEN, A. A correlation of optimal heat rejection pressures in transcritical carbon dioxide cycles. **Applied Thermal Engineering**, Elsevier, v. 20, n. 9, p. 831–841, 2000.

LLOYD, J.; MORAN, W. Natural convection adjacent to horizontal surface of various planforms. **Journal of Heat Transfer**, American Society of Mechanical Engineers, v. 96, n. 4, p. 443–447, 1974.

LOCKHART, R.; MARTINELLI, R. Proposed correlation of data for isothermal two-phase, two-component flow in pipes. **Chem. Eng. Prog**, v. 45, n. 1, p. 39–48, 1949.

MA, Y.; LIU, Z.; TIAN, H. A review of transcritical carbon dioxide heat pump and refrigeration cycles. **Energy**, Elsevier, v. 55, p. 156–172, 2013.

MACHADO, L.; HABERSCHILL, P.; LALLEMAND, M. Masse du fluide frigorigéne dans un évaporateur en fonctionnement permanent ou transitoire: Refrigerant mass inside an evaporator in a steady or non-steady state. **International journal of refrigeration**, Elsevier, v. 21, n. 6, p. 430–439, 1998.

MACHADO, L. **Modele de simulation et etude experimentale d'un evaporateur de machine frigorifique en regime transitoire**. 1996. PhD thesis – INSA, Lyon.

MAKHNATCH, P.; KHODABANDEH, R. Selection of low GWP refrigerant for heat pumps by assessing the Life Cycle Climate Performance (LCCP). In: 11TH International Energy Agency Heat Pump Conference. Montreal: International Energy Agency, 2014.

_____. The role of environmental metrics (GWP, TEWI, LCCP) in the selection of low GWP refrigerant. **Energy Procedia**, Elsevier, v. 61, p. 2460–2463, 2014.

MCADAMS, W. H. **Heat transmission**. London, 1954.

MINETTO, S. Theoretical and experimental analysis of a CO_2 heat pump for domestic hot water. **International journal of refrigeration**, Elsevier, v. 34, n. 3, p. 742–751, 2011.

MMA. **Convenção de Viena e Protocolo de Montreal**. 2017. Available from: ¡http://www.mma.gov.br/clima/protecao-da-camada-de-ozonio/convencao-de-viena-e-protocolo-de-montreal¿. Visited on: 8 May 2017.

_____. **Tratato de Paris**. 2017. Available from: ¡http://www.mma.gov.br/clima/convencao-das-nacoes-unidas/acordo-de-paris¿. Visited on: 15 May 2017.

MOHAMED, E.; RIFFAT, S.; OMER, S. Low-temperature solar-plates-assisted heat pump: a developed design for domestic applications in cold climate. **International Journal of Refrigeration**, Elsevier, 2017.

MOHR, P. J.; NEWELL, D. B.; TAYLOR, B. N. CODATA recommended values of the fundamental physical constants: 2014. **Journal of Physical and Chemical Reference Data**, NIST, v. 45, n. 4, p. 043102, 2016.

MORENO-RODRÍGUEZ, A. et al. Theoretical model and experimental validation of a direct-expansion solar assisted heat pump for domestic hot water applications. **Energy**, Elsevier, v. 45, n. 1, p. 704–715, 2012.

NEILS, G.; KLEIN, S. **Heat Transfer**. New York: Cambridge university press, 2009.

OLIVEIRA, R. N. de et al. Dynamic model and experimental validation for a gas cooler of a CO_2 heat pump for heating residential water. **Science and Technology for the Built Environment**, Taylor & Francis, v. 22, n. 1, p. 30–40, 2016.

PALM, B. Hydrocarbons as refrigerants in small heat pump and refrigeration systems–a review. **International journal of refrigeration**, Elsevier, v. 31, n. 4, p. 552–563, 2008.

QI, P.-C. et al. Experimental investigation of the optimal heat rejection pressure for a transcritical CO_2 heat pump water heater. **Applied Thermal Engineering**, Elsevier, v. 56, n. 1, p. 120–125, 2013.

REES, S. **Advances in ground-source heat pump systems**. [s.l.]: Woodhead Publishing, 2016.

REIS, R. V. d. M. **Análise experimental comparativa entre uma bomba de calor e uma resistência elétrica como dispositivo de apoio de energia para um aquecedor solar de água**. 2012. PhD thesis – UFMG.

RODRIGUEZ, O. R. S. **Desenvolvimento de um simulador de coletor solar para reprodução das condições de operação de uma bomba de calor para aquecimento de água residencial**. 2015. MA thesis – UFMG. Available from: ¡`http:
//www.bibliotecadigital.ufmg.br/dspace/handle/1843/BUBD-9WFGRC`¿.

ROHSENOW, W. M.; HARTNETT, J. P.; CHO, Y. I., et al. **Handbook of heat transfer**. New York: McGraw-Hill, 1998. v. 3, p. 4.1–99.

ROUHANI, S. Z.; AXELSSON, E. Calculation of void volume fraction in the subcooled and quality boiling regions. **International Journal of Heat and Mass Transfer**, Elsevier, v. 13, n. 2, p. 383–393, 1970.

SARBU, I. A review on substitution strategy of non-ecological refrigerants from vapour compression-based refrigeration, air-conditioning and heat pump systems. **International journal of refrigeration**, Elsevier, v. 46, p. 123–141, 2014.

SARKAR, J.; BHATTACHARYYA, S.; GOPAL, M. R. Simulation of a transcritical CO_2 heat pump cycle for simultaneous cooling and heating applications. **International Journal of Refrigeration**, v. 29, n. 5, p. 735–743, 2006.

SARKAR, J.; BHATTACHARYYA, S.; GOPAL, M. R. Optimization of a transcritical CO_2 heat pump cycle for simultaneous cooling and heating applications. **International Journal of Refrigeration**, Elsevier, v. 27, n. 8, p. 830–838, 2004.

SCARPA, F.; TAGLIAFICO, L. A. Exploitation of humid air latent heat by means of solar assisted heat pumps operating below the dew point. **Applied Thermal Engineering**, v. 100, p. 820–828, 2016.

SHAH, M. M. Chart correlation for saturated boiling heat transfer: equations and further study. **ASHRAE Trans.;(United States)**, v. 88, CONF-820112, 1982.

_____. Comprehensive correlations for heat transfer during condensation in conventional and mini/micro channels in all orientations. **International journal of refrigeration**, Elsevier, v. 67, p. 22–41, 2016.

_____. Unified correlation for heat transfer during boiling in plain mini/micro and conventional channels. **International Journal of Refrigeration**, Elsevier, v. 74, p. 604–624, 2017.

SHARPLES, S.; CHARLESWORTH, P. Full-scale measurements of wind-induced convective heat transfer from a roof-mounted flat plate solar collector. **Solar Energy**, Elsevier, v. 62, n. 2, p. 69–77, 1998.

SOARES, D. S. L. **Sobre o valor da aceleração da gravidade medido no Departamento de Física**. 2011. Available from: ¡`http://goo.gl/iIqYmq`¿. Visited on: 15 Feb. 2014.

SONNTAG, R. E. et al. **Fundamentals of thermodynamics**. New York: Wiley, 2003.

SUN, X. et al. Performance Comparison of Direct Expansion Solar-assisted Heat Pump and Conventional Air Source Heat Pump for Domestic Hot Water. **Energy Procedia**, v. 70, p. 394–401, 2015.

TEST, F.; LESSMANN, R.; JOHARY, A. Heat transfer during wind flow over rectangular bodies in the natural environment. **Journal of Heat Transfer**, American Society of Mechanical Engineers, v. 103, n. 2, p. 262–267, 1981.

THOM, J. Prediction of pressure drop during forced circulation boiling of water. **International journal of heat and mass transfer**, Elsevier, v. 7, n. 7, p. 709–724, 1964.

TORRES-REYES, E.; GORTARI, J. C. Optimal performance of an irreversible solar-assisted heat pump. **Exergy, An International Journal**, v. 1, n. 2, p. 107–111, 2001.

TORRES-REYES, E.; NUÑEZ, M. P.; GORTARI, J. C. de. Exergy analysis and optimization of a solar-assisted heat pump. **Energy**, v. 23, n. 4, p. 337–344, 1998.

TSAMOS, K. et al. Energy analysis of alternative CO_2 refrigeration system configurations for retail food applications in moderate and warm climates. **Energy Conversion and Management**, Elsevier, 2017.

TURNER, J.; WALLIS, G. The separate-cylinders model of two-phase flow, paper no. **NYO-3114-6Thayer's School Eng., Dartmouth College, Hanover, NH, USA**, 1965.

UNEP. **2014 Report of the Refrigeration, Air Conditioning and Heat Pumps Technical Options Committee.** Nairobi, 2015.

WANG, S. et al. Experimental investigation on air-source transcritical CO_2 heat pump water heater system at a fixed water inlet temperature. **international journal of refrigeration**, Elsevier, v. 36, n. 3, p. 701–716, 2013.

WATMUFF, J.; CHARTERS, W.; PROCTOR, D. Solar and wind induced external coefficients for solar collectors. Comples, 2. **Rev. Inter. Heliotech., Marseille**, 1977.

WOLDESEMAYAT, M. A.; GHAJAR, A. J. Comparison of void fraction correlations for different flow patterns in horizontal and upward inclined pipes. **International journal of multiphase flow**, Elsevier, v. 33, n. 4, p. 347–370, 2007.

XU, G. et al. Simulation of a photovoltaic/thermal heat pump system having a modified collector/evaporator. **Solar Energy**, v. 83, n. 11, p. 1967–1976, 2009.

XU, X.; HWANG, Y.; RADERMACHER, R. Performance comparison of R410A and R32 in vapor injection cycles. **International Journal of Refrigeration**, Elsevier, v. 36, n. 3, p. 892–903, 2013.

YANG, L. et al. Minimizing COP loss from optimal high pressure correlation for transcritical CO_2 cycle. **Applied Thermal Engineering**, Elsevier, v. 89, p. 656–662, 2015.

ZIVI, S. Estimation of steady-state steam void-fraction by means of the principle of minimum entropy production. **Journal of heat transfer**, American Society of Mechanical Engineers, v. 86, n. 2, p. 247–251, 1964.